UNIVERSITY OF CALIFORNIA, SAN DIEGO

Traffic Throughput and Safety Enhancement for Vehicular Traffic Networks

A dissertation submitted in partial satisfaction of the
requirements for the degree
Doctor of Philosophy

in

Electrical Engineering (Communication Theory and Systems)

by

Seokheon Cho

Committee in charge:

Professor Ramesh R. Rao, Chair
Professor Robert R. Bitmead
Professor William M. McEneaney
Professor Truong Q. Nguyen
Professor Mohan M. Trivedi

2014

The dissertation of Seokheon Cho is approved, and it is acceptable in quality and form for publication on microfilm and electronically:

_____

_____

_____

_____

_____

Chair

University of California, San Diego

2014

DEDICATION

To my father and mother, for guiding me through this life.

And to Misun, for her love and support.

TABLE OF CONTENTS

LIST OF FIGURES

LIST OF TABLES

ACKNOWLEDGEMENTS

I would first like to show my sincere appreciation to my advisor Professor Ramesh R. Rao for his valuable advice and continuous encouragement. He was a great advisor to help me to have constructive insight and to develop new ideas in my research. The work in this dissertation was made possible by his generous and constant support.

I would like to thank my former advisor Professor Rene L. Cruz for his timely advice and valuable help. He gave me a meaningful conjecture and a great deal of freedom in my work. His suggestions were very helpful in strengthening the basis of my dissertation. I hope he rests in peace.

I would also like to thank Professor William M. McEneaney for sharing his mathematical knowledge and guidance. He has helped me build a solid foundation for my interdisciplinary works, particularly on optimization problems and dynamic programmings.

I would like to thank the rest of my committee: Professors Truong Nguyen, Mohan M. Trivedi, and Robert R. Bitmead for their generous time and comments to improve my dissertation. Moreover, I would like to thank Anush Badii at the California Department of Transportation (Caltrans) for providing motivation and fundamental information on traffic flow dynamics.

Chapter 2, in full, is a reorganized version of the following publication in the Proceedings of the IEEE 79th Vehicular Technology Conference, 2014 Spring. Seokheon Cho, Anush Badii, Rene L. Cruz, and Ramesh R. Rao. "Time-gap based traffic model for vehicular traffic flow," in Proceedings of the IEEE 79th Vehicular Technology Conference (VTC Spring), pp. 1-5, May, 2014.

Chapter 3, in full, is a reorganized version of the following publication in the Proceedings of the IEEE 80th Vehicular Technology Conference, 2014 Fall. Seokheon Cho and Ramesh R. Rao. "Coordinated ramp-metering control using a time-gap based traffic model," in Proceedings of the IEEE 80th Vehicular Technology Conference (VTC Fall), pp. 1-6, Sep., 2014.

Chapter 4, in full, is a reorganized version of the following manuscript in preparation. Seokheon Cho and Ramesh R. Rao. "A new safety metric for vehicular traffic networks," *in preparation*.

Chapter 5, in full, is a reorganized version of the following manuscript in preparation. Seokheon Cho and Ramesh R. Rao. "Usability, safety, and capacity analysis for a target time-gap-based velocity update model," *in preparation*.

VITA

2000	B.S. in Electronic Engineering, Chonbuk National University, Jeonju, South Korea.
2002	M.S. in Information of Communications Engineering, Gwangju Institute of Science and Technology (GIST), Gwangju, South Korea.
2014	Ph.D. in Electrical and Computer Engineering (Communication Theory and Systems), University of California, San Diego.

PUBLICATIONS

Seokheon Cho, Anush Badii, Rene L. Cruz, and Ramesh R. Rao, "Time-gap Based Traffic Model for Vehicular Traffic Flow," in *Proceedings of the IEEE 79th Vehicular Technology Conference (VTC) Spring*, pp. 1-5, May 2014.

Seokheon Cho and Ramesh R. Rao, "Coordinated Ramp-metering Control Using a Time-gap Based Traffic Model," in *Proceedings of the IEEE 80th Vehicular Technology Conference (VTC) Fall*, pp. 1-6, Sep. 2014.

Seokheon Cho and Ramesh R. Rao, "A New Safety Metric for Vehicular Traffic Networks," *in preparation*.

Seokheon Cho and Ramesh R. Rao, "Usability, Safety, and Capacity Analysis for a Target Time-gap-based Velocity Update Model," *in preparation*.

ABSTRACT OF THE DISSERTATION

Traffic Throughput and Safety Enhancement for Vehicular Traffic Networks

by

Seokheon Cho

Doctor of Philosophy in Electrical Engineering (Communication Theory and Systems)

University of California, San Diego, 2014

Professor Ramesh R. Rao, Chair

For decades, one of the most significant challenges in vehicular traffic networks has been how to mitigate traffic congestion characterized by increased vehicle queueing and slower traffic speeds. Whereas traffic congestion is a complicated and subjective matter, congestion delay consists of recurrent delay and non-recurrent delay. Recurring congestion is attributed to high excess demand that constitutes about half of congestion delay, and most of the rest is non-recurring congestion mainly occurring due to incidents. In order to reduce congestion more effectively in vehicular traffic networks, it is necessary to focus on how to control high utility demand for using traffic systems and how to guarantee safety against incidents by using various strategies, instead of inefficiently widening roads. Therefore, this dissertation provides diverse approaches to improve system throughput as well as to enhance collision safety for vehicular traffic

networks through understanding of vehicular traffic flow, ramp-metering control, traffic safety metric, and inter-vehicle velocity control.

In Chapter 2, we provide a macroscopic traffic flow model called a time-gap-based traffic model, which is a good and simple representative model for vehicular traffic flow. The proposed time-gap-based traffic model is well validated with empirical traffic data using least squares matching and is consistent with previous research outcomes about propagation velocity. Moreover, two analysis techniques to estimate the time gap from traffic measurement data are suggested.

Chapter 3 presents two optimal coordinated ramp-metering algorithms based on the time-gap-based traffic model defined in Chapter 2. The purpose of the two optimization problems is to attain the maximum average system capacity for vehicular traffic networks. In addition, both of them are coordinated ramp-metering strategies that make use of the measurement data along a highway corridor to control all metered ramps simultaneously. One is a steady-state optimization problem used under supposition when the traffic system reaches a steady-state, whereas another optimal control is a time-variant optimization problem exploited when the traffic flow changes continuously with respect to time. The time-variant optimization problem considers an on-ramp queue management strategy.

We propose a traffic safety metric called a safety marginal value (SMV) to be applied to continuous-space and discrete-time vehicular traffic networks in Chapter 4. The SMV represents the safety level of collision risk at every time step and is bounded by two non-negative integers. However, the computational complexity in determining the SMV grows dramatically, particularly when the number of vehicles traveling on a roadway increases. Hence, a finite space horizon for the SMV is also developed in order to prune the computational complexity of our proposed traffic safety indicator. A safety analysis of a car-following model is conducted with the SMV and with a microscopic traffic simulation.

A car-following model called a target time-gap-based velocity update model is proposed in Chapter 5. Our proposed microscopic traffic flow model is used for inter-vehicle velocity control, which every vehicle exploits in order to refresh the velocity and position for the next time step. The microscopic traffic simulation results are matched

well with empirical traffic data. Thus, the target time-gap-based velocity update model is considered a representative car-following model that can accurately mimic typical driving behavior. The effective domains of the target time gap and the update time interval, which guarantee both collision-free movement of all vehicles and system capacity enhancement compared to the traffic data measured in the field, are examined.

Chapter 1

Introduction

1.1 Motivation

An annoying and bothersome phenomenon confronted frequently by commuters is traffic congestion, particularly in growing and large metropolitan regions across the world. There are many side effects of traffic jam: longer travel times for drivers, slower traffic speeds, wasted fuel consumption, increased air pollution, higher likelihood of collisions due to constant stop-and-go traffic, additional spillover traffic from congested roadways onto adjacent streets, unhoped-for road rage, and increased travel costs. Traffic congestion is categorized as recurrent delay or non-recurrent delay depending on the cause of congestion. Recurring congestion is attributed to high excess demand, whereas non-recurring congestion mainly occurs when there are unexpected incidents.

Examination of the causes of congestion is an essential prerequisite for relieving traffic jams [1, 2, 3]. Kwon *et al.* [2, 3] analyzed the traffic data measured on I-15N in San Diego, California, USA. According to their analysis, the measured total delay is classified into three components: (1) the congestion caused by incidents; (2) the potential mitigation in congestion that an optimal ramp-metering control can achieve; and (3) the remaining congestion due to all other causes such as non-collision incidents, lane closures, and weather. When traffic density exceeds the critical density by any cause mentioned above, traffic flow breaks down and thus severe congestion occurs. Collisions and potential mitigation constitute 31% and 46% of the total daily traffic congestion, respectively. This implies that optimal congestion mitigation strategies such

as ramp-metering and vehicular safety controls help to obtain the remarkable gain of reducing around 77% of the delay.

Kwon *et al.*'s statistics that collisions account for around $1/3$ of the total congestion causes are consistent with the numerical statement reported by the California Department of Transportation (Caltrans), USA. The average number of collisions per day and the average accident clearance time per collision collected from May 1-7 in 2012 in San Diego, California, USA are given in Table 1.1. The average number of collisions per day during rush hours on weekdays measured on highways I-5, I-15, and I-805 is 5.4, 2.2, and 4.5, respectively. In addition, it takes longer than 40 min on average to clear each collision during weekday rush hours. Since more time is needed to clear traffic congestion caused by incidents compared to collision clearance time, the average traffic congestion clearance time is much longer than 40 min. To top it off, this non-recurring delay intensifies the recurring congestion, in particular during rush hours, creating more severe congestion. There still exist incidents that incur unwanted and significant traffic jams during non-rush hours on weekdays, even though the average number of collisions that happen during off hours is less than during rush hours. This similar phenomenon can be observed on weekends even when there is no rush hours. Also, the average accident clearance time is longer than 43.8 min during non-rush hours on all highways except on a corridor of I-805 on weekends. Hence, the statistics shown in Table 1.1 imply that a collision gives rise to a serious traffic jam by itself during non-rush hours as well as aggravates recurring delays during rush hours.

According to another crash statistics conducted by the Missouri Department of Transportation (MoDOT), more than 80% of all crashes are related to collisions among neighboring vehicles [4]. Moreover, since most collisions are caused by drivers' faults, such as speeding, inattention by distraction, or intoxication, most incidents are avoidable through consistent, careful driving or through use of an auxiliary driving control such as autonomous driving and automatic cruise control. Therefore, various technical strategies to augment traffic safety through vehicle controls and improve traffic system capacity by mitigating congestion need to be investigated.

Table 1.1: Measurement traffic data collected from May 1 to May 7 in 2012 in San Diego, California, USA. (1) Average number of collisions per day. (2) Average accident clearance time per collision.

		Rush hours		Non-rush hours	
		Average number of collisions	Average accident clearance time per collision (min)	Average number of collisions	Average accident clearance time per collision (min)
Weekdays	I-5	5.4	40.1	2.6	57.5
	I-15	2.2	64.9	1.2	55
	I-805	4.5	58.3	2.6	47.7
Weekends	I-5	N/A	N/A	8.5	43.8
	I-15	N/A	N/A	1.5	50
	I-805	N/A	N/A	2.5	25.6

1.2 Contributions

The philosophy of this dissertation is shown in Fig. 1.1. The final purposes of the dissertation seek the traffic capacity and safety enhancement of vehicular traffic networks. Diverse approaches need to be considered to accomplish these compositive aims: (1) Develop a series of strategies to guarantee traffic safety and to relieve traffic congestion by first gaining an understanding of vehicular traffic flow as an essential prerequisite. As an analysis result of the empirical traffic data, a macroscopic traffic flow model called a time-gap-based traffic model is provided; (2) Create two coordinated ramp-metering controls, which use real-time measurement data along a system-wide highway corridor to control all metered ramps simultaneously, to maximize the average system throughput. A comparison between no ramp-metering and two coordinated ramp-metering strategies is conducted through both a macroscopic traffic simulator and a traffic flow estimation based on a time-gap-based traffic model; (3) Provide a traffic safety metric called an anterior safety marginal value (SMV). The anterior SMV indicates the safety level of collision risk with other vehicles, which is calculated at every discrete time step. A safety analysis of a car-following model is performed with this safety indicator under a microscopic traffic simulator. This induces safety enhancement for vehicular traffic networks; (4) Develop a car-following model called a target time-

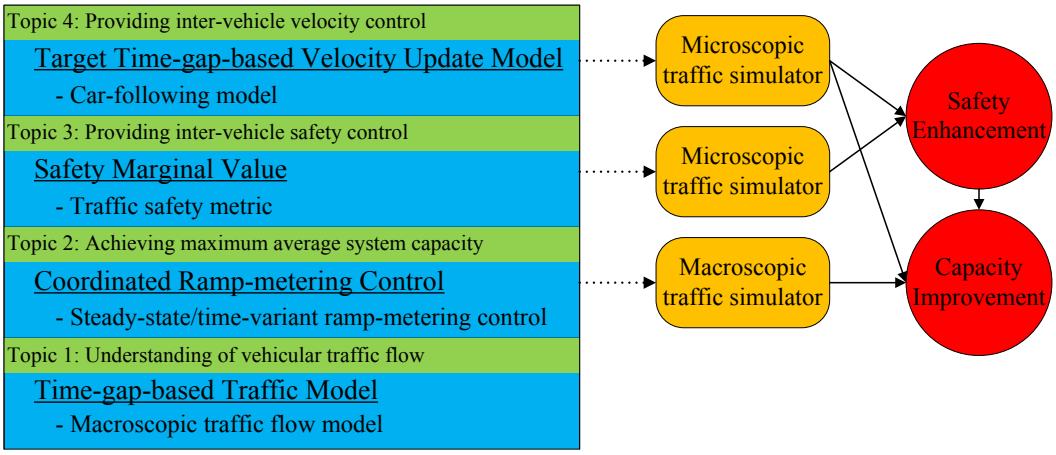

Figure 1.1: Philosophy of dissertation.

gap-based velocity update model. The target time-gap-based velocity update model is used for inter-vehicle velocity control. When every vehicle in vehicular traffic system uses the target time-gap-based velocity update model, the domains of the target time gap and the update time interval that guarantee both safety and capacity improvement are presented through a microscopic traffic simulator.

Most of studies for reducing traffic congestion have been conducted without fundamental knowledge of vehicular traffic flow, particularly such as drivers' behavior or their driving patterns; however, the understanding of vehicular traffic flow is a critical and essential prerequisite for developing a series of diverse strategies related to traffic flow dynamics, since the typical behavior of drivers is itself a creative and superior algorithm not only to avoid collision but also to reduce congestion. Hence, the development of a macroscopic traffic flow model through the analysis of traffic flow needs to precede the provision of various algorithms to accomplish these purposes. That is, diverse system-wide managements, which are based on a macroscopic traffic flow model reflecting the traffic flow characteristics well, will lead to a great synergistic effect to enhance throughput and safety for vehicular traffic networks.

Various ramp-metering controls have been examined and recognized as an effective method of relieving recurrent congestion on highways by regulating the inflow from on-ramps to the highway mainline; for example, ALINEA [5, 6, 7, 8, 9], BOTTLENECK [10], ZONE [11], SWARM [12], and METALINE [13, 14, 15, 16, 17] are famous

existing ramp-metering algorithms. These ramp-metering strategies seek to maximize capacity or to minimize the total travel times of vehicles on vehicular traffic systems. However, the selection of only a proper macroscopic traffic flow model, which represents the vehicular traffic features created by vehicles, brings about correct outcomes of the objective function defined for ramp-metering algorithms. Moreover, ramp-metering control is a partial solution to total travel delay on roadways, because it considers only recurrent congestion; that is, other studies, such as a traffic safety metric and inter-vehicle safety control, also need to be investigated to mitigate non-recurrent congestion and improve traffic safety.

A traffic safety metric is used to indicate safety level of collision risk and warn of dangerous traffic circumstances in advance. This safety indicator is a good auxiliary control in intelligent vehicles to mitigate collisions. In addition, a car-following model mimicking driving pattern needs to be developed, since typical driving behavior without distraction is itself a creative and superior algorithm. An investigation of the effective conditions for the proposed car-following model, which ensures collision-free movement and system capacity enhancement, is important. When all vehicles use inter-vehicle safety controls based on the effectual conditions of the model, a vehicular traffic network can improve its performance, such as safety and throughput.

Therefore, we first provide a macroscopic traffic flow model describing traffic flow and the typical behavior of drivers. We derive various strategies based on a macroscopic traffic flow model, which are (1) coordinated ramp-metering control to relieve the potential congestion incurred by excess demand as well as (2) inter-vehicle safety control using a car-following model to help to decrease accidents and congestion simultaneously. Moreover, a traffic safety metric is introduced to warn of and avoid collisions. These studies can be mapped to other areas beyond traffic flow dynamics, such as reducing packet transmission delay, enlarging data transmission rate, decreasing packet loss rate, and so on, in wireless communication systems.

1.3 Organization

The organization of this dissertation is as follows:

Chapter 2 provides a macroscopic traffic flow model called a time-gap-based traffic model, which is a good and simple representative model for vehicular traffic flow. The proposed time-gap-based traffic model is well validated with empirical traffic data using least squares matching and is consistent with previous research outcomes about propagation velocity. Moreover, two analysis techniques to estimate the time gap from traffic measurement data are suggested.

Chapter 3 proposes two optimal coordinated ramp-metering algorithms based on the time-gap-based traffic model defined in Chapter 2. The purpose of the two optimization problems is to attain the maximum average system capacity for vehicular traffic networks. In addition, both of them are coordinated ramp-metering strategies that make use of the measurement data along a highway corridor to control all metered ramps simultaneously. One is a steady-state optimization problem used under supposition when the traffic system reaches a steady-state, whereas another optimal control is a time-variant optimization problem exploited when the traffic flow changes continuously with respect to time. A time-variant optimization problem considers an on-ramp queue management strategy.

Chapter 4 provides a traffic safety metric called a safety marginal value (SMV) to be applied to continuous-space and discrete-time vehicular traffic networks. The SMV represents the safety level of collision risk at every time step and is bounded by two non-negative integers. However, the computational complexity in determining the SMV grows dramatically, particularly when the number of vehicles traveling on a roadway increases. Hence, a finite space horizon for the SMV is also developed in order to prune the computational complexity of our proposed traffic safety indicator. A safety analysis of a car-following model is conducted with the SMV and with a microscopic traffic simulation.

Chapter 5 proposes a car-following model called a target time-gap-based velocity update model. Our proposed microscopic traffic flow model is used for inter-vehicle velocity control, which every vehicle exploits in order to refresh the velocity and position for the next time step. The microscopic traffic simulation results are matched well with empirical traffic data. Thus, the target time-gap-based velocity update model is considered a representative car-following model that can accurately mimic typical

driving behavior. The effective domains of the target time gap and the update time interval, which guarantee both collision-free movement of all vehicles and system capacity enhancement compared to the traffic data measured in the field, are examined.

Chapter 6 concludes with a brief summary and remarks about the various strategies for the safety and throughput enhancements for vehicular traffic networks. Moreover, future research works that can be extended from the dissertation are discussed.

Chapter 2

Time-gap-based Traffic Model as a Macroscopic Traffic Flow Model

There have been many studies for modeling vehicular traffic flow using fluid models. However, these previous approaches do not accommodate realistic models for traffic density, flow, and velocity. The existing traffic flow models also fail to uncover the relationships among energy efficiency, capacity, and safety. In this Chapter, we investigate vehicular traffic networks from a system-level perspective. In result, we provide a time-gap-based mathematical traffic flow model for representing vehicular traffic flow on highways. Our proposed model explains the widely known triangular fundamental diagram, in particular by using three primary parameters: the maximum free-flow velocity, a typical safety length of vehicles, and a mean value of the time gap of the traffic data during congested conditions. A time-gap-based traffic flow model is also well validated with empirical traffic data using least squares matching and with previous research outcomes about propagation velocity. In addition, we suggest two distinct analysis techniques to estimate the time gap from the traffic data measured on highways.

2.1 Introduction

Many attempts to specify a relation among traffic flow, density, and speed have been made. A macroscopic traffic model to correlate them forms the so-called fun-

damental diagrams of traffic flow. Greenshields [18] derived a parabolic fundamental diagram between flow and density. Lighthill, Whitham, and Richards [19, 20] used Greenshields's hypothesis and a conservation law of vehicles to provide a concave fundamental diagram, which is called first order LWR model. Newell [21] proposed a triangular flow-density fundamental diagram as a simpler alternative to solve the LWR model. Only two velocities characterize this model: a maximum free-flow velocity in a free-flow regime and a propagation velocity for a congestion area. However, he did not explain the correlation between propagation velocity and driving patterns.

Banks [22] considered the time gap which is the time required to travel the distance between the front end of a vehicle to the back end of its leading vehicle, and showed the relation between the time gap and speed using real traffic data in the USA. He found that during congested times, the average time gap was relatively constant, while it diverges with large deviation during free-flow periods. However, he did not derive a fundamental diagram from the time gap nor an analysis method to estimate the time gap from raw traffic data.

The remainder of this Chapter is organized as follows: In Section 2.2, we present a fundamental traffic pattern to describe the Newell model in congested states, which we call a time-gap-based traffic model. We propose two different methods to estimate the time gap from real traffic data measured by a single-loop and double-loop system in Section 2.3. Section 2.4 shows various analysis results about the relation between the time gap and a triangular fundamental diagram, and validates our proposed time-gap-based traffic model with empirical traffic data.

2.2 Time-gap-based Traffic Model

In this Section, we derive a time-gap-based traffic model. The time gap, τ, is defined as the time required to travel to the bumper of the vehicle in front of a typical vehicle. We assume that highways can be divided into homogeneous sections with similar traffic characteristics and patterns at a local scale.

2.2.1 Time-gap-based triangular fundamental diagram

It has been empirically observed that drivers generally travel to maintain safe distance between themselves and the vehicles immediately in front of them in order to prevent collisions. Because of this distance, there exists a time gap guaranteeing at least a driver's minimum reaction time, which has some average value with slight variation by driver or by region. We also assume that there is a maximum free-flow velocity, v_f, imposed either by physical limitations of the vehicles or by speed limits of the road.

Let L_i denote the safety length of the ith vehicle for $i \in \mathbb{N}$ in feet. The safety length is a summed value of the actual physical length of a vehicle and the positive safety distance, say 0.1 feet, between any two consecutive vehicles on the same lane. In addition, let L denote the average safety length of vehicles in feet. Let ρ, q, and v denote the density, flow, and velocity for the homogeneous section considered. Their units are vehicles per mile (vpm), vehicles per hour (vph), and miles per hour (mph), respectively. Since one mile is 5280 feet, the maximum density ρ_{max} per a lane is $5280/L$ and thus $\rho \leq 5280/L$ for all sections and for all times. For a value of density $\rho \leq 5280/L$, the average distance between the front ends of vehicles is $5280\rho^{-1}$ and thus the average car spacing which is the distance from the front end of a vehicle to the back end of its leading vehicle is $d = 5280\rho^{-1} - L$ in feet. At a constant velocity of v, the time in seconds required to travel the car spacing d is $d/(\bar{c}v)$, where $\bar{c}$ is $5280/3600$ which is feet per second (fps). In order to follow the concept of the time gap τ, we must have $d/(\bar{c}v) \geq \tau$. This becomes

$$v \leq \frac{1}{\bar{c}} \cdot \frac{5280\rho^{-1} - L}{\tau}. \tag{2.1}$$

Since the velocity has the limitation $v \leq v_f$, by (2.1),

$$v \leq \min\left[v_f, \frac{5280\rho^{-1} - L}{\bar{c}\tau}\right].$$

Assuming that every driver travels as fast as possible, it is reasonable to suppose that this inequality is satisfied with equality. Hence,

$$v = \min\left[v_f, \frac{5280\rho^{-1} - L}{\bar{c}\tau}\right]. \tag{2.2}$$

Since the relationship among flow, density, and velocity satisfies with $q = \rho v$, by (2.2),

$$q = \min\left[\rho v_f, \frac{5280 - \rho L}{\bar{c}\tau}\right]. \tag{2.3}$$

This describes a relatively simple triangular fundamental diagram between the flow and density shown in Fig. 2.1. The vehicular traffic system for a considered homogeneous section has the maximum throughput q_{max} at a value of critical density $\rho = \rho_c$ such that

$$\rho_c v_f = \frac{5280 - \rho_c L}{\bar{c}\tau},$$

which becomes

$$\rho_c = \frac{5280}{\bar{c}\tau v_f + L}.$$

The corresponding maximal throughput achieved at the critical density ρ_c is given by

$$q_{max} = \rho_c v_f = \frac{5280 v_f}{\bar{c}\tau v_f + L}.$$

Our proposed time-gap-based triangular fundamental diagram describes two distinct regions; a free-flow regime where the density is less than the critical density and a congestion regime where the density exceeds the critical density. The positive slope in a free-flow regime of a triangular fundamental diagram is the maximum free-flow velocity v_f, while the negative slope in a congestion regime is $-L/(\bar{c}\tau)$ mainly consisting of the time gap τ by (2.3). Hence, we can explain how to derive a triangular fundamental diagram with both the maximum free-flow velocity and time gap. We can easily imagine that the larger the maximum velocity is in a homogeneous section, the greater the throughput is. Additionally, a smaller time gap value means that vehicles are tailgating closer to the vehicles immediately in front of them and thus allows for larger capacity on highways, as long as this tailgating behavior guarantees no crashes. This phenomenon can be also explained by our derivation (2.3); a smaller value of the time gap shows that a negative slope in a congestion regime of our proposed triangular fundamental diagram is steeper, because we fix a value of the safety length L and thus a maximum density ρ_{max} is predetermined as $5280/L$. Hence, a steeper negative slope under a predetermined maximum density causes both larger critical density and higher maximum flow, i.e. larger capacity.

Note that our proposed model describes how the flow varies with the density at a local point. In fact, a triangular fundamental diagram was provided as an idealized traffic approximation by Newell [21], who recognized that this model provides simple algorithms for maximizing throughput using ramp metering. However, even though

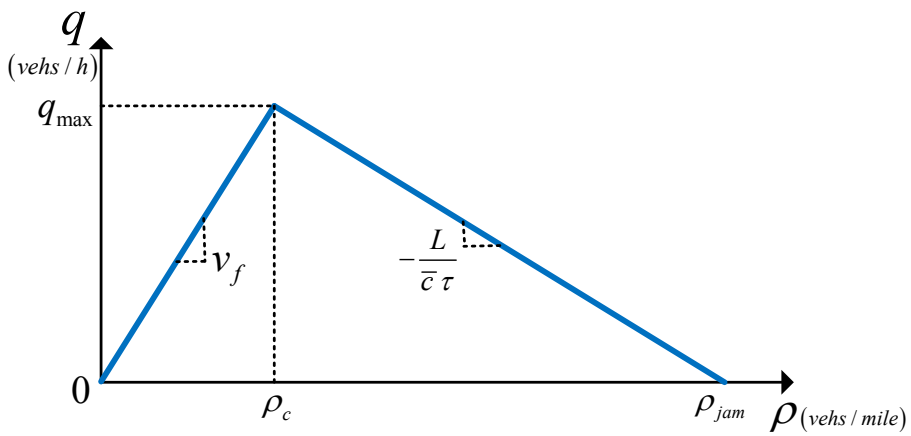

Figure 2.1: Traffic flow on a road.

he presented a car-following model which is consistent with a triangular fundamental diagram, he has not explained it in terms of the traffic parameters v_f, L, and τ, as we have done here.

2.3 Comparative Analysis of Time Gap from Measurement Data

Both the USA and South Korea commonly embed an induction loop detector on highways to collect real traffic data. However, induction loop detectors can measure up to three parameters, so we are required to estimate the time gap from these insufficient traffic observations. The USA uses a single-loop detector, whereas the South Korea employs a dual-loop detector constructed by two consecutive single-loop detectors feet apart. The type of measurement data collected from a single-loop detector is different from that by a dual-loop detector. Hence, we create the distinct methods to derive the time gap from measurement data of these two different detector systems.

2.3.1 Time gap analysis from single-loop detectors

Single-loop detectors deployed in the USA report the number of vehicles passing over a detector and the occupancy counts occupied by passing vehicles per lane every

30 seconds. Because the sampling rate is at 30 Hz, the occupancy counts range from 0 to 900 over the 30 second window. Let $n\left(kT\right)$ denote the number of passing vehicles per lane that is recorded during the kth time frame and reported at time kT, where T is the measurement interval (i.e., 30 seconds in this case). As another available raw data, the value of $o\left(kT\right)$ is the total number of clock ticks, known as the occupancy counts when a vehicle is present over a detector in the kth sampling period. Let l_d denote the length of a detector to be 10 feet. Since $l_d > 0$, this causes the duration of on-time of each pulse to be larger, i.e. a fraction $\left(L + l_d\right)/L$, than if the detector diameter were the ideal length $l_d = 0$. We assume that all vehicles are uniformly distributed for the same measurement period. The ratio that a vehicle is not present at a certain point of the detector, i.e. at its leading side, for the kth measurement period can be estimated as

$$\left(\frac{900 - o\left(kT\right) \cdot \frac{L}{L+l_d}}{900}\right).$$

Hence, the average estimated time gap for the kth measurement interval is

$$\tilde{\tau}\left(kT\right) = \frac{30\left(1 - \left(\frac{o(kT)}{900}\right) \cdot \left(\frac{L}{L+l_d}\right)\right)}{n\left(kT\right)} \tag{2.4}$$

seconds. The flow for the kth measurement period is estimated to be

$$\tilde{q}\left(kT\right) = \frac{n\left(kT\right)}{30} \cdot 3600 = 120n\left(kT\right) \tag{2.5}$$

vph. In addition, we assume that all vehicles travel with the same velocity within the detector diameter. If we assume that the vehicles passing over a detector during the kth interval travel the distance $n\left(kT\right)\left(L + l_d\right)$ feet for the time $\frac{o(kT)}{900}30$ seconds, then the average velocity for the kth interval is

$$\tilde{v}\left(kT\right) = n\left(kT\right)\left(L + l_d\right)\frac{30}{\bar{c}o\left(kT\right)} \tag{2.6}$$

mph. Now, by (2.5), (2.6), and the equation $\rho\left(kT\right) = q\left(kT\right)v\left(kT\right)$ for all $k \in \{0 \cup \mathbb{N}\}$, we can draw a flow-density fundamental diagram and show the estimated time gap value versus the density.

2.3.2 Time gap analysis from double-loop detectors

Even though the cost to deploy a double-loop detector is greater than a single-loop detector, it has added measuring ability. Since a double-loop detector can collect

the travel time data of each vehicle from the first loop to the second loop, it can calculate the speed of an individual vehicle between the two known consecutive loops. However, the speed provided from a dual-loop detector system is not the velocity of an individual vehicle but the average speed of vehicles passing during the kth measurement interval. We suppose that the velocity of every vehicle belonging to the same measurement interval is equal to the average velocity provided by a dual-loop detector. Let v_i denote the velocity of the ith vehicle and $v\left(kT\right)$ denote the average velocity for the kth measurement period. In addition, $\tilde{t}_i$ is the estimated passage time at which the ith vehicle passes over the leading side of the first loop. Then, $v_i = v\left(kT\right)$ for all i such that $\tilde{t}_i \in \left(\left(k-1\right)T, kT\right]$. Let $\tilde{t}_{d(i,i-1)}$ denote the time difference of the estimated passage times between the ith vehicle and $(i-1)$th vehicle. $x_{i-1|(x_i=0)}$ is the position of the $(i-1)$th vehicle when its following ith vehicle just arrives at the leading side of the first loop. In addition, let $\tilde{\tau}_i$ denote the estimated time gap of the ith vehicle at that position. We then assume every vehicle travels with the same velocity after it passes over a detector under the existing steady-state. Then,

$$v_{i-1} \cdot \tilde{t}_{d(i,i-1)} = x_{i-1|(x_i=0)} - L = v_i \cdot \tilde{\tau}_i.$$

This gives the estimated time gap for the ith vehicle

$$\tilde{\tau}_i = \frac{v_{i-1}}{v_i}\tilde{t}_{d(i,i-1)}. \tag{2.7}$$

Hence, since a dual-loop detector provides the number of passing vehicles $n\left(kT\right)$ during the kth measurement interval, by arithmetic average and (2.7), the average estimated time gap for the kth measurement period is

$$\tilde{\tau}\left(kT\right) = \frac{\sum_{i=1}^{n(kT)} \tilde{\tau}_i}{n\left(kT\right)} \tag{2.8}$$

for all i such that $\tilde{t}_i \in \left(\left(k-1\right)T, kT\right]$. Now, by using the measurement data with $n\left(kT\right)$ and $v\left(kT\right)$, we can easily get the density for the kth measurement period and thus show a flow-density fundamental diagram as well as the estimated time gap versus the density.

2.4 Analysis, Results, and Discussions

We have measurements data collected from a single-loop detector in the USA and from a dual-loop detector in the South Korea. One data set was measured on May 10, 2012, at La Jolla Village Dr. of I-805 SB, USA and the other set was collected on Apr. 02, 2012, at PM. 31.91 of Yeongdong Express EB, South Korea. The raw traffic data presented here is processed to remove potentially erroneous observations; some examples of such measurements include the low number of passing vehicles during one measurement interval representing a low density value in spite of erroneously high occupancy counts or an extremely low velocity values. This case occurs when a vehicle temporarily stops over a detector or a loop detector system is malfunctioning.

Fig. 2.2 shows the relationship between the traffic density and time gap estimated by the analysis methods above. Fig. 2.2(a) uses real traffic data measured in the USA, while Fig. 2.2(b) is the result of real traffic data from the South Korea. Each point in the scatter plots gives the estimated density and time gap using the analysis method above which are averaged over 30 seconds. Commonalities are apparent between the two different geographical data sets. It is seen that the time gap varies widely when the density is low. However, it is nearly constant when the density is above a critical density.

We show the average and standard deviation values of the estimated time gap versus density in Fig. 2.3. These time gap and density pairs are placed into bins according to their densities with a granularity of 1 vehicle per mile per lane per bin. The red starred points and blue-circled points represent the average and standard deviation of the estimated time gap for each density bin, respectively. Both the average and standard deviation of the time gap are large in a free-flow regime where the density is less than a critical density, i.e. 26 vpm for the USA data and 31 vpm for the South Korea. We will discuss later the method for how to get the critical density from real traffic data. As the density increases, both the average and standard deviation of the time gap decrease until the density value approaches the critical density. Compared to a free-flow regime, the data shows that the average time gap is fairly predictable as a constant value and that its standard deviation is relatively small in a congestion regime despite the existence of minor variation. The data shows several interesting points where average time gap values are large even under high densities being larger than 170 vpm. The number of

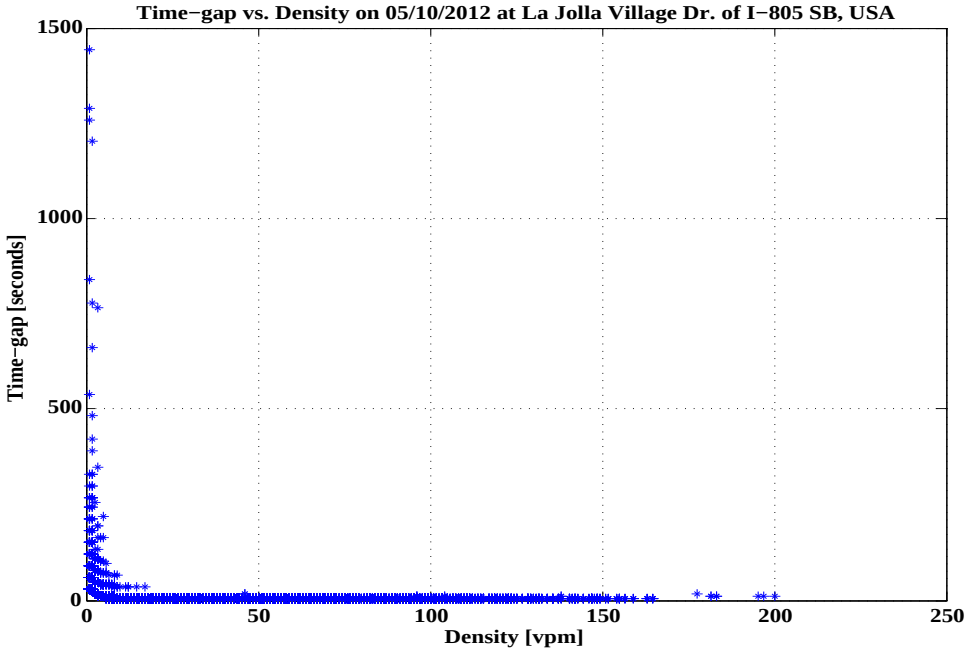

(a)

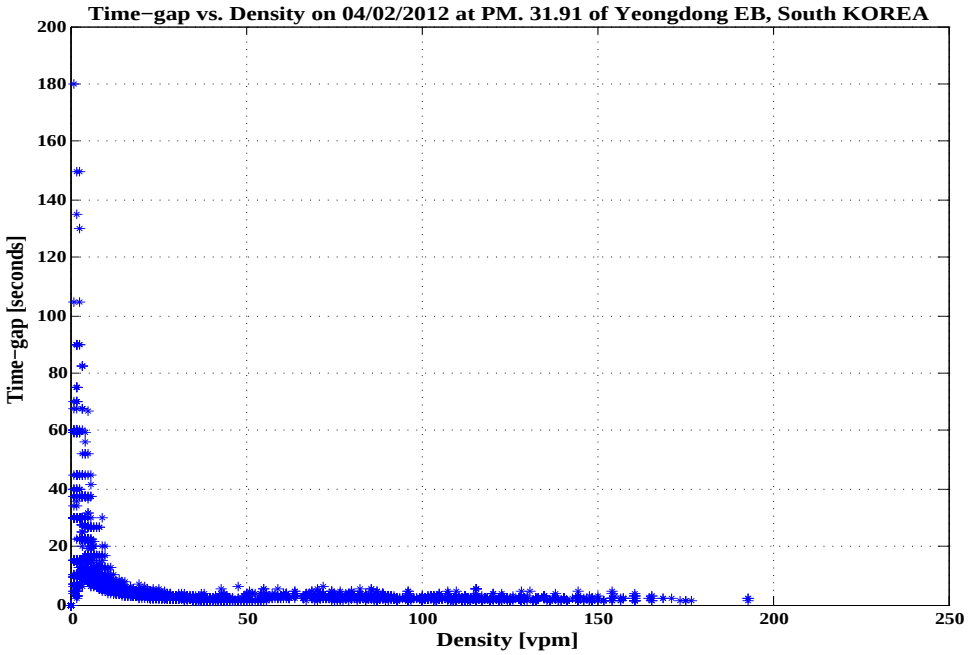

(b)

Figure 2.2: Estimated time gap vs. density. (a) Data measured on 05/10/2012 at La Jolla Village Dr. of I-805 SB, USA. (b) Data measured on 04/02/2012 at PM. 31.01 of Yeongdong EB, South Korea.

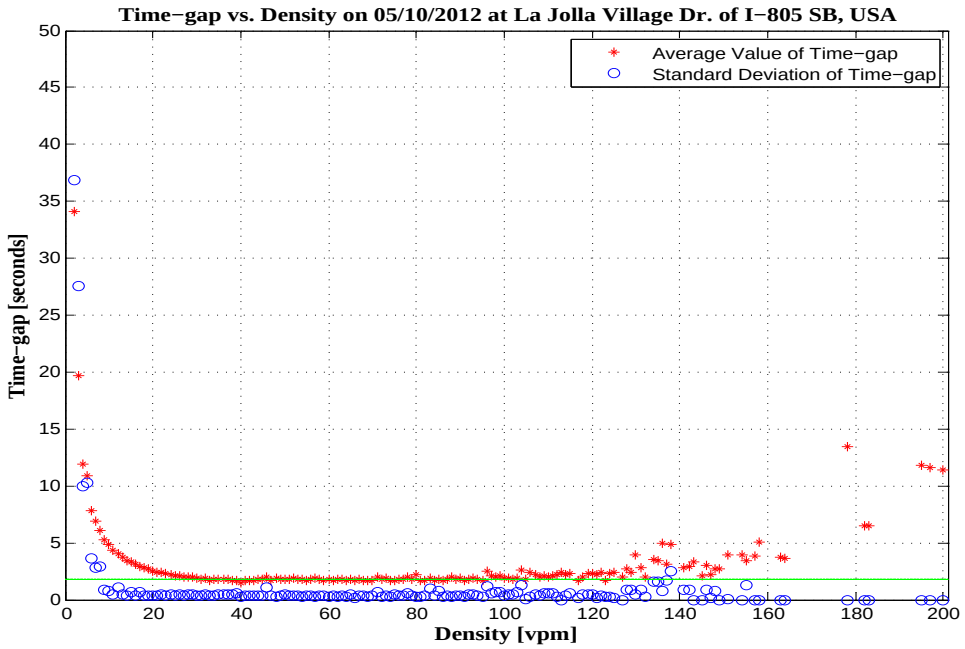

(a)

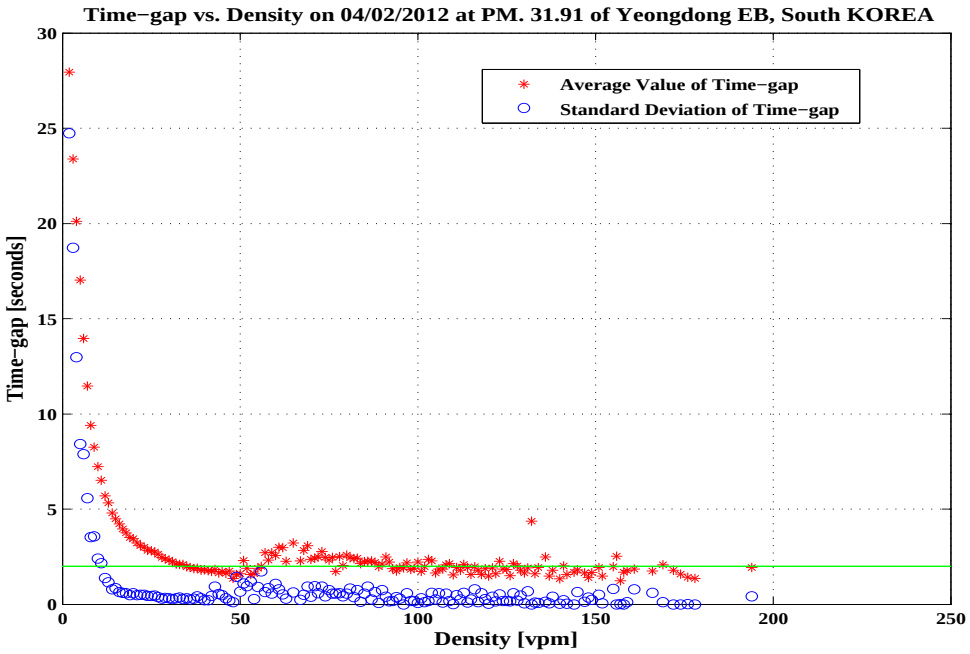

(b)

Figure 2.3: Average and standard deviation of estimated time gap vs. density. (a) Data measured on 05/10/2012 at La Jolla Village Dr. of I-805 SB, USA. (b) Data measured on 04/02/2012 at PM. 31.01 of Yeongdong EB, South Korea.

these interesting points is few, so this infrequent observation might be caused by erroneous instances when a vehicle stops just in front of a loop detector while maintaining a distance to its leading vehicle that does not adhere to the normal traffic patterns of following closely even under heavy congestion. A loop detector system error is also a possibility.

The green line in the above plots shows the arithmetic mean value of the estimated time gap for all measurement data points included in a congestion regime. The mean time gap in a congestion region are about $\tau = 1.78$ seconds in the USA and $\tau = 2.00$ seconds in the South Korea. It is obvious that drivers travel maintaining the positive time gap to their leading vehicles to avoid collision, which is related to the brake reaction time. The brake reaction time is defined as the amount of time required to apply the brakes upon recognition of danger. Many research studies about driver reaction times have been conducted. Green [23] showed that a driver's reaction time to a traffic event increases with the degree of surprise to the driver. He provided that the average reaction time to break for different situations is 0.75 seconds for an expected event, 1.20 to 1.35 seconds for an unexpected event such as brake lights of the lead vehicle, and 1.50 seconds for a sudden intrusion event. Mehmood [24] used a driving simulator to estimate the mean reaction time for the following three scenarios. The mean reaction time of a driver who is avoiding imminent collision is 0.92 to 1.94 seconds when he tries to decelerate at a normal deceleration rate, while the reaction time range decreases dramatically from 0.66 to 1.04 seconds when the driver decreases the velocity with a maximum deceleration rate. In addition, it is 0.58 to 0.94 seconds against a stationary leading vehicle. Taoka discussed a representative value of the reaction time for various drivers based on experimental investigations [25, 26, 27, 28]. According to his estimates of the break reaction time, the median range is from 1.07 to 1.14 seconds. Overall, we can observe that the mean value of the driver's reaction time is less than or almost equal to the average time gap defined in a congestion regime. This observation provides the insight that drivers subconsciously drive with their own time gap being larger than their reaction time so as to avoid a rear-end collision.

Fig. 2.4 shows the flow and estimated density pairs, and the corresponding fundamental diagram using the same data sets from the USA and South Korea. Each circle

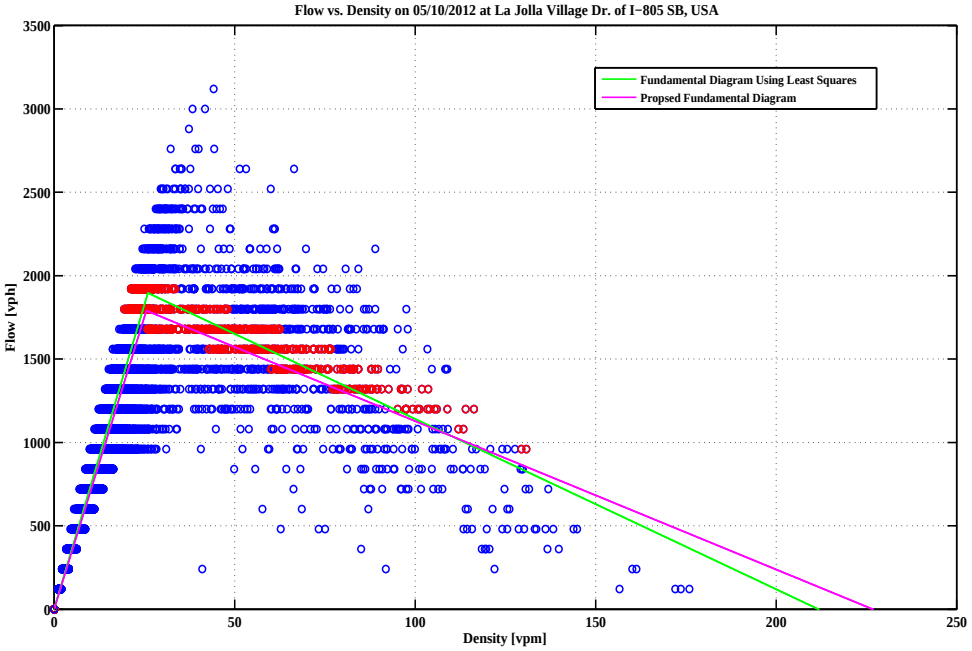

(a)

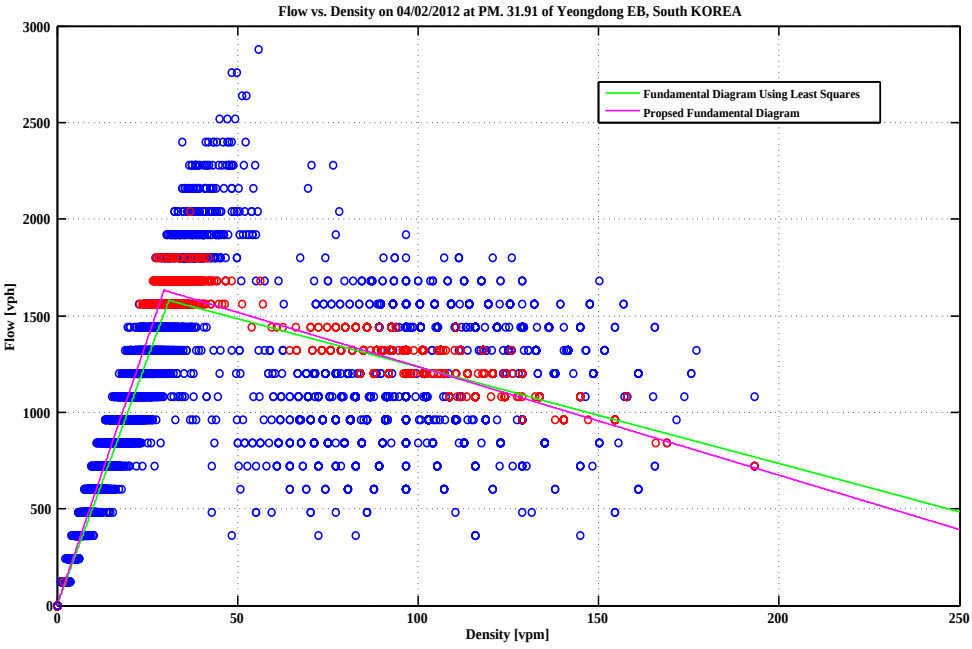

(b)

Figure 2.4: Measurement data of flow vs. density and a time-gap-based traffic model. (a) Data measured on 05/10/2012 at La Jolla Village Dr. of I-805 SB, USA. (b) Data measured on 04/02/2012 at PM. 31.01 of Yeongdong EB, South Korea.

in the scatter plots provides the flow and estimated density averaged over 30 seconds. For reference, we draw a green line as a triangular flow-density fundamental diagram by regression analysis with least squares from all data points. We can derive this line by adjusting three important parameters: the critical density, and the positive and negative slopes of a triangular fundamental diagram so as to best fit these flow and estimated density sets. These parameters adjusted by least squares are listed in Table 2.1. In the USA, the best fitted critical density, positive slope, and negative slope are 26 vpm, 72.95 mph, and -10.21 mph, respectively. The South Korea exhibits larger critical density and gentler slopes than the USA does. Since the speed limit of the measurement area in the South Korea is about 50 mph which is less than that in the USA with 65 mph, it is expected that the South Korea has a more gradual positive slope in a free-flow regime than the USA does.

A magenta line in Fig. 2.4 represents our proposed time-gap-based traffic model drawn by (2.3). We need to use three parameters to draw it, which are the maximum velocity, typical safety length of a vehicle, and the mean value of a time gap defined in a congestion regime. We added 5 mph to the pre-defined speed limit, because people normally travel with slightly higher speed than the regulated speed where there is no traffic. Therefore, we set a maximum velocity, v_f, as 70 and 55 mph for the USA and South Korea, respectively. We can get the best fit critical density by least squares from all data points. We then calculate the mean value of the time gap τ of the data points for which the density values are larger than the best fitted critical density, that is to say in a congestion regime. The calculated mean values of the time gap are approximately $\tau = 1.78$ seconds for the USA and $\tau = 2.00$ seconds for the South Korea. Finally, we can draw our proposed time-gap-based flow-density triangular fundamental diagram as shown in Fig. 2.4.

By comparing the green and magenta lines in Fig. 2.4, we can observe that our proposed time-gap-based traffic model almost corresponds to the best fit triangular fundamental diagram by least squares. Therefore, not only does our proposed time-gap-based traffic model explain well a triangular fundamental diagram provided by Newell [21] with both a maximum velocity and a mean value of the time gap defined in a congestion regime by (2.3), but also it is a good and simple representative model for

vehicular traffic flow.

There is additional indirect evidence of the validity of the time-gap-based traffic model for the fundamental diagram. When the traffic density changes, a shock wave is launched and travels against the direction of the traffic flow at an almost constant speed, which is called the propagation velocity. This propagation velocity, which is independent of the density in a congestion regime, has been studied for many years [29, 30, 31]. A positive propagation velocity is used throughout Chapter 2. Mika [29] showed that propagation velocity of stop-and-go traffic waves is around 6.22 to 12.42 mph. Windover [30] used real traffic measurement data from I-880 NB, in Oakland, California, which is identified as especially congested and showed that the propagation velocity was nearly constant with 10.56 to 12.43 mph over the homogeneous section. Muñoz and Zielke [31, 32] applied cross correlation of cumulative arrivals between two consecutive detector stations and provided that the shock wave propagates in reverse flow direction at speeds of about 11.81 to 12.43 mph. Smilowitz [33] used the Lighthill-Whitham-Richards (LWR) model [19, 20] to derive the wave velocity and showed that the wave velocities propagating upstream on a single lane of homogeneous highway section were 10.69 and 11.68 mph. Schönhof [34] investigated the real traffic data measured in Germany with many congested traffic states and found the propagation velocity was approximately 9.32 mph.

Thus, this previous research shows that the propagation velocity is consistent with our proposed time-gap-based traffic model, and in fact by (2.3), this time-gap-based traffic model predicts that the constant propagation velocity, v_p, is given by the simple formula

$$v_p = \frac{L}{\bar{c}\tau}.$$

Using $L = 22$ feet and $\tau = 1.78$ seconds, which is a mean value of the time gap estimated in the USA, the predicted propagation velocity is $v_p = 10.21$ mph as listed in Table 2.1. We can observe that this value is in range of the propagation velocity provided by the above papers and thus the propagation velocity derived by our proposed time-gap-based traffic model is consistent with earlier studies. Indeed, we believe that the characteristic properties in congested traffic can be largely explained using the model that we provide.

Table 2.1: Adjusted parameters by least squares.

Nation	Critical Density (vpm)	Positive Slope (mph) (Free-flow Velocity)	Negative Slope (mph) (Propagation Velocity)
USA	26	72.95	−10.21
South Korea	31	50.97	−5.00

2.5 Summary

We provided a time-gap-based traffic model, which explains well a triangular flow-density fundamental diagram proposed by Newell, in particular by using three principal parameters: maximum velocity, a typical safety length of vehicles, and a mean value of the time gap of traffic data under congested conditions. Also, we proposed two different analysis methods to estimate the time gap from real traffic data measured by a single-loop and a dual-loop detector system. We found that the average and standard deviation of the time gap vary widely when the traffic density is low, while its average is nearly constant and its standard deviation is small in a congestion regime. This observation agrees with our time-gap-based traffic model presented here, which shows that a mean value of the time gap is a major factor to characterize vehicular traffic flow, especially where the traffic is congested. A further meaningful observation is that a mean value of the time gap defined in a congestion area is larger than or almost equal to the average driver reaction time. This provides the insight that drivers unconsciously travel with their own time gap being larger than their reaction time so as to avoid a real-end collision towards their leading vehicles.

In conclusion, we have shown the validity of our proposed time-gap-based traffic model. The time-gap-based traffic model represented with the three parameters above almost corresponds with the best fitting triangular fundamental diagram by least squares to the measured traffic. Also, the propagation velocity derived by a mean value of the time gap is consistent with the propagation velocity studied for many years. Therefore, our proposed time-gap-based traffic model is a good and simple representative model for vehicular traffic flow.

Chapter Acknowledgments

Chapter 2, in full, is a reorganized version of the following publication in the Proceedings of the IEEE 79th Vehicular Technology Conference, 2014 Spring. Seokheon Cho, Anush Badii, Rene L. Cruz, and Ramesh R. Rao. "Time-gap based traffic model for vehicular traffic flow," in Proceedings of the IEEE 79th Vehicular Technology Conference (VTC Spring), pp. 1-5, May, 2014.

Chapter 3

Optimal Coordinated Ramp-metering Control

Numerous studies have examined ramp-metering control to relieve highway congestion. Unlike previous research, this Chapter presents two different optimization problems for achieving the maximum average system capacity over a highway corridor, using both a time-gap-based traffic model describing traffic flow and the limited traffic data measured by existing field facilities. Our proposed algorithms are coordinated ramp-metering strategies controlling the metered rates at system-wide entrance ramps. The origin-utilization relationship is taken into consideration in providing the mathematical derivation for the steady-state optimization problem. This scheme regulates on-ramp flows so as to keep traffic densities along the system below their critical densities. To prevent an increase in adjacent street traffic, which might be caused by this scheme, a time-variant linear programming problem is provided with both on-ramp queue control and traffic flow estimation. Comparative simulation results for two optimization problems are presented.

3.1 Introduction

Ramp-metering control has been recognized as an effective method of relieving congestion on highways by regulating the inflow from on-ramps to the highway mainline. Chen [35] used Greenshields's model to investigate on-ramp control for travel-rate

maximization over the traffic network. He assumed that traffic origin-destination information is available from the vehicular traffic network. However, this is not based on real-time and empirical measurements from existing detectors in the traffic networks. Realistically, it is desirable to control on-ramp flow using the limited traffic observations measured from the existing traffic network such as the mainline flow, average speed on the mainline, on-ramp flow, demand flow, and off-ramp flow during each time interval. In addition, Chen calculated the mainline flow of each section of the traffic network by summing up the mainline flow at the upstream-most section and on-ramp flows of its upstream sections. Chen calculated this under the restrictive assumption that traffic on all sections of the traffic network is in a free-flow regime; this can only be accomplished by letting fewer vehicles enter highways, as a decrease in vehicle entry onto highways causes unexpected interference with neighboring arterial roads. In order to avoid such interference, the system designer has no choice but to permit more vehicles to enter the highway mainline in spite of the mainline congestion. Hence, it is necessary to estimate traffic density and flow using a traffic model that specifically takes into account congested traffic states.

The ALINEA method proposed by Papageorgiou [6, 7, 36] is a traffic responsive ramp-metering control based on real-time measurements that seek to attain maximum capacity at the merge area of the on-ramp. This algorithm is simple and easily implemented, and it has been shown to decrease the total time spent (TTS) in traffic and thus to relieve congestion at a local scale. However, a significant drawback of the ALINEA is that it is not a coordinated ramp-metering system but is instead a local feedback control. Hence, we need to provide optimal ramp-metering control to improve system-level capacity.

Macroscopic traffic models to specify the relationship among traffic flow, density, and velocity form the so-called fundamental diagrams. Greenshields [18] derived a parabolic fundamental diagram between traffic flow and density with the assumption of a linear velocity-density relationship under uninterrupted traffic flow conditions. Lighthill, Whitham, and Richards (LWR) [19, 20] used Greenshields's hypothesis and a non-linear conservation law of vehicles to provide a concave fundamental diagram, which is called the first-order LWR model. Newell [21] proposed a triangular flow-

density fundamental diagram as a simpler alternative to the LWR model. A time-gap-based traffic model verified by empirical traffic data explains the Newell model with both a mean value of the time gap and a typical safety length of vehicles in a congestion regime [37].

In this Chapter, optimal coordinated ramp-metering control for maximizing average system-level throughput using a time-gap-based traffic model will be studied. In Section 3.2, we present vehicular traffic network assumptions and a time-gap-based traffic model used for estimating traffic flow and achieving optimal coordinated ramp-metering control. In Section 3.3, we propose a steady-state optimal control that regulates on-ramp flow rates at system-wide entrance ramps so as to keep traffic densities along the system below their critical densities. The origin-utilization relationship is introduced in providing the steady-state optimization problem. However, it causes on-ramp queue spillover onto adjacent local streets. In contrast, a time-variant optimal problem is derived considering an on-ramp queue control in order to diminish unexpected interference with neighboring arterial roads in Section 3.4. Section 3.5 shows the comparative simulation results of these optimization problems using a macroscopic traffic simulator.

3.2 Vehicular Traffic Network

In this Section, we describe a vehicular traffic network and specify the time-gap-based fundamental diagram used for achieving the maximum average system capacity for vehicular traffic networks.

3.2.1 Vehicular traffic network assumptions

Here, we first consider the vehicular traffic network shown in Fig. 3.1. We assume that there are I entrance ramps, J exit ramps, and M sections, where I, J, and M are bounded integer values. Let T be the time interval (e.g. 30 seconds) used for all controllers to measure traffic data and to apply the newly calculated metered rate along the highway corridor. Let $\rho\left(kT, x\right)$, $q\left(kT, x\right)$, and $v\left(kT, x\right)$ denote the average traffic density, flow, and velocity per lane that are reported at time kT and at point x with the traffic data measured during the kth time frame, where k is a non-negative integer. Their

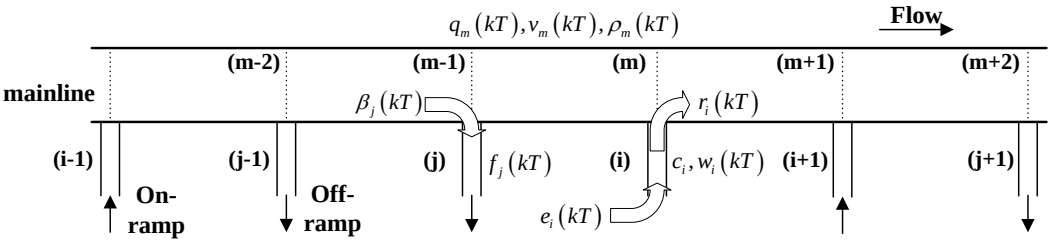

Figure 3.1: Vehicular traffic network.

units are vehicles per mile (vpm), vehicles per hour (vph), and miles per hour (mph), respectively. We suppose that highways can be divided into homogeneous sections with similar traffic characteristics and patterns. Let $\rho_m(kT)$, $q_m(kT)$, and $v_m(kT)$ denote the average traffic density, flow, and velocity per lane reported at time kT over the mth section for $m \in [1, M]$. Hence, by the homogeneity of section, $\rho(kT, x) = \rho_m(kT)$, $q(kT, x) = q_m(kT)$, and $v(kT, x) = v_m(kT)$ for all points x belonging to the mth section and for every time kT.

Let $e_i(kT)$ denote the demand flow in vph entering the ith on-ramp queue detected during the kth time frame for $i \in [1, I]$. Let $w_i(kT)$ denote the number of vehicles queued on the ith on-ramp queue at time kT. That is, $w_i(kT)$ is the queue length of the ith on-ramp queue. Let $r_i(kT)$ denote the metered rate of the ith on-ramp queue in vph, which is applied for the kth time frame.

Let $f_j(kT)$ denote the off-ramp flow to the jth exit ramp measured during the kth time frame. Let $\beta_j(kT)$ denote the split ratio, which is the ratio of the number of vehicles exiting to the jth off-ramp over the number of vehicles traveling on the upstream section immediately before the jth off-ramp during the kth time frame, or which is the ratio of the jth off-ramp flow to the total summed flow of the jth off-ramp flow and the mainline flow of the downstream section just after the jth off-ramp. This gives $\beta_j(kT) \in [0, 1]$ for all $j \in [1, J]$ with $\beta_0(kT) = 0$. Let $\tilde{m}^j$ denote the downstream section index immediately after the jth exit ramp. Then, $\beta_j(kT) = f_j(kT) / (f_j(kT) + q_{\tilde{m}^j}(kT))$ for all $j \in [1, J]$ and for all k.

3.2.2 Time-gap-based traffic model

The time-gap-based traffic model shown in Fig. 3.2 explains the triangular fundamental diagram proposed by Newell [21], particularly by using three principal parameters: the maximum free-flow velocity in a free-flow region, a typical safety length of vehicles, and a mean value of the time gap of traffic data under congested conditions [37]. Since this time-gap-based traffic model is not only supported by empirical traffic measurements but is also simple, we will use this model for estimating traffic flow and providing optimal coordinated ramp-metering control for achieving maximum system throughput. The traffic flow-density equation of a time-gap-based traffic model at time kT and for the mth section is given by

$$q_m\left(kT\right) = \min\left\{v_{f,m}\rho_m\left(kT\right), \frac{5280 - L\rho_m\left(kT\right)}{\bar{c}\tau_m}\right\}, \tag{3.1}$$

where $v_{f,m}$ is the maximum free-flow velocity for the mth section in mph, L is a typical safety length of vehicles in feet, τ_m is the mean value of the time gap defined in a congestion regime of the mth section in seconds, and $\bar{c}$ is a constant with $5280/3600$. The vehicular traffic network for the considered mth homogeneous section has the maximum capacity $q_{max,m}$ at a value of the critical density $\rho_m\left(kT\right) = \rho_{c,m}$ such that

$$v_{f,m}\rho_{c,m} = \frac{5280 - L\rho_{c,m}}{\bar{c}\tau_m},$$

which becomes

$$\rho_{c,m} = \frac{5280}{\bar{c}\tau_m v_{f,m} + L}. \tag{3.2}$$

The corresponding maximal throughput achieved at the critical density $\rho_{c,m}$ is given by

$$q_{max,m} = v_{f,m}\rho_{c,m} = \frac{5280 v_{f,m}}{\bar{c}\tau_m v_{f,m} + L} \tag{3.3}$$

and also $0 \leq q_m\left(kT\right) \leq q_{max,m}$ holds for all times kT and for all $m \in [1, M]$. We define the same value of the jam density for all $m \in [1, M]$ as $\rho_{jam} = 5280/L$. Note that $v_{f,m}$, τ_m, $\rho_{c,m}$, and $q_{max,m}$ are time-invariant.

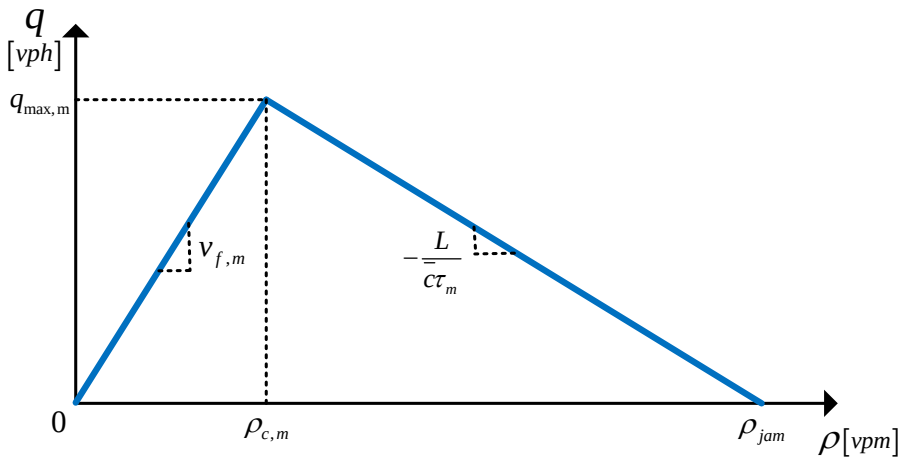

Figure 3.2: Time-gap-based traffic model.

3.3 Steady-state Optimization Problem for Maximum Capacity

In this Section, we consider a method of achieving ramp-metering control using steady-state optimization without on-ramp queue control. On-ramp queue management is used to prevent on-ramp queue spillover onto neighboring arterial streets by increasing ramp-metering rate [38, 39]. This strategy can have an adverse effect on highway mainline traffic and thus diminish the benefits of ramp-meter control. When the vehicular traffic network reaches the steady-state, traffic density of each homogeneous section is constant with respect to time kT. Likewise, traffic flow and velocity also become time-invariant in the steady-state. Thus, by the steady-state conditions, $\rho_m(kT) = \rho_m$, $q_m(kT) = q_m$, $v_m(kT) = v_m$, $r_i(kT) = r_i$, $f_j(kT) = f_j$, and $\beta_j(kT) = \beta_j$ for all $m \in [1, M]$, $i \in [1, I]$, $j \in [1, J]$ and for all times kT.

3.3.1 Traffic flow estimation

We consider that the last indices of the entrance ramp and exit ramp located just before the mth section for some $m \in [1, M]$ are $\bar{i}^m$ and $\bar{j}^m$, respectively. Then, $m = \bar{i}^m + \bar{j}^m$ for all $m \in [1, M]$. Let $\tilde{j}^{i,m}$ and $\bar{j}^{i,m}$ denote the indices of the upstream-most and downstream-most exit ramps located between the ith entrance ramp and mth

homogeneous section, respectively. We assume that vehicles traveling on the section located just before each off-ramp exit from a highway with uniform distribution, no matter which upstream entrance ramps they entered. By this hypothesis, the origin-utilization equation for traffic flow of the mth section is given by

$$q_m = \frac{1}{n_m} \sum_{i=1}^{\bar{i}^m} \left[\prod_{j=\tilde{j}^{i,m}}^{\bar{j}^{i,m}} (1 - \beta_j) \right] r_i, \tag{3.4}$$

where n_m is the number of lanes of the mth section. If a specific exit ramp cannot be defined for $\tilde{j}^{i,m}$, i.e. if there does not exist an exit ramp between the ith entrance ramp and mth section, then $\tilde{j}^{i,m} = 0$ and thus $\bar{j}^{i,m} = 0$.

3.3.2 Optimization problem

The main purpose of a ramp-metering algorithm is to control the metering rate at all entrance ramps and thus to relieve congestion on highways. The most important evaluation criteria for a ramp-metering strategy are total travel time (TTT) on the mainline, total waiting time (TWT) at the entrance ramp, and total time spent (TTS), which is the sum of TTT and TWT. That is, in order to improve system-wide total time spent, it is desirable to utilize the limited throughput of all sections as close as possible to their maximum capacity, $q_{max,m}$, for all $m \in [1, M]$. Hence, we pursue the steady-state optimization problem to maximize average system throughput on highways. In a steady-state, the average system throughput per lane along the highway corridor, J_C, is given by

$$J_C = \frac{1}{D} \sum_{m=1}^{M} q_m d_m, \tag{3.5}$$

where D is the total length of the vehicular traffic network and d_m is the length of the mth section. Substituting (3.4) into (3.5),

$$J_C = \frac{1}{D} \sum_{m=1}^{M} \left\{ \sum_{i=1}^{\bar{i}^m} \left[\prod_{j=\tilde{j}^{i,m}}^{\bar{j}^{i,m}} (1 - \beta_j) \right] r_i \right\} \frac{d_m}{n_m} = \frac{1}{D} \vec{r}^{\top} \mathbf{B} \vec{a},$$

where $\vec{a}$ is the $M \times 1$ vector whose element is the length over the number of lanes of the mth section (i.e. $a_m = d_m / n_m$ for all $m \in [1, M]$), $\vec{r}$ is the $I \times 1$ vector whose element

is the metered rate at the ith entrance ramp, $\mathbf{B}$ is the $I \times M$ origin-utilization matrix, and $(\cdot)^\top$ is the transpose of the vector or matrix. The elements of the origin-utilization matrix $\mathbf{B}$ are $\beta_{(i,m)}$, which refer to the proportion of vehicles entering from the ith on-ramp and traveling on the mth section, where $0 \leq \beta_{(i,m)} \leq 1$ for all $i \in [1, I]$ and all $m \in [1, M]$. If there exists $\hat{m}_i$ with $\hat{m}_i > i$ for each $i \in [1, I]$ such that

$$\begin{cases} \beta_{(i,m)} = 0 & \text{for all } \ m \in [1, \hat{m}_i), \\ \beta_{(i,m)} = 1 & \text{for } \ m = \hat{m}_i, \\ 0 \leq \beta_{(i,m)} \leq 1 & \text{for all } \ m \in (\hat{m}_i, M], \end{cases}$$

then the corresponding matrix $\mathbf{B}$ is called an upper unit trapezoidal matrix. Note that the original-utilization matrix $\mathbf{B}$ is an upper unit trapezoidal matrix, thus reducing the computational complexity needed to determine the average system throughput, J_C.

To utilize the limited throughput of the system fully, we need to prevent the sharp drop-off of traffic flow that occurs when traffic density is above critical density, which eventually causes serious congestion. Hence, it is desirable to control the metered rates at system-wide entrance ramps so as to keep traffic densities along the system below their critical densities; that is, $0 \leq \rho_m \leq \rho_{c,m}$ for all $m \in [1, M]$. By this optimization strategy and (3.2), for all $m \in [1, M]$,

$$0 \leq \rho_m \leq \frac{5280}{\bar{c}\tau_m v_{f,m} + L}. \tag{3.6}$$

By (3.1), for all $m \in [1, M]$,

$$\frac{q_m}{v_{f,m}} \leq \rho_m \leq \frac{5280 - \bar{c}\tau_m q_m}{L}. \tag{3.7}$$

Hence, by (3.6) and (3.7), the optimal traffic density range for the mth section is

$$\frac{q_m}{v_{f,m}} \leq \rho_m \leq \frac{5280}{\bar{c}\tau_m v_{f,m} + L}. \tag{3.8}$$

Therefore, by (3.3) and (3.8) the optimization problem for achieving maximum average system throughput, J_C, along the vehicular traffic network becomes

$$\max J_C = \frac{1}{D} \sum_{i=1}^{I} \left\{ \sum_{m=\tilde{m}^i}^{M} \left[\prod_{j=\tilde{j}^{i,m}}^{\bar{j}^{i,m}} (1 - \beta_j) \right] a_m \right\} r_i = \frac{1}{D} \vec{a}^\top \mathbf{B}^\top \vec{r}, \tag{3.9}$$

subject to, for all $m \in [1, M]$,

$$\begin{cases} 0 \leq \frac{1}{n_m} \sum_{i=1}^{\bar{i}^m} \left[\prod_{j=\tilde{j}^{i,m}}^{\bar{j}^{i,m}} (1 - \beta_j) \right] r_i \leq \frac{5280 v_{f,m}}{\bar{c}\tau_m v_{f,m} + L}, \\ \frac{1}{n_m v_{f,m}} \sum_{i=1}^{\bar{i}^m} \left[\prod_{j=\tilde{j}^{i,m}}^{\bar{j}^{i,m}} (1 - \beta_j) \right] r_i \leq \rho_m \leq \frac{5280}{\bar{c}\tau_m v_{f,m} + L}, \end{cases}$$

where $\tilde{k}^i$ is the downstream section index immediately after the ith entrance ramp.

3.4 Time-variant Optimization Problem for Maximum Capacity with On-ramp Queue Control

The optimization problem (3.9) for achieving maximum average system throughput in the steady-state described in Section 3.3 is valid as long as the traffic of the mth section is in a free-flow regime. Although this scheme shows the maximum system capacity, it causes additional long-term congestion on entrance ramps and unexpected interference with adjacent street traffic. In order to prevent this undesirable effect of ramp-metering control, we need to consider an on-ramp queue management strategy. However, if the high demand flow arrives at on-ramps continually, the activation of on-ramp queue control unintentionally leads to the inevitable congestion on the highway mainline. In this case, if the traffic flow summed up with the inflows from upstream on-ramp queues of the mth section is larger than the corresponding maximum flow, $q_{max,m}$, then the equation (3.9) cannot be used. Hence, we introduce a traffic flow estimation method using both a fundamental diagram such as the time-gap-based traffic model described in previous Section and the vehicle conservation law. The conservation law of vehicles describes a physical constraint that the change in the number of vehicles on a highway section is equivalent to the net difference between the inflowing number of vehicles and the outflowing number of vehicles to or from the corresponding section.

3.4.1 On-ramp queue control

Let $\hat{c}_i$ denote the maximum permissible queue length of the ith entrance ramp, which is strictly less than the ith entrance ramp's capacity, c_i, with $\hat{c}_i < c_i$. Let r_{min} denote the minimum on-ramp discharge rate, which is the same constant for all entrance

ramps $i \in [1, I]$, i.e. 240 vph. Some minimum on-ramp discharge rate must be supported because drivers want to stay on the entrance ramp for as short a time as possible. Thus, for all $i \in [1, I]$ and for every time kT,

$$r_{min} \leq r_i\left(kT\right). \tag{3.10}$$

Since the difference between the demand flow and metered rate should be less than or equal to the admissible on-ramp queue length, for all $i \in [1, I]$,

$$\left(e_i\left(kT\right) - r_i\left(\left(k+1\right)T\right)\right) \leq \frac{\left(\hat{c}_i - w_i\left(kT\right)\right)}{\hat{T}}, \tag{3.11}$$

where $\hat{T} = T/3600$. Also, since the metered rate should be less than or equal to the maximum possible inflow rate considering the demand flow and current on-ramp queue length, for all $i \in [1, I]$,

$$r_i\left(\left(k+1\right)T\right) \leq e_i\left(kT\right) + \frac{w_i\left(kT\right)}{\hat{T}}. \tag{3.12}$$

By (3.10), (3.11), and (3.12), and by letting $\eta_i\left(kT\right) = e_i\left(kT\right) + \frac{w_i(kT)}{\hat{T}}$, on-ramp queue control is satisfied with

$$\max\left\{\min\left\{r_{min}, \eta_i\left(kT\right)\right\}, \eta_i\left(kT\right) - \frac{\hat{c}_i}{\hat{T}}\right\} \leq r_i\left(\left(k+1\right)T\right) \leq \eta_i\left(kT\right) \tag{3.13}$$

for all $i \in [1, I]$ and for all k.

3.4.2 Traffic flow estimation

Homogeneous sections comprising vehicular traffic networks are attached to either the entrance ramp or exit ramp. In the case of a homogeneous section with an entrance ramp, there exists disturbance by the vehicles entering from the on-ramp queue. Hence, based on the vehicle conservation law, traffic density of the mth section with an entrance ramp at the next time $\left(k+1\right)T$ can be estimated by

$$\begin{aligned}\rho_m\left(kT\right) = \rho_m\left(\left(k-1\right)T\right) + \hat{T}\big[&n_{m-1}q_{m-1}\left(\left(k-1\right)T\right) - n_m q_m\left(\left(k-1\right)T\right) \\ &+ r_{\bar{i}^m}\left(\left(k-1\right)T\right)\big]\frac{1}{n_m d_m}.\end{aligned} \tag{3.14}$$

Unlike a homogeneous section with an entrance ramp, since input disturbance does not exist in a section attached to an exit ramp, the estimated traffic density is linearly dependent on that of its upstream section as

$$\rho_m\left(kT\right) = \left(1 - \beta_{\bar{j}^m}\left(\left(k-1\right)T\right)\right)\rho_{m-1}\left(\left(k-1\right)T\right). \tag{3.15}$$

We can determine the estimated flow of the mth section at time kT by substituting (3.14) or (3.15) in (3.1).

3.4.3 Optimization problem

The time-variant optimization problem to find the metered rate for each entrance ramp for achieving the maximum average system capacity per lane is a linear programming problem of choosing $r_i\left(kT\right)$ every time kT as, by (3.1), (3.3), and (3.13),

$$\max J_C\left(kT\right) = \frac{1}{D}\sum_{m=1}^{M} q_m\left(kT\right)d_m, \tag{3.16}$$

subjected to, for all $m \in [1, M]$,

$$\begin{cases} 0 \leq q_m\left(kT\right) \leq \frac{5280 v_{f,m}}{\bar{c}\tau_m v_{f,m} + L}, \\ \max\left\{\min\left\{r_{min}, \eta_{\bar{i}^m}\left(\left(k-1\right)T\right)\right\}, \eta_{\bar{i}^m}\left(\left(k-1\right)T\right) - \frac{\hat{c}_{\bar{i}^m}}{\hat{T}}\right\} \\ \qquad\qquad \leq r_{\bar{i}^m}\left(kT\right) \leq \eta_{\bar{i}^m}\left(\left(k-1\right)T\right), \\ 0 \leq \rho_m\left(kT\right) \leq \rho_{jam}, \end{cases}$$

where $\eta_{\bar{i}^m}\left(\left(k-1\right)T\right) = e_{\bar{i}^m}\left(\left(k-1\right)T\right) + \frac{w_{\bar{i}^m}\left(\left(k-1\right)T\right)}{\hat{T}}$ and $q_m\left(kT\right)$ is given by either (3.14) or (3.15) depending on the type of the section.

3.5 Analysis, Results, and Discussions

In this Section, we present the comparative simulation results of the average system capacity and velocity on a highway corridor with four different ramp-metering strategies: with no ramp-metering control, ALINEA, a steady-state optimization scheme, and a time-variant optimization method.

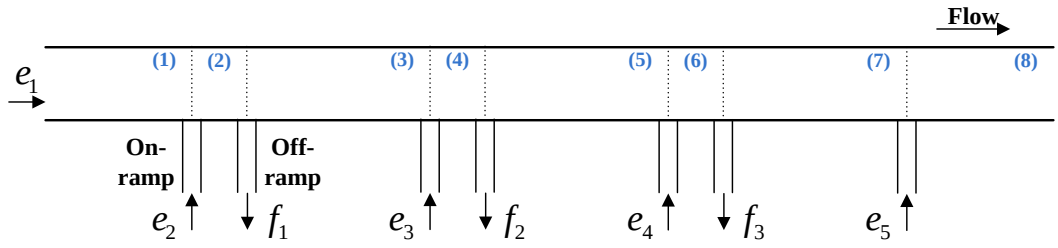

Figure 3.3: Highway corridor for simulation example.

3.5.1 Simulation scenario

Fig. 3.3 specifies a highway corridor that we consider for simulation; it consists of $M = 8$ sections, $I = 5$ entrance ramps including the first section that is the most upstream toward the mainline, and $J = 3$ exit ramps. The second section attaches to an entrance ramp and then each section contains, by turn, an entrance ramp and an exit ramp. Each section has $n_m = 4$ lanes for all $m \in [1, M]$. The length of section attached to an entrance ramp and an exit ramp is 1 and 0.1 miles, respectively. We set the average safety length of vehicles to $L = 22$ feet, maximum free-flow velocity to $v_{f,m} = 70$ mph, and mean value of the time gap under congested status to $\tau_m = 1.78$ seconds for all $m \in [1, M]$ as typically measured in the United States [37]. From this, we can determine the critical density $\rho_{c,m}$, jam density ρ_{jam}, and maximum flow $q_{max,m}$ for each section using a time-gap-based traffic model. We suppose that each on-ramp queue has the same permissible queue capacity of $\hat{c}_i = 200$ for all $i \in [1, I]$ and that the split ratio for each off-ramp is constant with $\beta_j(kT) = 0.2$ for all $j \in [1, J]$ and for all $k \geq 0$. In addition, we suppose that every section on the mainline has the same initial density of $\rho_m(0) = 10$ for all $m \in [1, M]$. Let the initial queue length on every on-ramp queue be $w_i(0) = 0$ for all $i \in [1, I]$.

The demand flow entering to each on-ramp queue for each period is listed in Table 3.1. The total simulation time is 5 hours and comprises three periods: we use the amount of demand flow vector defined in the free-flow period for the first hour, rush-hour period for the next 2 hours, and free-flow period again for the final 2 hours.

Table 3.1: Demand flow.

Entrance ramp number	Free-flow period (vph)	Rush-hour period (vph)
1	1000	1800
2, 3, 4, 5	200	1000

3.5.2 Simulation results

Fig. 3.4 shows the average system capacity over 5 hours on a sample highway corridor using the four specified ramp-metering controls. In addition, Fig. 3.5 shows the average system velocity of all vehicles traveling over the highway corridor during the specified 5-hour time frame. The average system flow is around 910 vph during the first free-flow period, which is the same without regard to the type of ramp-metering control and even under no ramp-metering operation. Once demand flow to all entrance ramps increases dramatically as occurs during the rush-hour period, all four ramp-metering methods show an instant throughput improvement approximate to the maximum system capacity around 1800 vph because of the sudden increase in traffic density. As high demand flow is injected into the vehicular traffic network continuously, no ramp-metering, ALINEA, and time-variant optimization controls lead to a gradual degradation of system throughput. However, steady-state optimization control method maintains a higher system flow by limiting the metered rates at system-wide entrance ramps so as to keep traffic densities along the system below their critical densities of about 25 vpm, causing on-ramp queue spillover to adjacent local streets. In contrast, following the rush-hour period, since density along the system decreases, no ramp-metering, ALINEA, and time-variant optimization controls show an increase in the average system capacity. Note that the system capacity recovering from congestion does not reach capacity before flow breakdown. This observation describes traffic hysteresis phenomena [40, 41]. After vehicles of all on-ramp queues are discharged or traffic density on the mainline of the system decreases below the critical density, average system throughput of all ramp-metering controls returns to the initial simulation state.

In contrast to the other three ramp-metering approaches described here, the steady-state optimization algorithm requires more than an hour to clear congestion; this is because the steady-state scheme must evacuate numerous vehicles waiting on

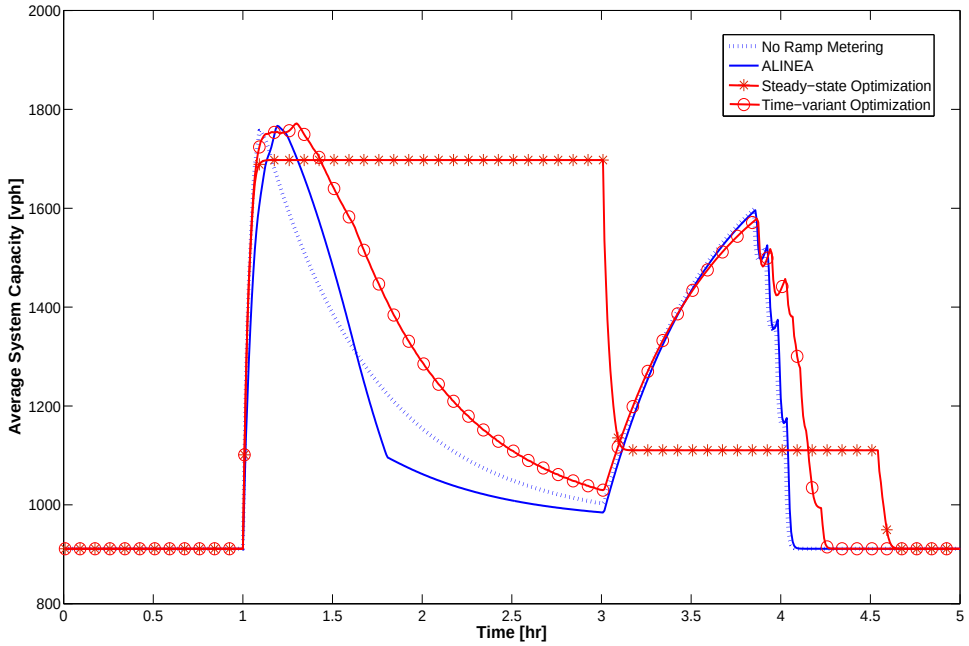

Figure 3.4: Average system capacity vs. time.

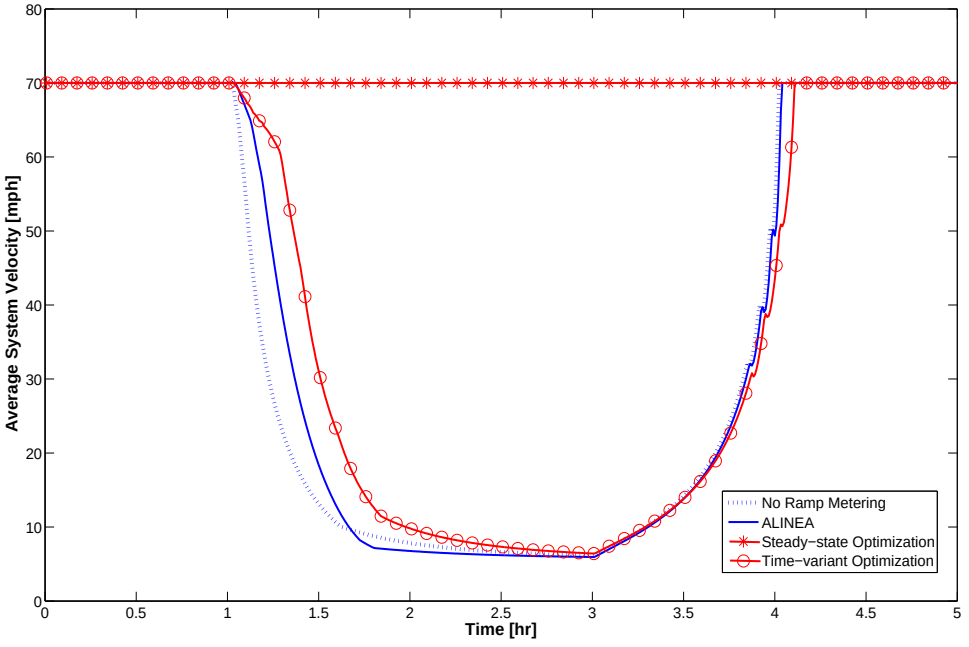

Figure 3.5: Average system velocity vs. time.

both entrance ramp queues and adjacent arterial roads. Since ALINEA also does not support on-ramp queue control, it incurs neighboring street traffic. However, the time-variant ramp-metering algorithm not only keeps the queue length on entrance ramps short enough to prevent build-up of vehicles at on-ramp queues, but it also generally improves the average system throughput, particularly during congestion conditions.

When we fulfill the requirements of the steady-state ramp-metering method, all vehicles on the mainline travel with a maximum free-flow velocity of 70 mph shown in Fig. 3.5, but it has the drawback of requiring longer congestion clearance time for dispersing vehicles both on entrance ramps and adjacent roads. Compared to the steady-state method, other three schemes show that the average system speed decreases as the number of vehicles wanting to use the highway network increases during the rush-hour period, but the average speed of traveling vehicles on the mainline increases until traffic returns to the normal free-flow state following the rush-hour period. As with the average system capacity results, the time-variant ramp-metering scheme allows vehicles on the highway mainline to travel with a higher velocity than is permitted by either ALINEA or no ramp metering.

3.6 Summary

The goal of the Chapter 3 is to provide two optimal ramp-metering controls for achieving maximum average system throughput on highways. The steady-state optimization problem limits the inflow rate from entrance ramps into the mainline so as to keep traffic densities along a highway corridor below their critical densities, whereas the time-variant programming problem adopts on-ramp queue control to prevent additional congestion onto neighboring arterial roads. The time-gap-based fundamental diagram is used for estimating traffic flow as well as for demonstrating the constraints of two optimization problems.

Use of the steady-state optimization scheme results in high average system capacity as well as increased average system velocity to the overall traffic network, but this method has the drawback of incurring significant on-ramp queue spillover on adjacent streets, thus requiring long congestion clearance time to return to the free-flow state.

In contrast, the time-variant optimization problem for achieving the maximum average system capacity is proven as an effective coordinated ramp-metering algorithm to provide higher system throughput and to increase the average system velocity, particularly under congestion situations.

Chapter Acknowledgments

The research provided in Chapter 3 was partially supported by professor Rene L. Cruz, now deceased. We truly appreciated his help.

Chapter 3, in full, is a reorganized version of the following publication in the Proceedings of the IEEE 80th Vehicular Technology Conference, 2014 Fall. Seokheon Cho and Ramesh R. Rao. "Coordinated ramp-metering control using a time-gap based traffic model," in Proceedings of the IEEE 80th Vehicular Technology Conference (VTC Fall), pp. 1-6, Sep., 2014.

Chapter 4

New Traffic Safety Metric

In this Chapter, we propose a traffic safety metric called the safety marginal value (SMV) to be applied to discrete-time and continuous-space vehicular traffic networks. Every vehicle in a network uses a set of vehicle states containing the position, velocity, and lane index of all vehicles on a roadway to determine the SMV, while also controlling its velocity for the next time step. The anterior SMV is defined as the minimum value from a set of the continuous safety level of collision risk with the leading vehicles predicted by the collision avoidance (CA) margin time of each vehicle and is bounded by two non-negative integers. The higher the anterior SMV, the lower the likelihood of a rear-end accident occurring. However, the computational complexity of our proposed safety metric grows dramatically as the number of vehicles traveling on a roadway increases, since a set of vehicle states for all vehicles is needed to determine the SMV. Thus, a finite space horizon for the anterior SMV is developed to reduce the computational complexity. That is, only a subset of vehicle states related to the finite number of vehicles defined by a space horizon is required to provide a precise anterior SMV. This simple and rigorous traffic safety metric will be useful in reducing vehicle-to-vehicle crashes and could thus relieve traffic congestion caused by accidents. Moreover, the anterior SMV can be used as a safety criterion to validate car-following models under various environmental variables or as a key parameter of an objective function to maximize safety levels on roadways. In particular, a safety analysis of the Gipps car-following model is performed with a microscopic traffic simulation as well as with our proposed safety indicator.

4.1 Introduction

There have been many attempts to specify the movement of vehicles traveling on vehicular traffic networks. In particular, existing car-following models describe the interactive characteristics of vehicles, such as time headway, velocity, and acceleration rate [42, 43, 44, 45, 46, 47]. The Gazis-Herman-Rothery (GHR) model [42], the most well-known car-following model, was developed based on the hypothesis that an individual driver's acceleration is proportional to the relative speed and car spacing to its leading vehicle. In addition to this assumption, Gipps [43] considered safety distance or collision avoidance with the reasonable supposition that a driver incorporates an additional braking reaction time for safety. Hence, the Gipps model described the behavior of real traffic in free-flow as well as in congested flow, which can be embedded in diverse microscopic traffic simulations. Wilson [44] provided a mathematical analysis of the Gipps car-following model. He derived the speed-headway function for the Gipps model with the numerical bound, where a physical solution can be defined, and analyzed the stability of the uniform flow solutions. The existing car-following models, such as the GHR model and the Gipps model, presented the driver's response to the behavior of the leading vehicle. However, these models cannot predict the risky and unexpected driving behavior of the leading vehicle, since they were developed based on unrealistic assumptions about the ideal safe behavior of drivers. Hence, these models can cause a rear-end collision under some combination of variables. A traffic safety metric therefore needs to be investigated as the basic essential for car-following models.

Kwon *et al.* [3] provided the evidence that most collisions are caused by human faults, such as speeding, intoxication, or inattention by distraction. Most crashes are rear-end and broadside collisions, but the main relevant accident to car-following models, unlike lane changing models, is a rear-end collision, which can be prevented with the help of a proper safety assessment tool. Meanwhile, many studies on driver assistance systems have been conducted for collision avoidance. In particular, adaptive cruise control (ACC) systems and braking assistance systems have been examined to mitigate rear-end collisions. These systems use various sensors on a vehicle to predict the driver's intent in different traffic situations, such as accelerating, braking, and changing lanes, and to help to reduce unexpected incidents [48, 49]. ACC systems as

an extension to the cruise control can help to enhance both safety and the driver's comfort [50]. The representative goals of ACC systems is to maintain a certain car spacing to the leading vehicle [51] and to automatically accelerate and brake [52]. In addition, probabilistic techniques have been used to analyze intentional driver behavior and predict driver reaction, which are hidden Markov models (HMMs) [53, 54] and sparse Bayesian learning [49]. However, driver assistance systems containing both ACC systems and probabilistic methods can not guarantee safe traffic patterns yet. Additional assessment techniques that determine the degree of safety and thus mitigate dangerous traffic circumstances are required for more controlled and advanced driver assistance systems. A traffic safety metric indicating safety level of collision risk can be a good auxiliary strategy in intelligent vehicles.

Hayward [55] initially defined Time-to-Collision (TTC) as a traffic safety indicator, which is the time required for two consecutive vehicles in the same lane to collide if they continuously travel at their current speed. TTC of the ith vehicle at time t is given by

$$TTC_i(t) = \frac{x_{i-1}(t) - x_i(t) - L_{i-1}}{v_i(t) - v_{i-1}(t)},$$

where $x_i(t)$ and $v_i(t)$ are the position and velocity of the ith vehicle at time t, respectively. In addition, L_i denotes the length of the ith vehicle, and the index of $(i-1)$ means the lead of the ith vehicle. TTC is defined only for $v_i(t) > v_{i-1}(t)$. TTC has proven to be an effective quantitative metric to rate the risk of collision [56, 57]. In general, TTC is inversely proportional to accident involvement. That is, a smaller value of TTC induces a higher level of crash risk. Another widely used safety measure is time headway, defined as the time it will take for a vehicle to travel the distance from its front end to the tip of its leading vehicle. By the definition of time headway, time headway of the ith vehicle at a certain location x is

$$TH_i(x) = t_i(x) - t_{i-1}(x),$$

where $t_i(x)$ denotes the time at which the ith vehicle passes the location x. There have been studies about the relationship between time headway and the occurrence of collisions [58, 59] that reveal an inverse relationship depending on traffic situations. In particular, Vogel [60] investigated the two safety indicators, TTC and time headway,

and claimed they are independent of each other. He found that these two measures are appropriate for different purposes; TTC can be used to evaluate the actual safety of the traffic environment, whereas the ease of observing and interpreting time headway makes it a criterion for preventing tailgating. Bevrani *et al.* [61] selected the bounds of TTC and time headway for the evaluation of a critical safety event and modified the Gipps car-following model under the performance results so as to remedy the unsafe vehicle movements of the Gipps model. Many studies used empirical traffic data or simulation to suggest suitable ranges of the two safety indicators, which guarantee collision-free trajectory [59, 62, 63, 64]. However, the proposed safety limits of TTC and time headway are not only various for different traffic situations, but also ambiguous for indicating the safety level of collision risk. For example, the recommend range of TTC is from 1.5 s to 5 s in urban areas. Nevertheless, even if a vehicle travels with a TTC of 1.4 s (being less than the lower bound), its movement can maintain a crash-free trajectory. Therefore, there is a need for a new safety metric that shows the likelihood of an accident occurring and applies identically, irrespective of diverse traffic conditions. We propose a safety indicator, called the safety marginal value (SMV), to predict and prevent a rear-end collision.

The remainder of this Chapter is organized as follows: In Section 4.2, we present the vehicular traffic system assumptions for determining the anterior SMV. We define the SMV as a rigorous safety metric in Section 4.3. In addition, we provide the anterior collision avoidance likelihood function to derive the anterior SMV mathematically, particularly for the following second vehicle. As its extension, Section 4.4 specifies the general form of the anterior SMV, when multiple vehicles exist on vehicular traffic networks. To derive the safety indicator, feasible combinations of trajectories of two consecutive vehicles are investigated. In addition, in order to reduce the dramatically growing computational complexity in determining the anterior SMV as the number of vehicles in system increases, a finite space horizon for the anterior SMV is introduced. In Section 4.5, we employ the Gipps car-following model to present simulation results. We show a steady-state that guarantees collision-free movements and a catastrophe state that results in collisions according to the different variables defined in the Gipps car-following model. Furthermore, our proposed anterior space horizon and corresponding

anterior SMV are examined under the various parameters of the model. In the resulting simulation, the anterior SMV is verified as a strong and rigorous safety metric to indicate the safety level of rear-end collision risk for a microscopic car-following model.

4.2 Vehicular Traffic Network

In this Section, we present the details of the vehicular traffic network overview for the SMV. We first provide several traffic system assumptions.

4.2.1 Vehicular traffic system assumptions

We consider traffic flow on a roadway shown in Fig. 4.1. Assuming that there are multiple vehicles traveling on a roadway, we use a set of vehicle states to determine the SMV. A set of vehicle states at time kT for $k \in \{0 \cup \mathbb{N}\}$ is given by $\mathbf{C}(kT) = \{C_i(kT) \mid \text{for all } i \in \mathbb{N}\}$, where $\mathbb{N}$ is a set of natural numbers and T is the update time interval. In other words, T is frequency of update in time to obtain the new SMV. $C_i(kT)$ denotes the vehicle states of the ith vehicle at time kT. A set of vehicle states consists of the position, velocity, and lane index for all vehicles and is newly updated at every time step. That is, the vehicle states of the ith vehicle are given by $C_i(kT) = \{x_i(kT), v_i(kT), l_i(kT)\}$, where $x_i(kT)$, $v_i(kT)$, and $l_i(kT)$ are the position, velocity, and lane index of the ith vehicle at time kT, respectively.

We suppose that every vehicle has the same maximum acceleration rate a^+_{max} and deceleration rate a^-_{max}, where $a^+_{max} > 0$ and $a^-_{max} < 0$ are finite bounded. In addition, we assume that every vehicle knows a set of vehicle states of all other vehicles on a roadway. Hence, each vehicle can predict the maximum and minimum trajectories of other vehicles for some future time at every time step kT. The maximum trajectory is the trajectory of a vehicle traveling with the maximum acceleration rate a^+_{max}, while the minimum trajectory is that of a moving vehicle with the maximum deceleration rate a^-_{max}. When a vehicle travels with the maximum deceleration rate, once it stops completely, its minimum trajectory stays stationary. Let $d_{i,max}(kT + \Delta t)$ and $d_{i,min}(kT + \Delta t)$ denote the maximum and minimum trajectories of the ith vehicle at time $(kT + \Delta t)$ for all $\Delta t \geq 0$, which are calculated from a set of vehicle states $\mathbf{C}(kT)$

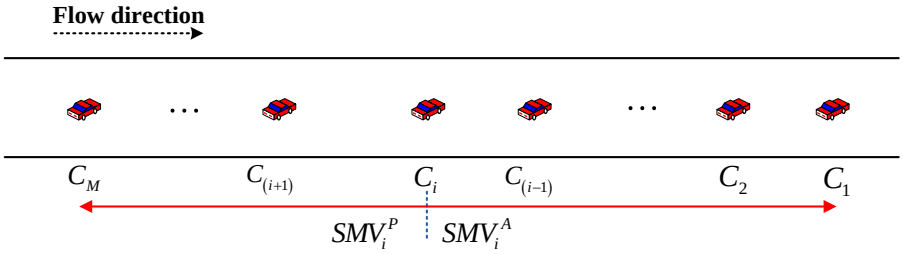

Figure 4.1: Vehicular traffic network.

at time kT, respectively. Assume that each vehicle calculates its collision avoidance (CA) margin time, which is the time required to stop completely with full application of the brakes. Let $h_i\,(kT)$ denote the CA margin time of the ith vehicle calculated at time kT, which is thus given by $-v_i\,(kT)\,/a_{max}^{-}$.

Note that the CA margin time is the critical time in determining a safety indicator. When a driver recognizes that a collision with the leading vehicle appears imminent, he must try to stop as soon as possible by braking with the maximum deceleration rate to prevent a rear-end crash, which leads to the minimum trajectory. In the case that the vehicle's path is the minimum trajectory, accident-free driving at the current time or even the subsequent time is not sufficient for complete safety, since if a collision happens by the CA margin time, it inevitably leads to a crash. That is to say, collision-free travel for the ith vehicle defined at time kT is determined by accident occurrence not by the next time step $(k+1)\,T$, but by the CA margin time $h_i\,(kT)$. Hence, each vehicle uses a set of vehicle states of all other vehicles to draw the maximum and minimum trajectories of all other automobiles by its calculated CA margin time in order to specify a safety indicator at every time step.

4.3 Anterior Safety Marginal Value

In this Section, we present the mathematical forms for the anterior SMV.

4.3.1 Safety marginal value property

Every vehicle uses a set of vehicle states $\mathbf{C}(kT)$ to determine two safety marginal values: the anterior SMV, $SMV_i^A(kT)$, and posterior SMV, $SMV_i^P(kT)$. The anterior SMV is used as a collision indicator against the leading vehicles. In contrast, when a vehicle changes lanes on a roadway, it is necessary to refer to a safety metric such as the posterior SMV. This metric utilizes the vehicle states of all following vehicles to measure the safety level of collision risk to those vehicles. That is, the ith vehicle needs a subset of vehicle states $\{C_1(kT), C_2(kT), \ldots, C_i(kT)\}$ to determine the anterior SMV and the other subset $\{C_i(kT), C_{i+1}(kT), \ldots, C_M(kT)\}$ to calculate the posterior SMV. In this Chapter, only the anterior SMV is described, since only this is associated with a rear-end collision.

The anterior safety marginal value function of the ith vehicle at time kT for every $i \in \mathbb{N}$ is given by

$$SMV_i^A(\{C_1(kT), C_2(kT), \ldots, C_i(kT)\}) \in [0, 1].$$

$SMV_i^A(kT) = 1$ implies that the ith vehicle will not collide with other leading vehicles by its CA margin time $h_i(kT)$. That is, the ith vehicle is absolutely safe from collision risk by its CA margin time. On the contrary, $SMV_i^A(kT) = 0$ implies that the ith vehicle will crash into vehicles ahead of it before its CA margin time. $SMV_i^A(kT) \in (0, 1)$ means that the ith vehicle is likely to crash into other leading vehicles by its CA margin time. The larger the SMV, the safer the vehicle is; that is, the lower the likelihood of a crash. The goal is to provide the anterior SMV at every time step, which can be used as an effective reference metric for controlling a vehicle for safe driving against a rear-end collision.

4.3.2 Anterior safety marginal value for the second vehicle

It can be assumed that the anterior SMV for the first vehicle is 1, as there is no vehicle in front of the first vehicle on a straight road as shown in Fig. 4.1. However, the anterior SMV for the following, second vehicle depends on the subset of vehicle states, which is $\{C_1(kT), C_2(kT)\} \subset \mathbf{C}(kT)$. Normally, the driving patterns of other drivers can be estimated based on the traffic flow status, and thus the velocity and position

of other vehicles can be predicted for some future time with positive error probability. Most people generally drive with the assumption that their acceleration rate has some distribution between the maximum acceleration rate and maximum deceleration rate; for example, a vehicle location between the maximum and minimum trajectories might follow a Gaussian distribution at any time. This implies that general driving patterns are based on an unreliable estimation of the position and velocity of other vehicles for some future time. This is not a particularly safe driving style, as this estimation does not actively take into consideration even the possibility of an unexpected crash. Hence, a worst-case driving scenario of the vehicles in front must be considered for safety. For instance, even though the immediately leading vehicle has enough car spacing with no accident risk, it might brake with intensity. However, if we assume that every vehicle is traveling with uncertainty of the position and velocity of other vehicles for some future time, then we can provide a tight and rigorous safety metric. Since a random parameter shows the highest entropy when it has a uniform distribution, we suppose that the trajectories of all vehicles have a uniform distribution between $d_{i,max}\left(kT+\Delta t\right)$ and $d_{i,min}\left(kT+\Delta t\right)$ at any time $\Delta t \geq 0$ with the magnitude $1/[d_{i,max}\left(kT+\Delta t\right) - d_{i,min}\left(kT+\Delta t\right)]$ for all $i \in \mathbb{N}$, where $d_{i,max}\left(kT+\Delta t\right)$ and $d_{i,min}\left(kT+\Delta t\right)$ are the maximum and minimum trajectories for the ith vehicle at time $(kT+\Delta t)$, respectively.

The maximum and minimum trajectories of the first two vehicles, and the corresponding collision and non-collision areas are shown in Fig. 4.2. The dotted (upper colored in blue) and dash-dotted (lower in blue) lines represent the maximum and minimum trajectories of the first vehicle, respectively. The solid line (in red) describes the minimum trajectory of the second vehicle. In addition, the circle (in blue) and star (in red) shown in Fig. 4.2 refer to the CA margin time for the first and second vehicles, respectively. The trajectories are obtained with the initial position vector $[15.2,\ 0]$ m and initial velocity vector $[48.3,\ 96.6]$ km/h of the first two vehicles. The second vehicle calculates the maximum and minimum trajectories of the first vehicle that is its leading vehicle, and its own minimum trajectory by its CA margin time $h_2\left(kT\right)$. We use the minimum trajectory of the second vehicle instead of its maximum trajectory for calculating the anterior SMV of the second vehicle because if the driver of the second vehicle recognizes that a collision with the first vehicle appears imminent, he must try to

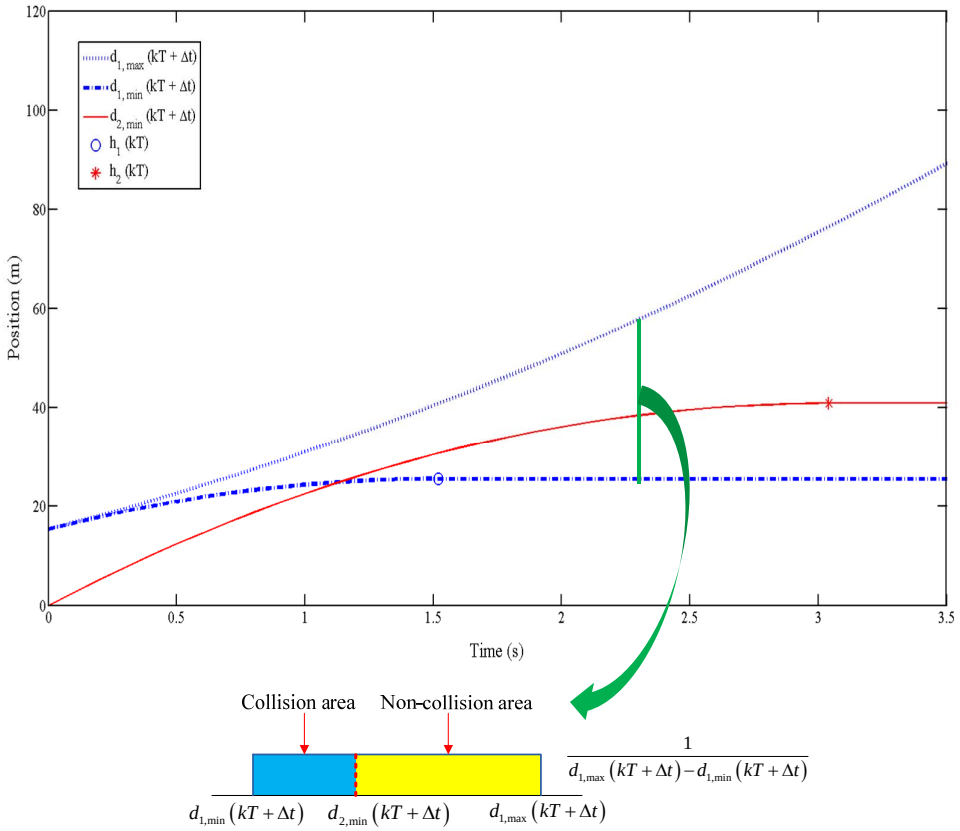

Figure 4.2: Collision and non-collision areas between two consecutive vehicles.

decrease the vehicle's velocity by fully applying the brakes, which draws the minimum trajectory.

Let us fix the time $\Delta\hat{t} \in (0, h_2(kT)]$. We cut the trajectory plane vertically at a certain time $\Delta\hat{t}$, so we specify two non-overlapped areas by the minimum trajectory of the second vehicle, which are said to be collision and non-collision areas. The first vehicle is located between $d_{1,max}\left(kT + \Delta\hat{t}\right)$ and $d_{1,min}\left(kT + \Delta\hat{t}\right)$ with a uniform distribution by supposition. For example, we assume that $\Delta\hat{t}$ is at the time indicated by a green vertical line as shown in Fig. 4.2. If the first vehicle is practically located between $d_{1,max}\left(kT + \Delta\hat{t}\right)$ and $d_{2,min}\left(kT + \Delta\hat{t}\right)$ under the condition $d_{1,max}\left(kT + \Delta\hat{t}\right) > d_{2,min}\left(kT + \Delta\hat{t}\right)$, then the second vehicle does not collide with the first vehicle at time $\left(kT + \Delta\hat{t}\right)$; this area is thus defined as a non-collision area, as the second vehicle must be located at $d_{2,min}\left(kT + \Delta\hat{t}\right)$ for active safe driving. In

contrast, if the first vehicle is located between $d_{2,min}\left(kT+\Delta\hat{t}\right)$ and $d_{1,min}\left(kT+\Delta\hat{t}\right)$ under the condition $d_{2,min}\left(kT+\Delta\hat{t}\right) > d_{1,min}\left(kT+\Delta\hat{t}\right)$, then the second vehicle will crash into the first vehicle; this area is thus said to be a collision regime.

Now, we provide the anterior collision avoidance likelihood and the anterior collision likelihood function for the second vehicle, which are continuous functions in time and are denoted by function $I_{\langle N(2,1)\rangle}\left(kT+\Delta t\right)$ and $I_{\langle A(2,1)\rangle}\left(kT+\Delta t\right)$, respectively. The anterior collision avoidance likelihood function shows the continuous safety level of collision risk toward any other leading vehicles. The anterior collision avoidance likelihood function and anterior collision likelihood function for the second vehicle at any given time $\Delta t \in (0, h_2(kT)]$ are given by

$$I_{\langle N(2,1)\rangle}\left(kT+\Delta t\right)=\left[\frac{d_{1,max}\left(kT+\Delta t\right)-d_{2,min}\left(kT+\Delta t\right)}{d_{1,max}\left(kT+\Delta t\right)-d_{1,min}\left(kT+\Delta t\right)}\right]_P, \tag{4.1}$$

$$I_{\langle A(2,1)\rangle}\left(kT+\Delta t\right)=\left[\frac{d_{2,min}\left(kT+\Delta t\right)-d_{1,min}\left(kT+\Delta t\right)}{d_{1,max}\left(kT+\Delta t\right)-d_{1,min}\left(kT+\Delta t\right)}\right]_P, \tag{4.2}$$

where $\langle N(i+1,i)\rangle$ means non-accident between two consecutive vehicles, the $(i+1)$st and ith vehicles, $\langle A(i+1,i)\rangle$ means accident occurrence between these two vehicles, and $[f(t)]_P$ is defined by

$$[f(t)]_P=\begin{cases}1 & \text{for } f(t)\geq 1,\\ f(t) & \text{for } 0<f(t)<1,\\ 0 & \text{for } f(t)\leq 0.\end{cases} \tag{4.3}$$

Note that $I_{\langle N(2,1)\rangle}\left(kT+\Delta t\right)+I_{\langle A(2,1)\rangle}\left(kT+\Delta t\right)=1$ for all $k\in\{0\cup\mathbb{N}\}$ and for all $\Delta t\in(0,h_2(kT)]$. Finally, the anterior SMV is defined as the minimum value from a set of the anterior collision avoidance likelihood function by the CA margin time. Therefore, the anterior SMV of the second vehicle at time kT is given by

$$SMV_2^A(kT)=\min_{\Delta t\in(0,h_2(kT)]} I_{\langle N(2,1)\rangle}\left(kT+\Delta t\right). \tag{4.4}$$

The anterior collision avoidance likelihood function and corresponding anterior SMV for the second vehicle are depicted in Fig. 4.3. The solid line describes an anterior collision avoidance likelihood function with respect to time from (4.1). The star shown here refers to the CA margin time of the second vehicle calculated at time kT, and

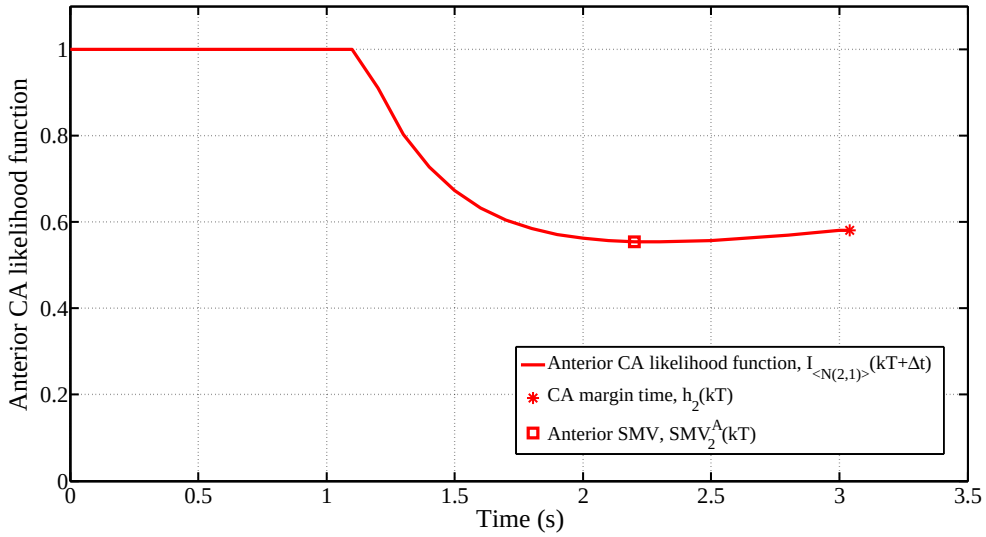

Figure 4.3: Anterior collision avoidance likelihood function and corresponding anterior SMV.

the square refers to the anterior SMV of the second vehicle, which is the minimum value of an anterior collision avoidance likelihood function by its CA margin time. This result is obtained under the same condition used for Fig. 4.2. As seen in Fig. 4.2, it can be observed that the minimum trajectory of the second vehicle overtakes that of the first vehicle after around 1.2 s, but it does not pass the maximum trajectory of the first vehicle up until the CA margin time of the second vehicle. If the first vehicle decreases its velocity with the maximum deceleration rate continuously from the time kT, which drives its minimum trajectory, then the second vehicle will collide with its leading vehicle around 1.2 s later, although the second vehicle decreases its velocity as quickly as possible via full application of the brakes. On the contrary, if the first vehicle increases its velocity constantly with the maximum acceleration rate, which drives its maximum trajectory, then the two vehicles will never crash by the CA margin time of the second vehicle; however, this does not assure collision-free movement at a later time than the CA margin time. That is, there might exist a nonzero collision possibility between two consecutive vehicles, which depends on their vehicle states updated at the next time step. By the definition of the anterior SMV (4.4), the anterior SMV of the second vehicle is about 0.55 under the scenario shown in Fig. 4.2.

4.4 General Form of Anterior Safety Marginal Value

In this Section, we provide the general form of the anterior SMV. In addition, we suggest using a finite space horizon for the anterior SMV in order to reduce the computational complexity in determining the anterior SMV.

4.4.1 Anterior safety marginal value of the ith vehicle

Suppose that all vehicles are in the same lane; that is, $l_i(kT) = l$ for all $i \in \mathbb{N}$ and for all $k \in \{0 \cup \mathbb{N}\}$. In that case, only the position and velocity from a set of vehicle states need to be considered to determine the anterior SMV. Also suppose that $x_i(kT) > x_{i+1}(kT)$ holds for all $i \in \mathbb{N}$ and for every time step kT; that is, the ith vehicle is followed by the $(i+1)$st vehicle. Let us fix $i \in \mathbb{N}$ and $k \in \{0 \cup \mathbb{N}\}$. The maximum and minimum trajectories of the ith vehicle at time $(kT + \Delta t)$, which are $d_{i,max}(kT + \Delta t)$ and $d_{i,min}(kT + \Delta t)$, are given by

$$d_{i,max}(kT + \Delta t) = x_i(kT) + v_i(kT)\Delta t + \frac{a^+_{max}}{2}\Delta t^2$$

for all $\Delta t \geq 0$, and

$$d_{i,min}(kT + \Delta t) = \begin{cases} x_i(kT) + v_i(kT)\Delta t + \frac{a^-_{max}}{2}\Delta t^2 \\ \qquad\qquad \text{for all } \Delta t \in [0, h_i(kT)], \\ x_i(kT) + v_i(kT)h_i(kT) + \frac{a^-_{max}}{2}h_i(kT)^2 \\ \qquad\qquad \text{for all } \Delta t > h_i(kT), \end{cases}$$

where $h_i(kT)$ is the CA margin time of the ith vehicle determined at time kT with $h_i(kT) = -v_i(kT)/a^-_{max}$. Note that $d_{i,max}(kT + \Delta t)$ is a strictly increasing function for all $\Delta t \geq 0$. $d_{i,min}(kT + \Delta t)$ is a strictly increasing function for all $\Delta t \in [0, h_i(kT)]$, while it is the same constant as $d_{i,min}(kT + h_i(kT))$ for all $\Delta t > h_i(kT)$. Also, we have two conditions such that $d_{i,max}(kT + \Delta t) = d_{i,min}(kT + \Delta t)$ for $\Delta t = 0$ and $d_{i,max}(kT + \Delta t) > d_{i,min}(kT + \Delta t)$ for all $\Delta t \in (0, h_i(kT)]$.

Note that the critical and non-trivial proofs only are included.

Lemma 4.1. *There exists $\epsilon_t > 0$ such that*

$$d_{i,min}(kT + \epsilon_t) > d_{i+1,max}(kT + \epsilon_t)$$

for all $i \in \mathbb{N}$ *and for every* $k \in \{0 \cup \mathbb{N}\}$.

Proof. Fix $i \in \mathbb{N}$ and $k \in \{0 \cup \mathbb{N}\}$.

$$d_{i,min}\left(kT+\epsilon_t\right) - d_{i+1,max}\left(kT+\epsilon_t\right)$$
$$= \left[x_i\left(kT\right) - x_{i+1}\left(kT\right)\right] + \left[v_i\left(kT\right) - v_{i+1}\left(kT\right)\right]\epsilon_t + \left(\frac{a_{max}^{-} - a_{max}^{+}}{2}\right){\epsilon_t}^2,$$

which as ϵ_t goes to 0,

$$\rightarrow \left[x_i\left(kT\right) - x_{i+1}\left(kT\right)\right]$$

Hence, since $\left[x_i\left(kT\right) - x_{i+1}\left(kT\right)\right] > 0$, and $i \in \mathbb{N}$ and $k \in \{0 \cup \mathbb{N}\}$ are arbitrary, there exists $\epsilon_t > 0$ such that $d_{i,min}\left(kT+\epsilon_t\right) > d_{i+1,max}\left(kT+\epsilon_t\right)$ for some $\epsilon_t > 0$ as required. □

Lemma 4.2. *Let* $v_i\left(kT\right) \geq v_{i+1}\left(kT\right)$ *for some* $i \in \mathbb{N}$ *and for some* $k \in \{0 \cup \mathbb{N}\}$. *Then,*

$$d_{i,max}\left(kT+\Delta t\right) > d_{i+1,max}\left(kT+\Delta t\right)$$

and

$$d_{i,min}\left(kT+\Delta t\right) > d_{i+1,min}\left(kT+\Delta t\right)$$

for all $\Delta t \in [0, h_i\left(kT\right)]$. *Furthermore,*

$$d_{i,max}\left(kT+\Delta t\right) > d_{i+1,min}\left(kT+\Delta t\right)$$

for all $\Delta t \in [0, h_i\left(kT\right)]$.

Proof. Suppose $v_i\left(kT\right) \geq v_{i+1}\left(kT\right)$. Then, $h_i\left(kT\right) \geq h_{i+1}\left(kT\right)$ holds by the definition of the CA margin time. Hence, we have

$$d_{i,min}\left(kT+\Delta t\right) - d_{i+1,min}\left(kT+\Delta t\right)$$
$$= \left[x_i\left(kT\right) - x_{i+1}\left(kT\right)\right] + \left[v_i\left(kT\right) - v_{i+1}\left(kT\right)\right]\Delta t$$

for all $\Delta t \in [0, h_{i+1}\left(kT\right)]$. By supposition, the relationship between the minimum trajectories of two consecutive vehicles satisfies $d_{i,min}\left(kT+\Delta t\right) > d_{i+1,min}\left(kT+\Delta t\right)$ for all $\Delta t \in [0, h_{i+1}\left(kT\right)]$. Since $d_{i,min}\left(kT+h_{i+1}\left(kT\right)\right) > d_{i+1,min}\left(kT+h_{i+1}\left(kT\right)\right)$,

$$0 < d_{i,min}\left(kT+h_{i+1}\left(kT\right)\right) - d_{i+1,min}\left(kT+h_{i+1}\left(kT\right)\right),$$

which by the definition of the minimum trajectory, for all $\Delta t \in \left(h_{i+1}\left(kT\right), h_i\left(kT\right)\right]$,

$$
\begin{aligned}
&< \left[x_i(kT) + v_i(kT)\Delta t + \frac{a_{max}^-}{2}\Delta t^2\right] \\
&\qquad - \left[x_{i+1}(kT) + v_{i+1}(kT)h_{i+1}(kT) + \frac{a_{max}^-}{2}h_{i+1}(kT)^2\right] \\
&= d_{i,min}(kT+\Delta t) - d_{i+1,min}(kT+\Delta t).
\end{aligned}
$$

Hence,

$$d_{i,min}(kT+\Delta t) > d_{i+1,min}(kT+\Delta t)$$

for all $\Delta t \in (h_{i+1}(kT), h_i(kT)]$ and thus this holds for all $\Delta t \in [0, h_i(kT)]$. Similarly, by the definition of the maximum trajectory and supposition,

$$d_{i,max}(kT+\Delta t) > d_{i+1,max}(kT+\Delta t)$$

is satisfied for all $\Delta t \in [0, h_i(kT)]$ as required. In addition, since $d_{i,max}(kT+\Delta t) \geq d_{i,min}\big(kT+\Delta t\big)$ for all $i \in \mathbb{N}$ and for all $\Delta t \in [0, h_i(kT)]$,

$$d_{i,max}(kT+\Delta t) > d_{i+1,min}(kT+\Delta t)$$

for all $\Delta t \in [0, h_i(kT)]$. □

Lemma 4.2 yields the following Corollary.

Corollary 4.3. *For some $i \in \mathbb{N}$ and for some $k \in \{0 \cup \mathbb{N}\}$, suppose that there exists $\Delta\hat{t} \in \big(0, \max\big\{h_i(kT), h_{i+1}(kT)\big\}\big]$ such that*

$$
\begin{aligned}
&d_{i,max}\left(kT+\Delta\hat{t}\right) \leq d_{i+1,max}\left(kT+\Delta\hat{t}\right), \\
&d_{i,min}\left(kT+\Delta\hat{t}\right) \leq d_{i+1,min}\left(kT+\Delta\hat{t}\right), \text{ or} \\
&d_{i,max}\left(kT+\Delta\hat{t}\right) \leq d_{i+1,min}\left(kT+\Delta\hat{t}\right).
\end{aligned}
$$

Then, $v_i(kT) < v_{i+1}(kT)$.

Lemma 4.4. *Suppose that there exists $\Delta\hat{t} \in (0, h_i(kT)]$ such that $d_{i,max}\left(kT+\Delta\hat{t}\right) = d_{i+1,max}\left(kT+\Delta\hat{t}\right)$. Then,*

$$d_{i,min}\left(kT+\Delta\hat{t}\right) = d_{i+1,min}\left(kT+\Delta\hat{t}\right)$$

holds and vice versa. Also, $d_{i+1,max}\left(kT+\Delta\hat{t}\right) > d_{i,min}\left(kT+\Delta\hat{t}\right)$. This implies that $v_i(kT) < v_{i+1}(kT)$. Hence,

$$d_{i,max}(kT+\Delta t) > d_{i+1,max}(kT+\Delta t) \;\; \textit{and} \;\; d_{i,min}(kT+\Delta t) > d_{i+1,min}(kT+\Delta t)$$

for all $\Delta t \in \left[0, \Delta\hat{t}\right)$*, and*

$$d_{i,max}\left(kT+\Delta t\right) < d_{i+1,max}\left(kT+\Delta t\right) \;\; \textit{and} \;\; d_{i,min}\left(kT+\Delta t\right) < d_{i+1,min}\left(kT+\Delta t\right)$$

for all $\Delta t \in \left(\Delta\hat{t}\,, h_{i+1}\left(kT\right)\right]$ *are satisfied.*

Proof. Suppose there exists $\Delta\hat{t} \in \left(0, h_i\left(kT\right)\right]$ such that the equality, $d_{i,max}\left(kT+\Delta\hat{t}\right) = d_{i+1,max}\left(kT+\Delta\hat{t}\right)$, holds. Then, by Corollary 4.3, $v_i\left(kT\right) < v_{i+1}\left(kT\right)$ and thus $h_i\left(kT\right) < h_{i+1}\left(kT\right)$. For some $\Delta\hat{t} \in \left(0, h_i\left(kT\right)\right]$,

$$\begin{aligned}
&d_{i,max}\left(kT+\Delta\hat{t}\right) - d_{i+1,max}\left(kT+\Delta\hat{t}\right) \\
&\quad= \left[x_i\left(kT\right) + v_i\left(kT\right)\Delta\hat{t} + \frac{a^+_{max}}{2}\Delta\hat{t}^2\right] - \left[x_{i+1}\left(kT\right) + v_{i+1}\left(kT\right)\Delta\hat{t} + \frac{a^+_{max}}{2}\Delta\hat{t}^2\right] \\
&\quad= \left[x_i\left(kT\right) + v_i\left(kT\right)\Delta\hat{t} + \frac{a^-_{max}}{2}\Delta\hat{t}^2\right] - \left[x_{i+1}\left(kT\right) + v_{i+1}\left(kT\right)\Delta\hat{t} + \frac{a^-_{max}}{2}\Delta\hat{t}^2\right] \\
&\quad= d_{i,min}\left(kT+\Delta\hat{t}\right) - d_{i+1,min}\left(kT+\Delta\hat{t}\right).
\end{aligned}$$

This shows that $d_{i,max}\left(kT+\Delta\hat{t}\right) = d_{i+1,max}\left(kT+\Delta\hat{t}\right)$ is satisfied for some $\Delta\hat{t} \in \left(0, h_i\left(kT\right)\right]$ if and only if $d_{i,min}\left(kT+\Delta\hat{t}\right) = d_{i+1,min}\left(kT+\Delta\hat{t}\right)$ holds. In addition, since $d_{i,max}\left(kT+\Delta t\right) > d_{i,min}\left(kT+\Delta t\right)$ for all $\Delta t \in \left(0, h_i\left(kT\right)\right]$ and for all $i \in \mathbb{N}$, $d_{i+1,max}\left(kT+\Delta\hat{t}\right) > d_{i,min}\left(kT+\Delta\hat{t}\right)$. We note that, by supposition,

$$\Delta\hat{t} = -\frac{x_i\left(kT\right) - x_{i+1}\left(kT\right)}{v_i\left(kT\right) - v_{i+1}\left(kT\right)} \quad \in \left(0, h_i\left(kT\right)\right]. \tag{4.5}$$

Since $v_i\left(kT\right) < v_{i+1}\left(kT\right)$, (4.5) yields

$$-\left[v_i\left(kT\right) - v_{i+1}\left(kT\right)\right]\Delta t < \left[x_i\left(kT\right) - x_{i+1}\left(kT\right)\right]$$

for any $\Delta t \in \left[0, \Delta\hat{t}\right)$. This gives

$$\begin{aligned}
0 <\; &\left[x_i\left(kT\right) - x_{i+1}\left(kT\right)\right] + \left[v_i\left(kT\right) - v_{i+1}\left(kT\right)\right]\Delta t \\
&= d_{i,max}\left(kT+\Delta t\right) - d_{i+1,max}\left(kT+\Delta t\right),
\end{aligned}$$

which since $\Delta t < \Delta\hat{t} \le h_i\left(kT\right) < h_{i+1}\left(kT\right)$,

$$= d_{i,min}\left(kT+\Delta t\right) - d_{i+1,min}\left(kT+\Delta t\right).$$

Accordingly, we have $d_{i,max}\left(kT+\Delta t\right) > d_{i+1,max}\left(kT+\Delta t\right)$ and $d_{i,min}\left(kT+\Delta t\right) > d_{i+1,min}\left(kT+\Delta t\right)$ for all $\Delta t \in \left[0, \Delta\hat{t}\right)$. In a similar way, by (4.5), we can show

that $d_{i,max}\left(kT+\Delta t\right) < d_{i+1,max}\left(kT+\Delta t\right)$ is satisfied for all $\Delta t \in \left(\Delta\hat{t}, h_{i+1}\left(kT\right)\right]$ and $d_{i,min}\left(kT+\Delta t\right) < d_{i+1,min}\left(kT+\Delta t\right)$ holds for all $\Delta t \in \left(\Delta\hat{t}, h_i\left(kT\right)\right]$. Now, we need to show that $d_{i,min}\left(kT+\Delta t\right) < d_{i+1,min}\left(kT+\Delta t\right)$ holds even for all $\Delta t \in \left(h_i\left(kT\right), h_{i+1}\left(kT\right)\right]$. Since $\Delta\hat{t} \leq h_i\left(kT\right)$, by (4.5), we have

$$\left[x_i\left(kT\right)+v_i\left(kT\right)h_i\left(kT\right)+\frac{a_{max}^{-}}{2}h_i\left(kT\right)^2\right] \leq \left[x_{i+1}\left(kT\right)+v_{i+1}\left(kT\right)h_i\left(kT\right)+\frac{a_{max}^{-}}{2}h_i\left(kT\right)^2\right], \quad (4.6)$$

which since $h_i\left(kT\right) < h_{i+1}\left(kT\right)$,

$$< d_{i+1,min}\left(kT+\Delta t\right)$$

for all $\Delta t \in \left(h_i\left(kT\right), h_{i+1}\left(kT\right)\right]$. Also, the left-hand side of the inequality (4.6) is equivalent to $d_{i,min}\left(kT+\Delta t\right)$ for all $\Delta t \in \left(h_i\left(kT\right), h_{i+1}\left(kT\right)\right]$. Consequently, $d_{i,min}\left(kT+\Delta t\right) < d_{i+1,min}\left(kT+\Delta t\right)$ for all $\Delta t \in \left(h_i\left(kT\right), h_{i+1}\left(kT\right)\right]$ and thus this holds for all $\Delta t \in \left(\Delta\hat{t}, h_{i+1}\left(kT\right)\right]$ as required. □

The proofs for the following Lemmas 4.5 and 4.6 are similar to that of Lemma 4.4, so we skip their proofs.

Lemma 4.5. *Let there exist* $\Delta\hat{t} \in \left(h_i\left(kT\right), h_{i+1}\left(kT\right)\right]$ *such that* $d_{i,max}\left(kT+\Delta\hat{t}\right) = d_{i+1,max}\left(kT+\Delta\hat{t}\right)$. *Then,*

$$\begin{cases} d_{i,max}\left(kT+\Delta t\right) > d_{i+1,max}\left(kT+\Delta t\right) & \textit{for all } \Delta t \in \left[0, \Delta\hat{t}\right), \\ d_{i,max}\left(kT+\Delta t\right) < d_{i+1,max}\left(kT+\Delta t\right) & \textit{for all } \Delta t \in \left(\Delta\hat{t}, h_{i+1}\left(kT\right)\right], \\ d_{i,min}\left(kT+\Delta t\right) > d_{i+1,min}\left(kT+\Delta t\right) & \textit{for all } \Delta t \in \left[0, \Delta\hat{t}\right]. \end{cases}$$

Lemmas 4.4 and 4.5 imply that if the speed of the $(i+1)$st vehicle is faster than that of its leading vehicle at some time kT and for some $i \in \mathbb{N}$, $v_i\left(kT\right) < v_{i+1}\left(kT\right)$ but $x_i\left(kT\right) > x_{i+1}\left(kT\right)$, then there might exist time $\Delta\hat{t} > 0$ such that the maximum trajectories of two consecutive vehicles coincide, $d_{i,max}\left(kT+\Delta\hat{t}\right) = d_{i+1,max}\left(kT+\Delta\hat{t}\right)$. After their rencounter, the maximum trajectory of the $(i+1)$st vehicle keeps ahead of that of the ith vehicle by its CA margin time $h_{i+1}\left(kT\right)$. This is also well explained by the fact that the change of relative difference of the two vehicles' maximum trajectories, $\left[d_{i,max}\left(kT+\Delta t\right) - d_{i+1,max}\left(kT+\Delta t\right)\right]$, has the constant negative slope with $\left[v_i\left(kT\right) - v_{i+1}\left(kT\right)\right] < 0$ for all $\Delta t \in \left[0, h_{i+1}\left(kT\right)\right]$.

Lemma 4.6. *Let there exist* $\Delta\hat{t} \in (h_i(kT), h_{i+1}(kT)]$ *such that* $d_{i,min}\left(kT+\Delta\hat{t}\right) = d_{i+1,min}\left(kT+\Delta\hat{t}\right)$. *Then,*

$$\begin{cases} d_{i,min}(kT+\Delta t) > d_{i+1,min}(kT+\Delta t) & \text{for all } \Delta t \in \left[0, \Delta\hat{t}\right), \\ d_{i,min}(kT+\Delta t) < d_{i+1,min}(kT+\Delta t) & \text{for all } \Delta t \in \left(\Delta\hat{t}, h_{i+1}(kT)\right], \\ d_{i,max}(kT+\Delta t) < d_{i+1,max}(kT+\Delta t) & \text{for all } \Delta t \in \left[\Delta\hat{t}, h_{i+1}(kT)\right]. \end{cases}$$

Lemma 4.7. *Suppose that there exists* $\Delta\hat{t} \in \left(0, \max\left\{h_i(kT), h_{i+1}(kT)\right\}\right]$ *such that* $d_{i,min}\left(kT+\Delta\hat{t}\right) = d_{i+1,max}\left(kT+\Delta\hat{t}\right)$. *Then,*

$$\begin{cases} d_{i,min}(kT+\Delta t) > d_{i+1,max}(kT+\Delta t) & \text{for all } \Delta t \in \left[0, \Delta\hat{t}\right), \\ d_{i,min}(kT+\Delta t) < d_{i+1,max}(kT+\Delta t) & \\ & \text{for all } \Delta t \in \left(\Delta\hat{t}, \max\left\{h_i(kT), h_{i+1}(kT)\right\}\right]. \end{cases}$$

Furthermore,

$$d_{i,max}(kT+\Delta t) > d_{i+1,max}(kT+\Delta t) \text{ and } d_{i,min}(kT+\Delta t) > d_{i+1,min}(kT+\Delta t)$$

hold for all $\Delta t \in \left[0, \Delta\hat{t}\right]$.

Proof. Suppose that there exists $\Delta\hat{t} \in \left(0, \max\left\{h_i(kT), h_{i+1}(kT)\right\}\right]$ such that $d_{i,min}\left(kT+\Delta\hat{t}\right) = d_{i+1,max}\left(kT+\Delta\hat{t}\right)$. Let

$$\bar{d}(kT+\Delta t) = d_{i+1,max}(kT+\Delta t) - d_{i,min}(kT+\Delta t)$$

for all $\Delta t \in (0, \max\{h_i(kT), h_{i+1}(kT)\}]$. Since $[a^+_{max} - a^-_{max}] > 0$, $\bar{d}(kT+\Delta t)$ is an upward quadratic function for all $\Delta t \in [0, \max\{h_i(kT), h_{i+1}(kT)\}]$. Let Δt^* denote the minima of the function, $\bar{d}(kT+\Delta t)$. Then, we have

$$\Delta t^* = -\frac{[v_{i+1}(kT) - v_i(kT)]}{[a^+_{max} - a^-_{max}]}.$$

In addition, the slope of $\bar{d}(kT+\Delta t)$ is given by

$$\left(a^+_{max} - a^-_{max}\right)\Delta t + [v_{i+1}(kT) - v_i(kT)]$$

for all $\Delta t \in [0, \max\{h_i(kT), h_{i+1}(kT)\}]$. If $\Delta t = 0$, by the initial position condition,

$$\bar{d}(kT) = [x_{i+1}(kT) - x_i(kT)] < 0.$$

Suppose $v_i(kT) \geq v_{i+1}(kT)$. Then, $\Delta t^* \geq 0$. Since $\bar{d}(kT+\Delta t)$ has the positive slope for all $\Delta t \in (\Delta t^*, h_i(kT)]$, the function $\bar{d}(kT+\Delta t)$ is a strictly increasing function for all $\Delta t > \Delta t^*$. Hence, if there exists $\Delta\hat{t} \in (0, \max\{h_i(kT), h_{i+1}(kT)\}]$ such that $d_{i,min}\left(kT+\Delta\hat{t}\right) = d_{i+1,max}\left(kT+\Delta\hat{t}\right)$ with $v_i(kT) \geq v_{i+1}(kT)$, then the first claim here holds.

Now, suppose that $v_i(kT) < v_{i+1}(kT)$. Then, the minima of the function, $\bar{d}(kT+\Delta t)$, is less than 0. Since $\bar{d}(kT+\Delta t)$ has the positive slope for all $\Delta t \in [0, h_{i+1}(kT)]$, the function $\bar{d}(kT+\Delta t)$ is a strictly increasing function for all $\Delta t \geq 0$. Hence, if there exists $\Delta\hat{t} \in (0, \max\{h_i(kT), h_{i+1}(kT)\}]$ such that $d_{i,min}\left(kT+\Delta\hat{t}\right) = d_{i+1,max}\left(kT+\Delta\hat{t}\right)$ with $v_i(kT) < v_{i+1}(kT)$, then the first claim here is satisfied as required.

Consequently, since $d_{i,max}(kT+\Delta t) > d_{i,min}(kT+\Delta t)$ is always true for all $\Delta t > 0$ and for all $i \in \mathbb{N}$, by the first claim,

$$d_{i,max}(kT+\Delta t) > d_{i+1,max}(kT+\Delta t) \text{ and } d_{i,min}(kT+\Delta t) > d_{i+1,min}(kT+\Delta t)$$

are satisfied for all $\Delta t \in \left[0, \Delta\hat{t}\right]$ as required. □

The proof for the following Lemma 4.8 is similar to that of Lemma 4.7, so we skip its proof.

Lemma 4.8. *Suppose that there exist(s)* $\Delta\hat{t_j} \in (0, h_{i+1}(kT)]$ *for* $j = 1$ *and* 2 *such that* $d_{i,max}\left(kT+\Delta\hat{t_j}\right) = d_{i+1,min}\left(kT+\Delta\hat{t_j}\right)$. *Then, if* $\Delta\hat{t_1} = \Delta\hat{t_2} = \Delta\hat{t}$,

$$d_{i,max}(kT+\Delta t) > d_{i+1,min}(kT+\Delta t)$$

for all $\Delta t \in [0, h_{i+1}(kT)]$ *with* $\Delta t \neq \Delta\hat{t}$, *or if* $\Delta\hat{t_1} < \Delta\hat{t_2}$,

$$\begin{cases} d_{i,max}(kT+\Delta t) > d_{i+1,min}(kT+\Delta t) \\ \qquad \textit{for all } \Delta t \in \left[0, \Delta\hat{t_1}\right) \textit{ or for all } \Delta t \in \left(\min\left\{\Delta\hat{t_2}, h_{i+1}(kT)\right\}, h_{i+1}(kT)\right], \\ d_{i,max}(kT+\Delta t) < d_{i+1,min}(kT+\Delta t) \\ \qquad \textit{for all } \Delta t \in \left(\Delta\hat{t_1}, \min\left\{\Delta\hat{t_2}, h_{i+1}(kT)\right\}\right). \end{cases}$$

A combination of trajectories shows the location relationship among the maximum and minimum trajectories of any two vehicles at a certain time. Combining Lemmas 4.2 and 4.4 to 4.8 immediately yields the following.

Theorem 4.9. *For any* $\Delta t \in \left[0, \max\left\{h_i\left(kT\right), h_{i+1}\left(kT\right)\right\}\right]$*, the relationship among the maximum and minimum trajectories of two consecutive vehicles is expressed as only one single case from the following* 10 *combinations of trajectories:*

1. $d_{i,max}\left(kT+\Delta t\right) > d_{i,min}\left(kT+\Delta t\right) > d_{i+1,max}\left(kT+\Delta t\right) > d_{i+1,min}\left(kT+\Delta t\right)$,
2. $d_{i,max}\left(kT+\Delta t\right) > d_{i,min}\left(kT+\Delta t\right) = d_{i+1,max}\left(kT+\Delta t\right) > d_{i+1,min}\left(kT+\Delta t\right)$,
3. $d_{i,max}\left(kT+\Delta t\right) > d_{i+1,max}\left(kT+\Delta t\right) > d_{i,min}\left(kT+\Delta t\right) > d_{i+1,min}\left(kT+\Delta t\right)$,
4. $d_{i,max}\left(kT+\Delta t\right) = d_{i+1,max}\left(kT+\Delta t\right) > d_{i,min}\left(kT+\Delta t\right) = d_{i+1,min}\left(kT+\Delta t\right)$,
5. $d_{i+1,max}\left(kT+\Delta t\right) > d_{i,max}\left(kT+\Delta t\right) > d_{i+1,min}\left(kT+\Delta t\right) > d_{i,min}\left(kT+\Delta t\right)$,
6. $d_{i,max}\left(kT+\Delta t\right) = d_{i+1,max}\left(kT+\Delta t\right) > d_{i,min}\left(kT+\Delta t\right) > d_{i+1,min}\left(kT+\Delta t\right)$,
7. $d_{i+1,max}\left(kT+\Delta t\right) > d_{i,max}\left(kT+\Delta t\right) > d_{i,min}\left(kT+\Delta t\right) > d_{i+1,min}\left(kT+\Delta t\right)$,
8. $d_{i+1,max}\left(kT+\Delta t\right) > d_{i,max}\left(kT+\Delta t\right) > d_{i,min}\left(kT+\Delta t\right) = d_{i+1,min}\left(kT+\Delta t\right)$,
9. $d_{i+1,max}\left(kT+\Delta t\right) > d_{i,max}\left(kT+\Delta t\right) = d_{i+1,min}\left(kT+\Delta t\right) > d_{i,min}\left(kT+\Delta t\right)$,
10. $d_{i+1,max}\left(kT+\Delta t\right) > d_{i+1,min}\left(kT+\Delta t\right) > d_{i,max}\left(kT+\Delta t\right) > d_{i,min}\left(kT+\Delta t\right)$.

Lemma 4.10. *Let there exist* $\Delta\tilde{t}$ *and* $\Delta\hat{t} \in \left(0, h_{i+1}\left(kT\right)\right]$ *with* $h_i\left(kT\right) < h_{i+1}\left(kT\right)$ *such that*

$$d_{i,min}\left(kT+\Delta\tilde{t}\right) = d_{i+1,max}\left(kT+\Delta\tilde{t}\right)$$

and

$$d_{i,max}\left(kT+\Delta\hat{t}\right) = d_{i+1,max}\left(kT+\Delta\hat{t}\right).$$

Then, $\Delta\tilde{t} < \Delta\hat{t}$.

Proof. Since $d_{i,max}\left(kT+\Delta t\right) > d_{i,min}\left(kT+\Delta t\right)$ for all $\Delta t > 0$, by the first supposition,

$$d_{i,max}\left(kT+\Delta\tilde{t}\right) > d_{i+1,max}\left(kT+\Delta\tilde{t}\right).$$

Hence, by Lemmas 4.4, 4.5 and the second supposition, $\Delta\tilde{t} < \Delta\hat{t}$ holds as required. □

The proof for the following Lemma 4.11 is similar to that of Lemma 4.10, so we skip its proof.

Lemma 4.11. *Let there exist* $\Delta\tilde{t}$ *and* $\Delta\hat{t} \in (0, h_{i+1}(kT)]$ *with* $h_i(kT) < h_{i+1}(kT)$ *such that*

$$d_{i,min}\left(kT + \Delta\tilde{t}\right) = d_{i+1,min}\left(kT + \Delta\tilde{t}\right)$$

and

$$d_{i,max}\left(kT + \Delta\hat{t}\right) = d_{i+1,min}\left(kT + \Delta\hat{t}\right).$$

Then, $\Delta\tilde{t} < \Delta\hat{t}$.

Theorem 4.12. ***Anterior SMV of the*** i***th Vehicle***

Suppose that there are multiple vehicles traveling in the same lane. Let $SMV_i^A(kT)$ *be the anterior SMV of the* i*th vehicle at time* kT*. Then, the anterior SMV of the* i*th vehicle at time* kT *is given by*

$$SMV_i^A(kT) = \min_{\Delta t \in (0, h_i(kT)]} \left\{ \left[\frac{\min\limits_{l\in[1,(i-1)]} \{d_{l,max}(kT+\Delta t)\} - d_{i,min}(kT+\Delta t)}{\min\limits_{l\in[1,(i-1)]} \{d_{l,max}(kT+\Delta t)\} - \min\limits_{l\in[1,(i-1)]} \{d_{l,min}(kT+\Delta t)\}} \right]_P \right\}. \tag{4.7}$$

Proof. We will use mathematical induction. By (4.1) and (4.4), the anterior SMV (4.7) holds for $i = 2$.

Suppose that the anterior SMV defined in (4.7) is true for some $i \in \mathbb{N}$. Let $I^A_{\langle N(\vec{i})\rangle}(kT + \Delta t)$ denote the anterior collision avoidance likelihood function of the ith vehicle at time $(kT + \Delta t)$ toward any other leading vehicles. This shows the continuous safety level of collision risk of the ith vehicle toward any other leading vehicles in time. Then, we have

$$I^A_{\langle N(\vec{i})\rangle}(kT + \Delta t) = \left[\frac{\min\limits_{l\in[1,(i-1)]} \{d_{l,max}(kT+\Delta t)\} - d_{i,min}(kT+\Delta t)}{\min\limits_{l\in[1,(i-1)]} \{d_{l,max}(kT+\Delta t)\} - \min\limits_{l\in[1,(i-1)]} \{d_{l,min}(kT+\Delta t)\}} \right]_P. \tag{4.8}$$

Now, we need to show that the anterior SMV (4.7) holds also for $i+1$. By the definition of the anterior SMV and (4.8), it is sufficient to prove that

$$I^A_{\left\langle N\left(\overrightarrow{i+1}\right)\right\rangle}\left(kT+\Delta t\right)=\left[\frac{\min\limits_{l\in[1,i]}\left\{d_{l,max}\left(kT+\Delta t\right)\right\}-d_{i+1,min}\left(kT+\Delta t\right)}{\min\limits_{l\in[1,i]}\left\{d_{l,max}\left(kT+\Delta t\right)\right\}-\min\limits_{l\in[1,i]}\left\{d_{l,min}\left(kT+\Delta t\right)\right\}}\right]_P, \tag{4.9}$$

because it immediately yields

$$SMV^A_{i+1}\left(kT\right)=\min_{\Delta t\in(0,h_{i+1}(kT)]} I^A_{\left\langle N\left(\overrightarrow{i+1}\right)\right\rangle}\left(kT+\Delta t\right).$$

Using the law of total probability into the anterior collision avoidance likelihood function of the $(i+1)$st vehicle,

$$\begin{aligned} I^A_{\left\langle N\left(\overrightarrow{i+1}\right)\right\rangle}\left(kT+\Delta t\right)=&\, I^A_{\left\langle N(i+1,i)|N\left(\vec{i}\right)\right\rangle}\left(kT+\Delta t\right)\cdot I^A_{\left\langle N\left(\vec{i}\right)\right\rangle}\left(kT+\Delta t\right)\\ &+I^A_{\left\langle N(i+1,i)|A\left(\vec{i}\right)\right\rangle}\left(kT+\Delta t\right)\cdot I^A_{\left\langle A\left(\vec{i}\right)\right\rangle}\left(kT+\Delta t\right), \end{aligned} \tag{4.10}$$

where $I^A_{\left\langle N(i+1,i)|N\left(\vec{i}\right)\right\rangle}\left(kT+\Delta t\right)$ and $I^A_{\left\langle N(i+1,i)|A\left(\vec{i}\right)\right\rangle}\left(kT+\Delta t\right)$ specify the anterior collision avoidance likelihood function of the $(i+1)$st vehicle toward the ith vehicle, given the conditions that the ith vehicle does not collide with any other leading vehicles and that there exists an accident between the ith vehicle and any other leading vehicles, respectively. In addition, $I^A_{\left\langle N\left(\vec{i}\right)\right\rangle}\left(kT+\Delta t\right)$ denotes the anterior collision avoidance likelihood function of the ith vehicle, while $I^A_{\left\langle A\left(\vec{i}\right)\right\rangle}\left(kT+\Delta t\right)$ represents its anterior collision likelihood function. It is supposed that the law of inertia is negligible when any two consecutive vehicles crash. In other words, two vehicles are stationary at the very accident site where they crash. If the ith vehicle does not crash into any other leading vehicles, then the feasible maximum position of the accident-free ith vehicle is the minimum value between $\min_{1\le l\le(i-1)}\left\{d_{l,max}\left(kT+\Delta t\right)\right\}$ and $d_{i,max}\left(kT+\Delta t\right)$, while its possible minimum position is $d_{i,min}\left(kT+\Delta t\right)$. Furthermore, the ith vehicle must be located farther than the maximum position between $d_{i,min}\left(kT+\Delta t\right)$ and $d_{i+1,min}\left(kT+\Delta t\right)$, so that the $(i+1)$st vehicle does not collide with the accident-free ith vehicle. That is, the ith vehicle is located between

$$\min\left\{\min_{1\le l\le(i-1)}\left\{d_{l,max}\left(kT+\Delta t\right)\right\},d_{i,max}\left(kT+\Delta t\right)\right\}$$

and

$$\max\left\{d_{i,min}\left(kT+\Delta t\right),d_{i+1,min}\left(kT+\Delta t\right)\right\}.$$

Let

$$d_{\hat{l},max}\left(kT+\Delta t\right)=\min_{1\leq l\leq(i-1)}\left\{d_{l,max}\left(kT+\Delta t\right)\right\}, \tag{4.11}$$

$$d_{\tilde{l},min}\left(kT+\Delta t\right)=\min_{1\leq l\leq(i-1)}\left\{d_{l,min}\big(kT+\Delta t\big)\right\}. \tag{4.12}$$

Hence, the anterior collision avoidance likelihood function of the $(i+1)$st vehicle toward the ith vehicle under the condition that the ith vehicle does not collide with any other leading vehicles becomes

$$I^{A}_{\left\langle N(i+1,i)|N\left(\vec{i}\right)\right\rangle}\left(kT+\Delta t\right)=\left[\frac{\alpha_1\left(kT+\Delta t\right)-\alpha_2\left(kT+\Delta t\right)}{\alpha_1\left(kT+\Delta t\right)-d_{i,min}\left(kT+\Delta t\right)}\right]_P, \tag{4.13}$$

where

$$\alpha_1\left(kT+\Delta t\right)=\min\left\{d_{\hat{l},max}\left(kT+\Delta t\right),d_{i,max}\left(kT+\Delta t\right)\right\}$$

and

$$\alpha_2\left(kT+\Delta t\right)=\max\left\{d_{i,min}\left(kT+\Delta t\right),d_{i+1,min}\left(kT+\Delta t\right)\right\}.$$

In contrast, if the ith vehicle collides with any other leading vehicles, then the feasible maximum position of the crashed ith vehicle is the minimum value between $\min_{1\leq l\leq(i-1)}\left\{d_{l,max}\left(kT+\Delta t\right)\right\}$ and $d_{i,min}\left(kT+\Delta t\right)$, while its possible minimum position is $\min_{1\leq l\leq(i-1)}\left\{d_{l,min}\left(kT+\Delta t\right)\right\}$. In order for the $(i+1)$st vehicle not to crash into the ith vehicle under this given condition, the ith vehicle must be located farther than the maximum position between $\min_{1\leq l\leq(i-1)}\left\{d_{l,min}\left(kT+\Delta t\right)\right\}$ and $d_{i+1,min}\left(kT+\Delta t\right)$ and thus it places between

$$\min\left\{\min_{1\leq l\leq(i-1)}\left\{d_{l,max}\left(kT+\Delta t\right)\right\},d_{i,min}\left(kT+\Delta t\right)\right\}$$

and

$$\max\left\{\min_{1\leq l\leq(i-1)}\left\{d_{l,min}\left(kT+\Delta t\right)\right\},d_{i+1,min}\left(kT+\Delta t\right)\right\}.$$

Therefore, the anterior collision avoidance likelihood function of the $(i+1)$st vehicle toward the ith vehicle given the condition that there exists an accident between the ith vehicle and any other leading vehicles is

$$I^{A}_{\left\langle N(i+1,i)|A\left(\vec{i}\right)\right\rangle}\left(kT+\Delta t\right)=\left[\frac{\alpha_3\left(kT+\Delta t\right)-\alpha_4\left(kT+\Delta t\right)}{\alpha_3\left(kT+\Delta t\right)-d_{\tilde{l},min}\left(kT+\Delta t\right)}\right]_P, \tag{4.14}$$

where

$$\alpha_3\left(kT+\Delta t\right)=\min\left\{d_{\hat{l},max}\left(kT+\Delta t\right),d_{i,min}\left(kT+\Delta t\right)\right\}$$

and

$$\alpha_4\left(kT+\Delta t\right)=\max\left\{d_{\tilde{l},min}\left(kT+\Delta t\right),d_{i+1,min}\left(kT+\Delta t\right)\right\}.$$

By the fact that $I^A_{\langle N(\vec{i})\rangle}\left(kT+\Delta t\right)+I^A_{\langle A(\vec{i})\rangle}\left(kT+\Delta t\right)=1$ holds for all $i\in\mathbb{N}$ and for all for all $\Delta t\in(0,h_i\left(kT\right)]$, (4.8), (4.11), and (4.12), the ith vehicle obtains the anterior collision avoidance likelihood function and the anterior collision likelihood function towards any other leading vehicles at time kT

$$I^A_{\langle N(\vec{i})\rangle}\left(kT+\Delta t\right)=\left[\frac{d_{\hat{l},max}\left(kT+\Delta t\right)-d_{i,min}\left(kT+\Delta t\right)}{d_{\hat{l},max}\left(kT+\Delta t\right)-d_{\tilde{l},max}\left(kT+\Delta t\right)}\right]_P \tag{4.15}$$

and

$$I^A_{\langle A(\vec{i})\rangle}\left(kT+\Delta t\right)=\left[\frac{d_{i,min}\left(kT+\Delta t\right)-d_{\tilde{l},min}\left(kT+\Delta t\right)}{d_{\hat{l},max}\left(kT+\Delta t\right)-d_{\tilde{l},min}\left(kT+\Delta t\right)}\right]_P, \tag{4.16}$$

respectively.

The maximum and minimum trajectories of all leading vehicles of the ith vehicle are considered in determining its anterior SMV. Instead of employing all these trajectories, however, only two paths are required for specifying the safety level of collision risk of the ith vehicle: the upper path consisting of minimum values among the maximum trajectories of the leading vehicles in time and the lower path constituting minimum values among their minimum trajectories. These upper and lower paths are represented by (4.11) and (4.12), respectively. Even though the number of vehicles in front of the ith vehicle is in practice $(i-1)$, a platoon of these leading vehicles can be regarded as one single virtual vehicle. In addition, we define the maximum and minimum trajectories of a leading virtual vehicle as the upper and lower paths described here, respectively. In other words, $d_{\hat{l},max}\left(kT+\Delta t\right)$ denotes the maximum trajectory of a leading virtual vehicle and $d_{\tilde{l},min}\left(kT+\Delta t\right)$ describes its minimum trajectory. Recall that $d_{i,max}\left(kT+\Delta t\right)$ and $d_{i,min}\left(kT+\Delta t\right)$ are increasing continuous functions for all $i\in\mathbb{N}$ and for all $\Delta t\in(0,\max_{i\in\mathbb{N}}\left\{h_i\left(kT\right)\right\}]$. Since the minimum of finite continuous functions is a continuous function, and the minimum of finite increasing functions is an increasing function, both $d_{\hat{l},max}\left(kT+\Delta t\right)$ and $d_{\tilde{l},min}\left(kT+\Delta t\right)$ are increasing continuous functions. Hence, we can apply Theorem 4.9 to two consecutive vehicles between

the ith vehicle and its leading virtual vehicle. That is, we can imagine that there exist 10 combinations of trajectories between the ith vehicle and its consecutive leading virtual vehicle. We will show that (4.9) is equivalent to (4.10) under the first case of Theorem 4.9, which is given by

$$d_{\hat{l},max}\left(kT+\Delta t\right) > d_{\tilde{l},min}\left(kT+\Delta t\right) > d_{i,max}\left(kT+\Delta t\right) > d_{i,min}\left(kT+\Delta t\right) \quad (4.17)$$

for some $\Delta t \in \left[0, \max_{0\le l\le(i+1)} \left\{ h_l\left(kT\right) \right\}\right]$. Let us fix the time $\Delta t \in \left[0, \max_{0\le l\le(i+1)} \left\{ h_l\left(kT\right) \right\}\right]$. Substituting (4.17) in (4.15) and (4.16) yields, by (4.3),

$$I^A_{\left\langle N\left(\vec{i}\right)\right\rangle}\left(kT+\Delta t\right) = 1 \text{ and } I^A_{\left\langle A\left(\vec{i}\right)\right\rangle}\left(kT+\Delta t\right) = 0,$$

and thus, by (4.10), (4.13), and (4.17),

$$\begin{aligned} I^A_{\left\langle N\left(\overrightarrow{i+1}\right)\right\rangle}\left(kT+\Delta t\right) &= I^A_{\left\langle N(i+1,i)|N\left(\vec{i}\right)\right\rangle}\left(kT+\Delta t\right) \\ &= \left[\frac{d_{i,max}\left(kT+\Delta t\right) - \max\left\{d_{i,min}\left(kT+\Delta t\right), d_{i+1,min}\left(kT+\Delta t\right)\right\}}{d_{i,max}\left(kT+\Delta t\right) - d_{i,min}\left(kT+\Delta t\right)}\right]_P . \quad (4.18) \end{aligned}$$

We suppose that $d_{i,min}\left(kT+\Delta t\right) \le d_{i+1,min}\left(kT+\Delta t\right)$. From (4.18), we have

$$I^A_{\left\langle N\left(\overrightarrow{i+1}\right)\right\rangle}\left(kT+\Delta t\right) = \left[\frac{d_{i,max}\left(kT+\Delta t\right) - d_{i+1,min}\left(kT+\Delta t\right)}{d_{i,max}\left(kT+\Delta t\right) - d_{i,min}\left(kT+\Delta t\right)}\right]_P,$$

which by (4.17),

$$= \left[\frac{\min\limits_{l\in[1,i]}\left\{d_{l,max}\left(kT+\Delta t\right)\right\} - d_{i+1,min}\left(kT+\Delta t\right)}{\min\limits_{l\in[1,i]}\left\{d_{l,max}\left(kT+\Delta t\right)\right\} - \min\limits_{l\in[1,i]}\left\{d_{l,min}\left(kT+\Delta t\right)\right\}}\right]_P,$$

which is exactly equivalent to (4.9).

Suppose that $d_{i,min}\left(kT+\Delta t\right) > d_{i+1,min}\left(kT+\Delta t\right)$. From (4.18), we have

$$I^A_{\left\langle N\left(\overrightarrow{i+1}\right)\right\rangle}\left(kT+\Delta t\right) = I^A_{\left\langle N(i+1,i)|N\left(\vec{i}\right)\right\rangle}\left(kT+\Delta t\right) = 1,$$

which is also identical with (4.9) easily obtained by employing (4.3) and (4.17) into (4.9). Thus, note that (4.9) holds if (4.8) is true under the first case of Theorem 4.9. We can show this claim holds under the other nine combinations of trajectories defined in Theorem 4.9.

Consequently, by the principle of mathematical induction, we conclude that

$$I^A_{\left\langle N\left(\vec{i}\right)\right\rangle}\left(kT+\Delta t\right) = \left[\frac{\min\limits_{l\in[1,(i-1)]}\left\{d_{l,max}\left(kT+\Delta t\right)\right\} - d_{i,min}\left(kT+\Delta t\right)}{\min\limits_{l\in[1,(i-1)]}\left\{d_{l,max}\left(kT+\Delta t\right)\right\} - \min\limits_{l\in[1,(i-1)]}\left\{d_{l,min}\left(kT+\Delta t\right)\right\}}\right]_P$$

is true for all $i \in \mathbb{N}$ and for every $k \in \{0 \cup \mathbb{N}\}$ and thus, by the definition of the anterior SMV, the anterior SMV of the ith vehicle at time kT is defined as

$$SMV_i^A(kT) = \min_{\Delta t \in (0, h_i(kT))} \left\{ \left[\frac{\min\limits_{l \in [1,(i-1)]} \{d_{l,max}(kT+\Delta t)\} - d_{i,min}(kT+\Delta t)}{\min\limits_{l \in [1,(i-1)]} \{d_{l,max}(kT+\Delta t)\} - \min\limits_{l \in [1,(i-1)]} \{d_{l,min}(kT+\Delta t)\}} \right]_P \right\}.$$

□

We interpret the general formula for the anterior SMV of the ith vehicle as follows: physically, there exist $(i-1)$ vehicles in front of the ith vehicle. However, we regard a platoon consisting of the leading $(i-1)$ vehicles as one single virtual vehicle, which affects the anterior SMV of the ith vehicle. The maximum and minimum trajectories of a single virtual vehicle in front of the ith vehicle are

$$\min_{1 \le l \le (i-1)} d_{l,max}(kT+\Delta t) \quad \text{and} \quad \min_{1 \le l \le (i-1)} d_{l,min}(kT+\Delta t),$$

respectively. This implies that the maximum trajectory of a leading virtual vehicle is described as the upper path consisting of minimum values among the maximum trajectories of other leading vehicles in time, while its minimum trajectory is characterized as the lower path constituting minimum values among its other leading vehicles' minimum trajectories. The concept of the maximum and minimum trajectories of a leading virtual vehicle is well supported by the fact that minimum values, not maximum values, among the maximum and minimum trajectories of the leading vehicles actually have a decisive effect on the safety level of rear-end collision risk. We note that, by (4.1) and (4.4), the anterior SMV of the ith vehicle (4.7) is exactly identical to that of the second vehicle, which follows a single virtual vehicle whose maximum and minimum trajectories are $\min_{1 \le l \le (i-1)} d_{l,max}(kT+\Delta t)$ and $\min_{1 \le l \le (i-1)} d_{l,min}(kT+\Delta t)$, respectively.

4.4.2 Computational complexity reduction for the anterior safety marginal value

As the value of i increases, the computational complexity for the anterior SMV (4.7) in Theorem 4.12 dramatically grows because this formula considers all of the lead-

ing vehicles in determining the anterior SMV. Let us consider that the finite space horizon that affects the anterior SMV of the ith vehicle. The space horizon is defined as the number of leading vehicles that are needed in order to affect non-unity SMV. Let $SH_i^A(kT)$ denote the space horizon for the anterior SMV of the ith vehicle at time kT. The definition of the anterior space horizon yields its mutual relation with the anterior SMV.

Lemma 4.13. *$SH_i^A(kT) = 0$ if and only if $SMV_i^A(kT) = 1$. However, $SH_i^A(kT) \in \mathbb{N}$ if and only if $SMV_i^A(kT) \in [0, 1)$.*

Note that the zero value of the anterior space horizon guarantees collision-free travel by the CA margin time, whereas the non-zero value implies that a rear-end collision might occur with some positive probability. For example, if the anterior space horizon is 1 for the ith vehicle, it is likely that the ith vehicle will crash into only the $(i-1)$th vehicle; that is, it will never collide with any other leading vehicles except the $(i-1)$st vehicle by the CA margin time of the ith vehicle. In this case, an interesting observation provides that the minimum trajectories of any other leading vehicles in front of the $(i-1)$st vehicle are farther than that of the ith vehicle consistently by the CA margin time of the ith vehicle; that is, $d_{j,min}(kT + \Delta t) > d_{i,min}(kT + \Delta t)$ holds for all $j \in [1, i-2]$ and for all $\Delta t \in [0, h_i(kT)]$, and there exists some $\Delta\hat{t} \in (0, h_i(kT)]$ such that $d_{i-1,min}(kT + \Delta t) = d_{i,min}(kT + \Delta t)$. In addition, $d_{i-1,min}(kT + \Delta t) > d_{i,min}(kT + \Delta t)$ for all $\Delta t \in \left[0, \Delta\hat{t}\right)$ and $d_{i-1,min}(kT + \Delta t) < d_{i,min}(kT + \Delta t)$ for all $\Delta t \in \left(\Delta\hat{t}, h_i(kT)\right]$.

Theorem 4.14. ***Finite Anterior Space Horizon***

Suppose that there exists $j_i = \max \mathcal{J}_i(kT)$ for every $i \geq 2$ and for every $k \in \{0 \cup \mathbb{N}\}$ such that

$$\mathcal{J}_i(kT) = \underset{l \in [1,i]}{\operatorname{argmin}} \left\{ d_{l,max}(kT + h_i(kT)) \right\}.$$

Then, the finite anterior space horizon of the ith vehicle at time kT is given by

$$SH_i^A(kT) = (i - j_i) \tag{4.19}$$

and its corresponding anterior SMV is

$$SMV_i^A(kT) = \min_{\Delta t \in (0, h_i(kT)]} \left\{ \left[\frac{\min\limits_{l \in [j_i,(i-1)]} \{d_{l,max}(kT+\Delta t)\} - d_{i,min}(kT+\Delta t)}{\min\limits_{l \in [j_i,(i-1)]} \{d_{l,max}(kT+\Delta t)\} - \min\limits_{l \in [j_i,(i-1)]} \{d_{l,min}(kT+\Delta t)\}} \right]_P \right\}. \tag{4.20}$$

Proof. Fix $i \geq 2$ and $k \in \{0 \cup \mathbb{N}\}$. Note that $\mathcal{J}_i(kT) \neq \emptyset$ and $\mathcal{J}_i(kT) \subset \{1, 2, \cdots, i\}$. Hence, by the supposition, there exists $j_i = \max \mathcal{J}_i(kT)$ such that

$$d_{j_i,max}(kT + h_i(kT)) \leq d_{l,max}(kT + h_i(kT)) \tag{4.21}$$

for all $l \in [1, i]$.

We suppose that $j_i = i$. By Lemmas 4.4 and 4.5, (4.21) yields

$$d_{i,min}(kT+\Delta t) < \min_{l \in [1,(i-1)]} \{d_{l,min}(kT+\Delta t)\}$$

for all $\Delta t \in (0, h_i(kT)]$, which gives

$$\begin{aligned} &\min_{l \in [1,(i-1)]} \{d_{l,max}(kT+\Delta t)\} - d_{i,min}(kT+\Delta t) \\ &\quad > \min_{l \in [1,(i-1)]} \{d_{l,max}(kT+\Delta t)\} - \min_{l \in [1,(i-1)]} \{d_{l,min}(kT+\Delta t)\} \end{aligned} \tag{4.22}$$

for all $\Delta t \in (0, h_i(kT)]$. Let us fix $\Delta\hat{t} \in (0, h_i(kT)]$. Let

$$d_{\bar{l},max}\left(kT+\Delta\hat{t}\right) = \min_{l \in [1,(i-1)]} \left\{d_{l,max}\left(kT+\Delta\hat{t}\right)\right\}.$$

Since $d_{\bar{l},min}(kT+\Delta t) < d_{\bar{l},max}(kT+\Delta t)$ for all $\Delta t \in (0, h_i(kT)]$, we have

$$\begin{aligned} \min_{l \in [1,(i-1)]} \left\{d_{l,min}\left(kT+\Delta\hat{t}\right)\right\} &\leq d_{\bar{l},min}\left(kT+\Delta\hat{t}\right) \\ &< d_{\bar{l},max}\left(kT+\Delta\hat{t}\right) = \min_{l \in [1,(i-1)]} \left\{d_{l,max}\left(kT+\Delta\hat{t}\right)\right\}. \end{aligned} \tag{4.23}$$

Since $\Delta\hat{t} \in (0, h_i(kT)]$ is arbitrary, by (4.23),

$$\min_{l \in [1,(i-1)]} \{d_{l,max}(kT+\Delta t)\} - \min_{l \in [1,(i-1)]} \{d_{l,min}(kT+\Delta t)\} > 0 \tag{4.24}$$

for all $\Delta t \in (0, h_i(kT)]$. Hence, by (4.3), (4.22), (4.24), and Theorem 4.12, $SMV_i^A(kT) = 1$ also satisfies (4.20). Further, by the definition of the anterior space horizon or Lemma 4.13, $SH_i^A(kT) = (i - i) = 0$, which supports (4.19).

Now, we suppose that $j_i \neq i$. By the definition of the anterior space horizon, we need to show that $SH_i^A(kT) = (i - j_i) \in \mathbb{N}$ such that $SMV_i^A(kT) \in [0, 1)$. By Theorem 4.12, it is sufficient to prove that there exists some $\Delta t \in (0, h_i(kT)]$ such that

$$\left[\frac{\min\limits_{l \in [1,(i-1)]} \{d_{l,max}(kT + \Delta t)\} - d_{i,min}(kT + \Delta t)}{\min\limits_{l \in [1,(i-1)]} \{d_{l,max}(kT + \Delta t)\} - \min\limits_{l \in [1,(i-1)]} \{d_{l,min}(kT + \Delta t)\}} \right] < 1. \tag{4.25}$$

By Lemmas 4.4, 4.5, and (4.21), we have

$$d_{i,min}(kT + h_i(kT)) > d_{j_i,min}(kT + h_i(kT)) \geq \min_{l \in [1,(i-1)]} \{d_{l,min}(kT + h_i(kT))\},$$

which by (4.21) again,

$$\left[\frac{\min\limits_{l \in [1,(i-1)]} \{d_{l,max}(kT + h_i(kT))\} - d_{i,min}(kT + h_i(kT))}{\min\limits_{l \in [1,(i-1)]} \{d_{l,max}(kT + h_i(kT))\} - \min\limits_{l \in [1,(i-1)]} \{d_{l,min}(kT + h_i(kT))\}} \right] < 1.$$

This inequality specifies that there exists $\Delta t = h_i(kT)$ such that (4.25) holds and thus $SH_i^A(kT) = (i - j_i) \geq 1$ such that $SMV_i^A(kT) \in [0, 1)$, which supports (4.19).

Finally, we will show that (4.7) of Theorem 4.12 has a simplified version of (4.20), which is the corresponding anterior SMV to the finite space horizon $SH_i^A(kT) = (i - j_i)$. By (4.21),

$$d_{j_i,max}(kT + h_i(kT)) \leq d_{l,max}(kT + h_i(kT))$$

for all $l \in [1, j_i]$, which by Lemmas 4.4 and 4.5,

$$d_{j_i,max}(kT + \Delta t) = \min_{l \in [1,j_i]} \{d_{l,max}(kT + \Delta t)\} \tag{4.26}$$

and

$$d_{j_i,min}(kT + \Delta t) = \min_{l \in [1,j_i]} \{d_{l,min}(kT + \Delta t)\} \tag{4.27}$$

for all $\Delta t \in (0, h_i(kT)]$. Substituting (4.26) and (4.27) in (4.7) yields a reduced form of the anterior SMV for the ith vehicle at time kT

$$SMV_i^A(kT) = \min_{\Delta t \in (0, h_i(kT)]} \left\{ \left[\frac{\min\limits_{l \in [j_i,(i-1)]} \{d_{l,max}(kT + \Delta t)\} - d_{i,min}(kT + \Delta t)}{\min\limits_{l \in [j_i,(i-1)]} \{d_{l,max}(kT + \Delta t)\} - \min\limits_{l \in [j_i,(i-1)]} \{d_{l,min}(kT + \Delta t)\}} \right]_P \right\}$$

as required. □

Note that the larger the value of i, the more complicated the formula of the anterior SMV. However, we can dramatically prune the general form of the anterior SMV with the following easy search at the CA margin time of the ith vehicle by examining the anterior space horizon $(i - j_i)$, where $j_i = \max \mathcal{J}_i(kT)$ such that

$$\mathcal{J}_i(kT) = \underset{l \in [1,i]}{\operatorname{argmin}} \{d_{l,max}(kT + h_i(kT))\}.$$

4.5 Simulation Results and Discussions

In this Section, we examine the simulation results of the proposed anterior space horizon and corresponding anterior SMV; the former is used to reduce the computational complexity dramatically required to determine the latter.

4.5.1 Description of the simulation environment

It is assumed that a string of vehicles is moving on a long corridor of a 2 km looping road. Unlike a straight road, every vehicle uses the vehicle states of all vehicles to provide the anterior SMV, since all vehicles except itself are its leading vehicles on a looping road. For instance, when the number of vehicles traveling on our considered roadway is M, the leading vehicles of the first vehicle (i.e., lead-most vehicle) are from the Mth vehicle (i.e., last-most vehicle) to the second vehicle. Also, the velocity and position of the first vehicle are influenced by its leading vehicles. There are two critical reasons why we prefer a looping road rather than a straight road for simulation: 1) the given constant density can be maintained until the simulation is terminated; and 2) no boundary condition for the lead-most vehicle is necessary. Furthermore, Mason *et al.* [65] showed that traffic characteristics such as stability and the propagation of disturbances are observed for looping and linear roads in the case that a large number of vehicles travel on a long roadway. In that regard, many researchers in practice have been carrying out computer simulations on a long corridor of looping roads.

We use the initial conditions for simulation that every vehicle starts to move with zero velocity and at a random location on a given looping system. We also suppose that every traveling vehicle on a vehicular traffic network employs the same car-following

model to update its vehicle states. The example car-following model exploited in this Chapter is the Gipps car-following model. This model consists of a few parameters mimicking the behavior of real traffic. A different combination of parameters affects the safety level of collision risk. In addition, it is reasonable to assume that vehicles in a platoon travel on a single-lane road where there is no overtaking, because we only examine the anterior SMV as a traffic safety indicator for a rear-end collision without taking account of lane changing models. Therefore, we observe our developed anterior SMV under various variables provided from the Gipps car-following model. Note that the proposed safety assessment tool does not aim at comparison with car-following models to figure out the best. Its true purpose is to provide an unbiased safety evaluator for a certain combination of parameters defined in a car-following model and to specify a realistic safety reference for an auxiliary driving control such as autonomous driving and automatic cruise control.

We define several states as a result of our simulation: a global steady-state, a local steady-state, and a catastrophe state. In general, the local traffic flow characteristics, such as the density, velocity, and flow, vary as functions of the position. However, when all vehicles move at the same speed with respect to time without crashes, it should be treated as a steady-state. Furthermore, if all vehicles maintain constant and time independent car spacing, we can specify that the traffic system realizes a global steady-state. This implies that the traffic flow on a corridor of a vehicular network is constant in a global steady-state. On the contrary, if we look at a sufficiently small part of a vehicle platoon, both velocity and car spacing are essentially constants only for each part of a string. The main difference compared to a global steady-state is that constant car spacing is valid only microscopically, when this small traffic system reaches a local steady-state. Since we assume that the same car-following model is applied to all vehicles and thus driving characteristics are the same for every vehicle in our simulation, once the vehicular traffic system establishes a steady-state, all vehicles remain in corresponding steady-states without a rear-end collision. In other words, before reaching a steady-state, we can observe an accident according to the values of variables of a car-following model, which is defined as a catastrophe state.

4.5.2 Gipps car-following model

We employ the Gipps car-following model to examine traffic safety through the help of the anterior SMV. Gipps provided a car-following model describing the behavior of driver response based on the supposition that a driver incorporates an additional breaking reaction time for safety [43, 44]. The new velocity of the ith vehicle for the next time step, $v_i\left(\left(k+1\right)T\right)$, is determined from the Gipps car-following model given by

$$v_i\left(\left(k+1\right)T\right) = \min\left\{v_i\left(kT\right) + 2.5\,a_{i,max}^{+}T\left(1-\frac{v_i\left(kT\right)}{v_f}\right)\sqrt{0.025+\frac{v_i\left(kT\right)}{v_f}},\right.$$
$$\left. b_i\left(\frac{T}{2}+\theta\right)+\sqrt{b_i^2\left(\frac{T}{2}+\theta\right)^2 - b_i\left\{2s_i\left(kT\right)-v_i\left(kT\right)T-\frac{v_{i-1}\left(kT\right)^2}{\hat{b}_{i-1}}\right\}}\right\}, \tag{4.28}$$

where $s_i\left(kT\right)$ is the car spacing between two consecutive vehicles, the ith and $(i-1)$st vehicles, defined as $s_i\left(kT\right) = \left[x_{i-1}\left(kT\right) - x_i\left(kT\right) - l_{i-1}\right]$ at time kT, $a_{i,max}^{+}$ denotes the maximum acceleration rate for the ith vehicle to be willing to undertake, v_f is the maximum velocity that is the same for all vehicles, θ is a safety margin time that is an additional delay for safety, b_i is the most severe deceleration rate undertaken by the ith vehicle, and $\hat{b}_{i-1}$ is the brake rate of the $(i-1)$st vehicle predicted by its following, the ith vehicle. Gipps initially used the braking reaction time, which is the elapsed time between the recognition of a safety hazard and the commencement of the brakes, instead of the update time interval (T) in (4.28). However, we interpret the braking reaction time as the update time interval, according to his remark that traffic flow behaves well even when it is replaced with T. The first argument of the the Gipps traffic model (4.28) is attained in free-flow condition, whereas the second argument is dominated in a congested traffic situation. We note that the newly generated velocity is truncated by both 0 and v_f.

4.5.3 Simulation results

In our simulation, we use the following parameters: All vehicles in a traffic system generate the vehicle states at every time step of $T = 60$ s. The maximum

acceleration rate, $a^{+}_{i,max}$, is a constant of $a^{+}_{max} = 4.41\ m/s^2$ for all vehicles. v_f is equal to 117 km/h, which is the average value of the maximum velocity measured in the USA [37]. This typical measured maximum velocity is greater than the speed limit, because people normally drive faster than the speed regulated by law. We set a safety margin time of θ to 0 s to ensure that the time interval to update both the vehicle states and the anterior SMV depends on only T, not on θ. The length of the ith vehicle, l_i, is equal to L for all vehicles, where L denotes the average safety length of vehicles of 6.7 m. The most severe deceleration rate and estimated brake rate are constants for all vehicles with $b_i = b = 3\ m/s^2$ and $\hat{b}_i = \hat{b}$. The density is 31 v/km/lane (50 v/mile/lane) with the units presenting the number of vehicles per kilometer (or mile) per lane. The given value is a so-called low-congested density.

We take three different values of the estimated deceleration rate of the vehicle in front, $\hat{b}$, with the fixed value of b. Our conjecture about the relationship between the most severe brake rate and estimated retardation rate is as follows: as the value of $\hat{b}$ decreases, given the fixed value of the true applied brake rate of b, the traffic system is transformed from a collision-free state to a catastrophe state of inevitable rear-end collisions. The reason is that every vehicle brakes much harder than the following vehicle expects, incurring a terrible tailgating phenomenon by the following vehicle. We will illustrate the simulation results regarding the anterior space horizon and corresponding anterior SMV depending on the value of $\hat{b}$.

Global Steady-state

We set $\hat{b} = 5\ m/s^2$. Comparing it with $b = 3\ m/s^2$ means that every vehicle decelerates less than its following vehicle predicts. This leads to enough car spacing between any two consecutive vehicles, ensuring no risk of collision. In other words, every vehicle behind performs perfect defensive driving.

Various simulation results using the Gipps car-following model under $\hat{b} = 5m/s^2 > b = 3m/s^2$ are shown in Figs. 4.4 and 4.5. These are truncated by the simulation time of 1500 s, since the vehicular system reaches a steady-state and thus there is no longer an observable change. Fig. 4.4(a) depicts the average speed of all vehicles over a long corridor of 2 km. The vehicular system in this scenario establishes a steady-state, because

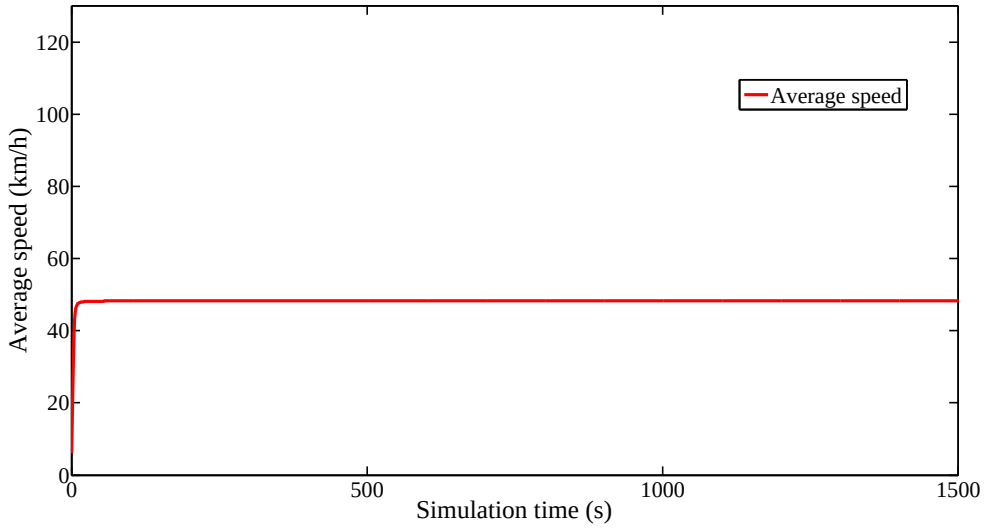

(a)

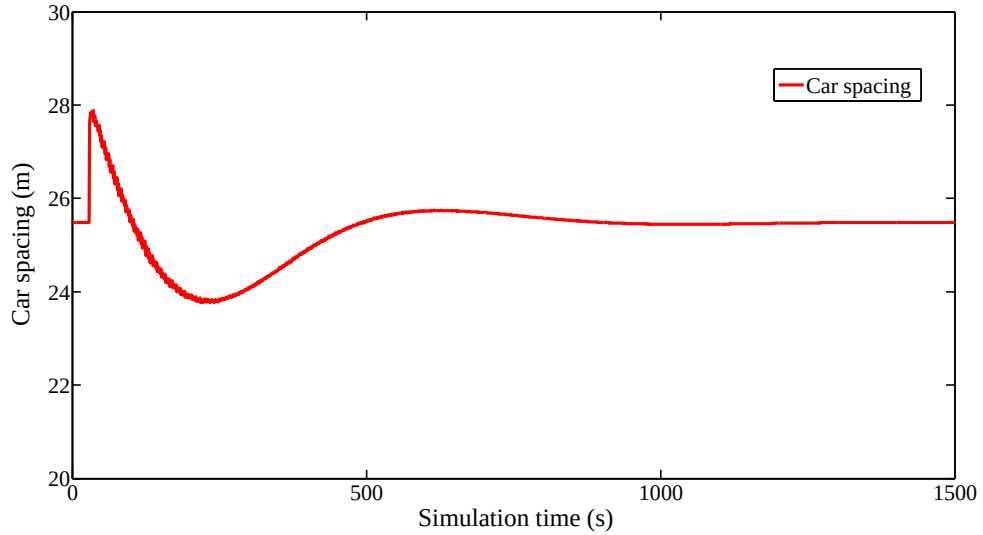

(b)

Figure 4.4: Simulation results of the Gipps car-following model under $\hat{b} = 5m/s^2 > b = 3m/s^2$. (a) Average speed of vehicles in simulation time. (b) Average car spacing of vehicles passing at a certain microscopic spot in simulation time.

the average speed of all vehicles, as well as the velocity of each individual vehicle, converge to around 50 km/h, as the simulation time goes. Defensive driving explains why the observed average speed is much less compared to the maximum velocity of $v_f = 117$ km/h. This light traffic congestion can be relieved by decreasing the value of $\hat{b}$ under the given b. In addition, we measure the car spacing data of the vehicles passing at a certain

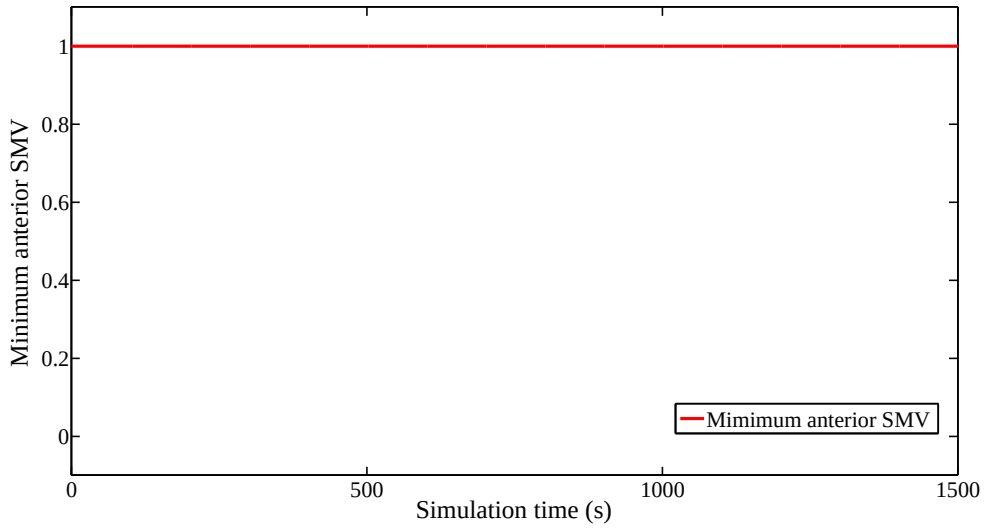

(a)

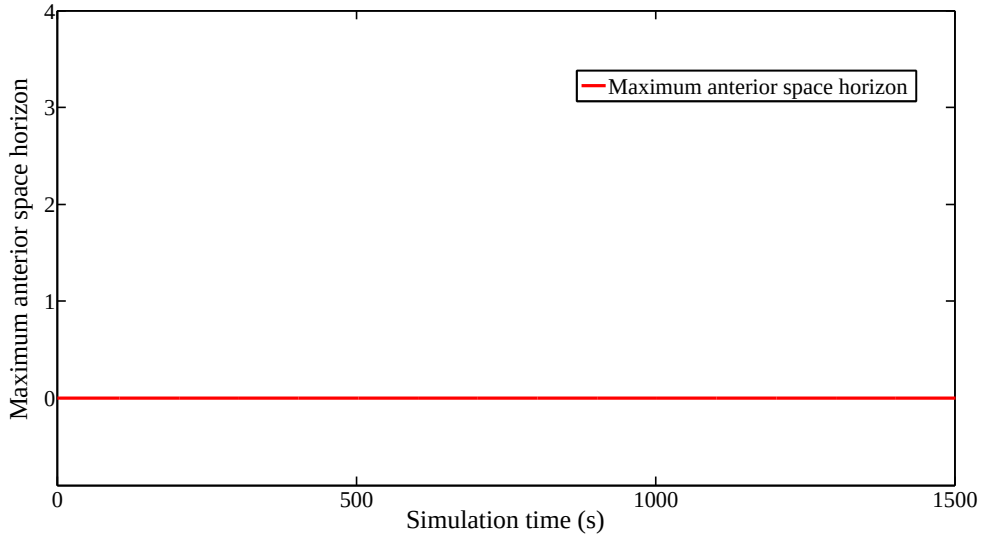

(b)

Figure 4.5: Safety indicator results of the Gipps car-following model under $\hat{b} = 5m/s^2 > b = 3m/s^2$. (a) Minimum value of anterior SMVs of all vehicles in simulation time. (b) Maximum value of their anterior space horizons in simulation time.

point of a road over every single update time interval and take its average. The average car spacing of any two consecutive vehicles passing at a microscopic spot is represented in Fig. 4.4(b). Its initial fluctuation between 23.5 m and 28 m decays as the simulation time goes. This observation implies that every vehicle keeps traveling with the same car

spacing of around 25.5 m towards the vehicle immediately in front it, which is defined as a global steady-state.

All vehicles calculate their anterior space horizon and corresponding anterior SMV at every time step, which refer to (4.19) and (4.20), respectively. The minimum value of the computed anterior SMVs of all vehicles with respect to time is shown in Fig. 4.5(a), while the maximum value of their anterior space horizons in simulation time is represented in Fig. 4.5(b). The minimum value of the anterior SMV and maximum value of the anterior space horizon in time can be denoted as

$$\min_{i\in[1,M]} \left\{SMV_i^A\left(kT\right)\right\} \quad \text{and} \quad \max_{i\in[1,M]} \left\{SH_i^A\left(kT\right)\right\}$$

for every $k \in \{0 \cup \mathbb{N}\}$, respectively. Here, M denotes the number of vehicles traveling on a vehicular traffic network. Since the minimum value of the anterior SMVs is 1 by the end of the simulation, we note that every vehicle always has an anterior SMV of 1. By the definition of the anterior SMV, this implies that every vehicle will always travel without collision unless an abrupt perturbation exists. Similarly, according to the simulation result related to the anterior space horizon, no leading vehicle influences its following vehicles to have non-unity anterior SMV. These two results show coherence to Lemma 4.13.

Therefore, this experiment enables the vehicular traffic system to achieve a global steady-state as well as to support perfect safety, if every vehicle uses the defensive driving habits with enough car spacing based on the presumption that its leading vehicle brakes less than expected. Now, we will investigate the other two states by decreasing only the value of $\hat{b}$.

Local Steady-state

We set the estimated deceleration rate of the vehicle ahead to $\hat{b} = 2.6m/s^2$, which is slightly less than $b = 3m/s^2$. It can be understood that every vehicle brakes slightly harder than its following vehicle anticipates.

The average speed of all vehicles and average car spacing of two consecutive vehicles are shown in Fig. 4.6(a) and 4.6(b), respectively. The average speed approaches the maximum velocity of $v_f = 117km/h$. In contrast, the car spacing fluctuates constantly between around 23.5 m and 27.5 m. These two results produce the traffic flow

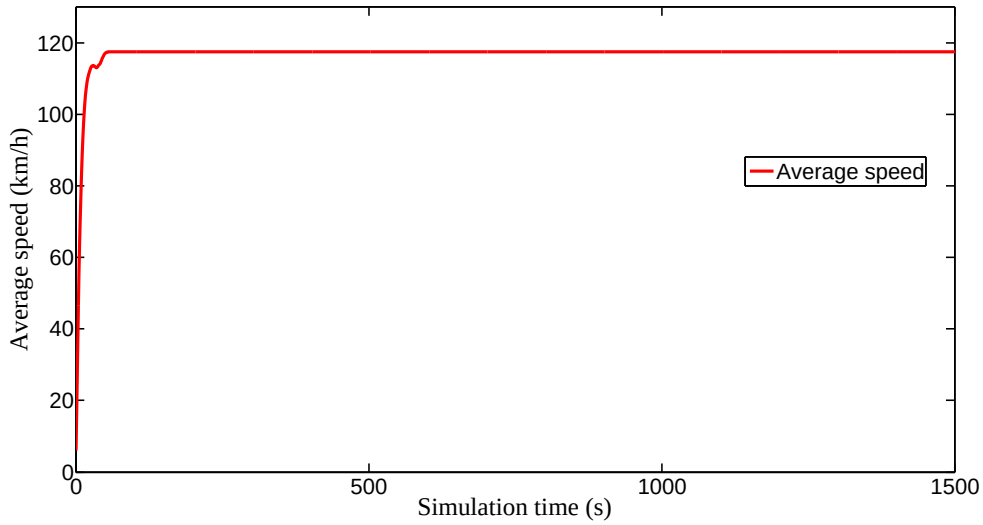

(a)

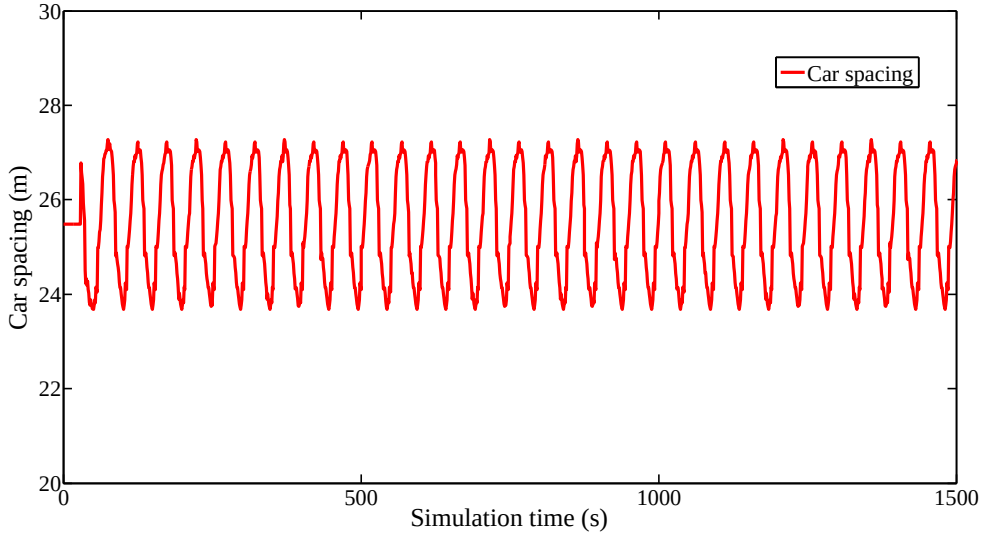

(b)

Figure 4.6: Simulation results of the Gipps car-following model under $\hat{b} = 2.6m/s^2 < b = 3m/s^2$. (a) Average speed of vehicles in simulation time. (b) Average car spacing of vehicles passing at a certain microscopic spot in simulation time.

characterizing a local steady-state. In other words, once vehicles travel as fast as the maximum velocity, the system reaches a steady-state; each vehicle has the same velocity of v_f, but with different and time-invariant car spacing. A set of car spacings for all vehicles fixed in a local steady-state is formed according to their initial random locations.

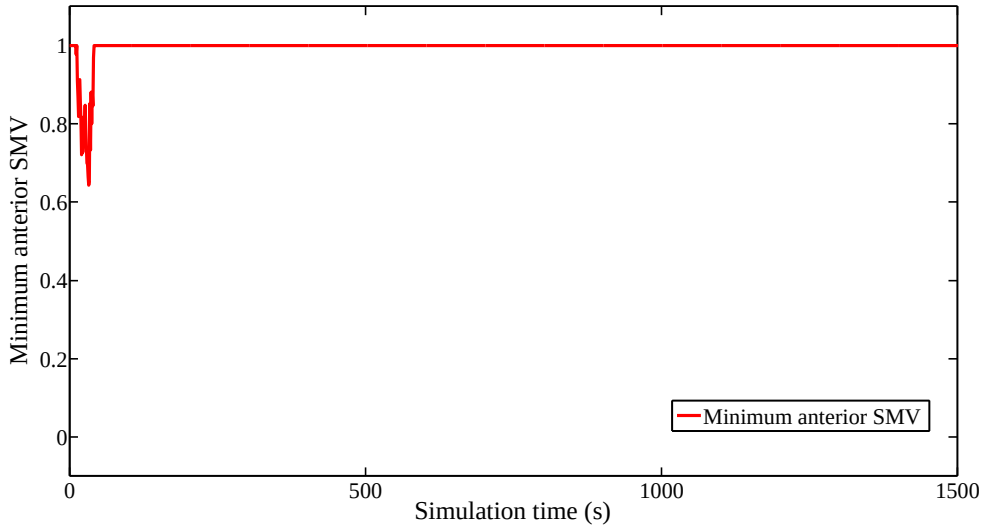

(a)

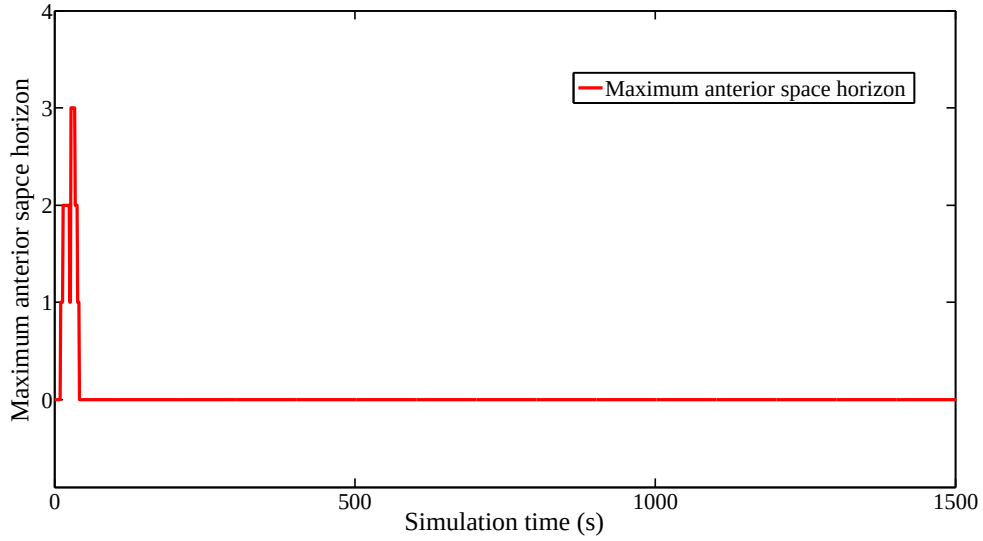

(b)

Figure 4.7: Safety indicator results of the Gipps car-following model under $\hat{b} = 2.6m/s^2 < b = 3m/s^2$. (a) Minimum value of anterior SMVs of all vehicles in simulation time. (b) Maximum value of their anterior space horizons in simulation time.

Fig. 4.7 describes the evolution of the minimum anterior SMV and maximum anterior space horizon for every vehicle in simulation time. One observes that at least one vehicle provides non-unity anterior SMV and non-zero anterior space horizon before establishing a steady-state of around 100 s as shown in Fig. 4.6(a). The minimum anterior

SMV falls to around 0.65, whereas the maximum anterior space horizon increases to 3. This indicates that the vehicle travels with mounting collision risk. Fortunately, $\hat{b}$ and b are similar in rate, which means the vehicle can escape gradually from a dangerous accident zone by performing moderate driving. A driver having moderate driving behavior is neither a slowpoke nor a tailgater. He is in between these two extremes and is described as a generally typical driver. Finally, once the vehicular traffic system reaches a steady-state, no vehicle has a leading vehicle that affects non-unity anterior SMV. Thus, a platoon of vehicles using the Gipps car-following model with the variables defined in this experiment can travel under perfectly safe conditions in spite of the existence of rear-end collision risk possibility in the early simulation phase.

Catastrophe State

We reduce the estimated brake rate to $\hat{b} = 1.4m/s^2$, which is much less than the most severely applied brake rate of $b = 3m/s^2$. This relation signifies that every vehicle brakes much harder than its following vehicle expects, which results in car spacing being narrow enough to be about to collide. In other words, drivers under these conditions can be considered as tailgaters.

The changes of the safety indicator values in time, up until a rear-end collision occurs, are shown in Fig. 4.8. Since vehicles are tailgating recklessly, a crash can be observed at barely 12 s. There exists at least one vehicle having non-unity anterior SMV and anterior space horizon of 1 from 6 s. Hence, owing to the vehicle's stubborn tailgating driving, it finally causes an accident with the vehicle in front. This could be avoided by creating enough car spacing through a decrease in its velocity. However, a string of vehicles traveling with an adversely big gap between two brake rates has no choice but to land in a catastrophe state.

Different simulation experiments for establishing a local steady-state or a catastrophe state show non-unity anterior SMV during the initial simulation times. The estimated brake rate being slightly less than the practical deceleration rate lets the vehicle with non-unity anterior SMV have an opportunity to gradually escape from the dangerous accident zone. However, if the anticipated brake rate is much less than the practical deceleration rate, the vehicle with non-zero anterior space horizon must collide with the

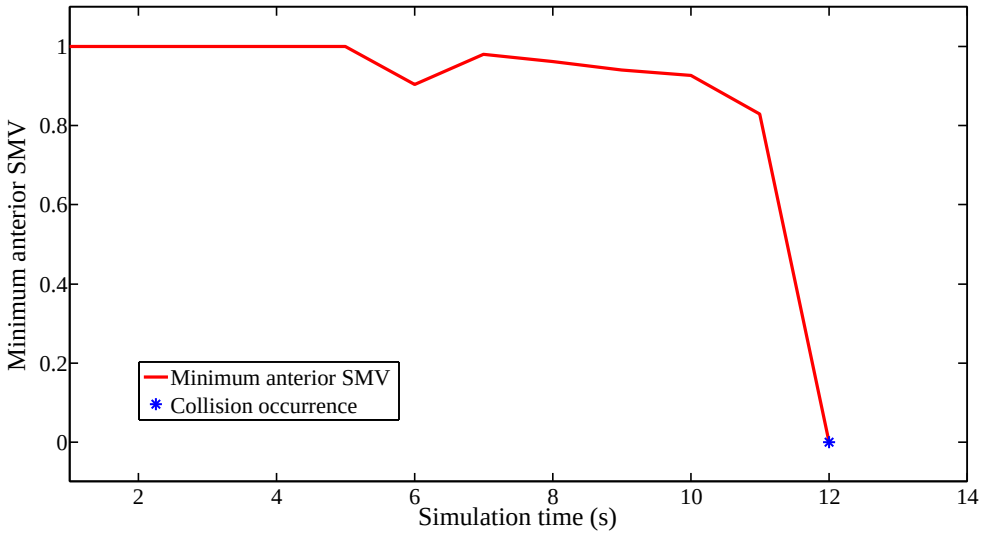

(a)

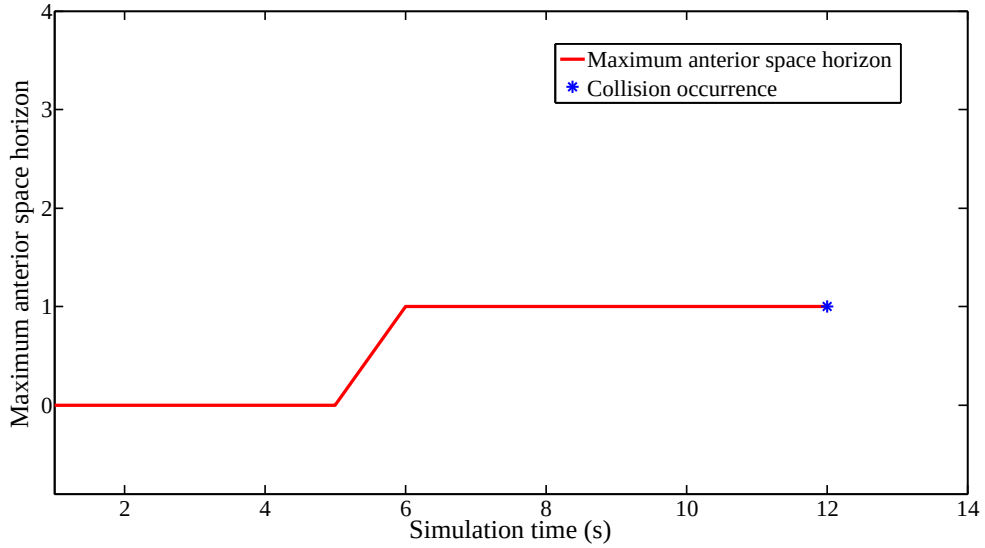

(b)

Figure 4.8: Safety indicator results of the Gipps car-following model under $\hat{b} = 1.4m/s^2 < b = 3m/s^2$. (a) Minimum value of anterior SMVs of all vehicles in simulation time. (b) Maximum value of their anterior space horizons in simulation time.

vehicle in front by maintaining the value of the predicted brake rate as shown in a catastrophe state. This comparison gives us remarkable results. When a vehicle controlled by the Gipps car-following model provides non-unity anterior SMV, if it automatically increases the estimated brake rate for its leading vehicle, it can provide an increase in

the collision avoidance possibility. Therefore, our proposed anterior SMV is verified as a rigorous and magnificent safety indicator to warn of the likelihood of a collision and to prevent a rear-end crash.

4.6 Summary

The proposed safety marginal value (SMV) can be utilized as a traffic safety metric to prevent unexpected vehicle-to-vehicle collisions on roadways. The anterior SMV indicates the safety level of a rear-end accident with the vehicles ahead, as calculated by its collision avoidance (CA) margin time. Every vehicle on a vehicular traffic network uses a set of vehicle states to determine the anterior SMV for every time step. The vehicle states contain the position, velocity, and lane index of all vehicles.

We have provided a simpler, general form for the anterior SMV, even in instances when multiple vehicles travel on roadways. However, since this general form requires an explosive increase in computational complexity with respect to the number of vehicles, we defined the space horizon for the anterior SMV, which is the finite number of leading vehicles that affect non-unity anterior SMV. In other words, the finite anterior space horizon obtained by an easy search at the CA margin time remarkably prunes the computational complexity in determining the anterior SMV. To show the effectiveness and efficiency of our proposed anterior SMV, we employed the Gipps car-following model to present simulation results. The non-unity value of the anterior SMV implies the existence of collision likelihood by the CA margin time. Our simulation showed that the vehicular traffic network reaches two different states upon non-unity anterior SMV. A vehicle with positive collision possibility escapes from a dangerous collision zone by driving moderately, and thus the system realizes a collision-free steady-state. On the contrary, a vehicle will ultimately crash into other leading vehicles by performing stubborn tailgating driving in spite of the alarm by the anterior SMV warning of imminent danger of collision.

Therefore, we conclude that the anterior SMV can be used as a rigorous safety criterion to indicate the collision avoidance level of rear-end collision risk when evaluating various conditions consisting of different variables provided in a car-following

model. As further work, we need to investigate how to use the calculated anterior SMV in controlling the velocity of a vehicle for the next time step so as to guarantee collision-free driving. In addition, it will be necessary to study how to extend the concept of our proposed safety metric into a primary parameter of an objective function to maximize safety or to minimize congestion in vehicular traffic networks.

Chapter Acknowledgments

Chapter 4, in full, is a reorganized version of the following manuscript. Seokheon Cho and Ramesh R. Rao. “A new safety metric for vehicular traffic networks,” *in preparation*.

Chapter 5

A Target Time-gap-based Velocity Update Model

We provide a car-following model called a target time-gap-based velocity update model in this Chapter. Every vehicle in a vehicular traffic network uses our proposed model to refresh its velocity and position for the next time step based on the given target time gap. The allocation of the target time gap value for an individual vehicle can be utilized in various ways; for example, the target time gap can be the constant for every vehicle, or it can follow a distribution. The results of a microscopic traffic simulation based on our proposed car-following model are well validated with empirical traffic data. This implies that a target time-gap-based velocity update model mimics the typical behavior of drivers. A safety analysis of a target time-gap-based velocity update model is performed with the help of the anterior SMV, which is a traffic safety metric to indicate the likelihood of accident occurrence. Using the anterior safety marginal value (SMV) as a tool, three different regions are defined with respect to the traffic density, the constant target time gap applied for all vehicles, and the update time interval needed to refresh the velocity of vehicles: a collision-free region, a transition region, and a catastrophe region. A collision-free area is the sub domain of the target time gap and the update time interval under fixed traffic density, which always assures the collision-free movement of vehicles unless an abrupt perturbation exists. On the contrary, a catastrophe area is the sub domain that will result in accidents. We also provide the mathematical analysis for a steady-state of a target time-gap-based velocity update model and compare it with the

microscopic traffic simulation results. Finally, the effective domain of the target time gap and the update time interval is presented, assuring both collision-free movements of vehicles and a system capacity improvement compared to the traffic measurement data.

5.1 Introduction

The provisions of a macroscopic traffic flow model are considered fundamentally essential to understand traffic flow dynamics. A macroscopic traffic flow model forms the basis of the fundamental diagram delineating the relationship among traffic density, flow, and velocity on highways. A macroscopic fundamental diagram is used to estimate traffic flow and to regulate the metered rate at entrance ramps along a highway corridor. The first attempt at modeling traffic flow at the macroscopic level was made by Greenshields [18]. He proposed a linear velocity-density fundamental diagram, which implies a parabolic shaped flow-density curve, under uninterrupted traffic flow conditions. Lighthill, Whitham, and Richards (LWR) [19, 20] developed a concave fundamental diagram, called the first-order LWR model, based on Greenshields's hypothesis and a nonlinear conservation law of vehicles. Despite its simplicity and its successful explanation for the formation and backward propagation of traffic disturbances, the first-order LWR model fails to describe various traffic features, such as capacity drop and traffic hysteresis. Several high-order macroscopic traffic flow models were developed in order to resolve the drawbacks of the LWR model. These include the second-order Payne-Whitham (PW) model [66, 67], the second-order Aw-Rascle-Zhang (ARZ) model [68, 69], and the third-order model introduced by Helbing [70]. Newell [21] initially proposed a triangular flow-density fundamental diagram, which is a simpler alternative to the first-order LWR model. The Newell model is characterized by two velocities: a maximum free-flow velocity in a free-flow regime and a propagation velocity in a congested situation. However, the Newell model is limited because it does not specify the relation between propagation velocity and the typical behavior of drivers. The time-gap-based traffic model introduced by Cho *et al.* [37] is also a triangular flow-density curve such as the Newell model, but it is generally verified by empirical traffic data irrespective of highway areas, and it specifically explains the Newell model

by using three major parameters: the maximum free-flow velocity in a free-flow regime, a typical safety length of vehicles, and an average value of the measured time gap in a congestion condition.

In contrast to a macroscopic fundamental diagram, a microscopic traffic flow model specifies the microscopic dynamic properties, such as the velocity and position, of a single vehicle. In particular, a car-following model describes the behavior of driver response to the leading vehicle in the same lane. Car-following models are generally divided into three types according to the formation hypothesis of each model: the Gazis-Herman-Rothery (GHR) family of models, the safety distance or collision avoidance (CA) models, and the psychophysical or action point (AP) models. The GHR model [42], the most well-known car-following model, states that an individual driver's acceleration is proportional to the velocity of his vehicle, relative speed, and car spacing to its leading vehicle. The representative safety distance or CA model introduced by Gipps [43] has an assumption that the driver of a following vehicle incorporates a braking reaction time in order to keep an adequate distance from its leading vehicle for safety. In particular, the Gipps model describes the behavior of following vehicles subjected to different traffic conditions, such as free-flow and congested flow. AP models initially discussed by Michaels [71] use thresholds where a vehicle changes its dynamic properties. That is, a vehicle reacts to variations in relative speed or car spacing to the vehicle in front of it only when the relevant defined thresholds are reached [72, 73]. The existing car-following models, such as the GHR model, the CA model, and the AP model, describe a driver's response to the behavior of a leading vehicle, and their results match with empirical traffic data. However, they lack in an investigation of their usability, safety, and capacity analysis. These models cannot be correlated with any existing macroscopic traffic flow model to show how they would function from the point of view of flow characteristics. Another drawback of these models is that the macroscopic level results obtained from them cannot support macroscopic traffic features such as capacity drop and traffic hysteresis. These two weaknesses suggest that the usability of the existing car-following models is limited. The capacity drop is defined as a discharge flow drop after a local traffic disruption becomes active [74, 75, 76]. In particular, Koshi *et al.* [74] suggested that the traffic flow-density relationship resembles a reversed λ shape

with a capacity drop of 1% to 18% from the achievable maximum flow in a free-flow regime to that in a congested region at the same density value [77, 78, 79, 80]. Traffic hysteresis is explained by the phenomenon of the acceleration curve lying below the deceleration curve at the same density [41, 81, 82]. In other words, vehicular traffic networks exhibit traffic hysteresis when average traffic flow measured in the onset of congestion is higher than that observed while congestion is released. Also, since the existing car-following models were developed based on unrealistic suppositions that every driver always seeks safety without distraction, they cannot predict the unexpected and risky driving behavior of the vehicle in front. These models can predict incidents under some combinations of parameters defined in themselves, which raises doubts about perfect safety. Therefore, a new car-following model needs to be designed that possesses the following properties: (1) the model should mimic the typical behavior of drivers, (2) the model should have a close connection with a macroscopic fundamental diagram, (3) the results obtained from the model should describe the traffic flow characteristics such as capacity drop and traffic hysteresis, (4) the analysis of usability, safety, and capacity for the model should be feasible, and (5) the parameters in the model should be provided, particularly for ensuring safety and capacity enhancements.

If all vehicles in a vehicular traffic network use the same car-following model, they tend to form a platoon of finite vehicles. The selection of values for the parameters defined in a car-following model decides whether a string of vehicles either reach a steady-state or make collisions. The so-called string stability containing a steady-state car-following mode have been studied [83, 84]. Four control policies, which maintain constant car spacing, constant time headway, constant velocity, and constant safety factor, have been mainly considered for vehicle follower systems. The string stability ensures that errors of this individual control policy decrease as it propagates along the vehicle stream. Vehicle-to-vehicle (V2V) wireless communication was shown to be important in order to achieve string stability with the given control policies, particularly with the constant car spacing [85]. Centralized control as well as decentralized regulation for a string of coupled traveling vehicles have been examined [83, 86]. When a discrete-time and continuous-space car-following model is considered, its string stability is able to depend on traffic density and the update time interval being frequency of

update in time. Therefore, an analysis of safety and capacity of a car-following model, when a vehicular traffic system reaches string stability, is necessary according to the key parameters, such as traffic density, the update time interval, and so on, defined in the model.

A traffic safety indicator can be used to analyze the safety of a car-following model. Hayward [55] initially introduced Time-to-Collision (TTC), which is the time required for two consecutive vehicles in the same lane to collide if they consistently move at their current velocity. The smaller the TTC, the higher the risk of a rear-end collision. TTC has been verified as an effective quantitative indicator to rate collision risk. Another widely known safety measure is time headway, which is defined as the time it takes to travel the distance from the front end of a vehicle to that of the vehicle in front. Suitable ranges of the safety indicators, such as TTC and time headway, have been studied to ensure collision-free movements of all vehicles through empirical traffic data or microscopic traffic simulation results [59, 63, 64]. However, the suggested bounds of TTC and time headway change for different traffic conditions and are ambiguous for specifying the safety level of collision risk. In order to resolve the limitations of the TTC and time headway, a safety metric called the anterior safety marginal value (SMV) was presented in Chapter 4. The anterior SMV has the efficient capability to provide a numerical value that shows the likelihood of incident occurrence and applies identically to all vehicles, irrespective of various traffic situations.

The remainder of this paper is organized as follows: In Section 5.2, a brief explanation of the target time-gap-based traffic model, which is a macroscopic fundamental diagram, and the reasonable justification for its extension to a car-following model are stated. In addition, we provide a new car-following model, called a target time-gap-based velocity update model, which is developed from the the time-gap-based traffic model. We present a vehicular traffic network for various analysis of our proposed car-following model in Section 5.3. In Section 5.4, the average time gap with respect to traffic density and traffic flow with respect to density under various target time gap values are obtained in order to show the usability of the target time-gap-based velocity update model. We mention the anterior SMV as a traffic safety metric used to analyze the safety of the model in Section 5.5. Rear-end collision risk evolutions in simulation time

are observed under four scenarios depending on the values of the target time gap and the update time interval with the help of the safety indicator. In addition, the collision ratio according to a combination of three key parameters in the target time-gap-based velocity update model is examined. We introduce three different regions to describe the collision ratio and emphatically assert the importance of the selection of three primary parameters' values for collision-free movements of vehicles in our considered vehicular traffic flow. In Section 5.6, the average practical time gap and the average system velocity in a steady-state of the model are analyzed mathematically and verified with the corresponding simulation results. In addition, the numerical capacity obtained from the analysis about the average system velocity and the empirical capacity measured in a highway are compared. The effective domain of the target time gap and the update time interval for each traffic density is presented, which ensures both system throughput improvement based on the comparative result in a steady-state and collision-free movements of vehicles.

5.2 A Target Time-gap-based Velocity Update Model

In this Section, we present a target time-gap-based velocity update model that is a simple and adequate car-following model. In addition, a time-gap-based traffic model [37], which is a macroscopic traffic flow model, is explained as a triggering point of a target time-gap-based velocity update model.

5.2.1 Time-gap-based traffic model

The time-gap-based traffic model shown in Fig. 5.1 is well validated with the traffic data measured from single-loop and double-loop detector systems using least squares matching, and with previous research on propagation velocity and driver reaction times [37]. In that regard, the time-gap-based traffic model is considered to be a good and simple representative fundamental diagram for describing traffic flow. The time gap is defined as the time required to travel the car spacing between two consecutive vehicles. In particular, the provided time-gap-based traffic model explains a triangular flow-density traffic model initially proposed by Newell [21], by using three

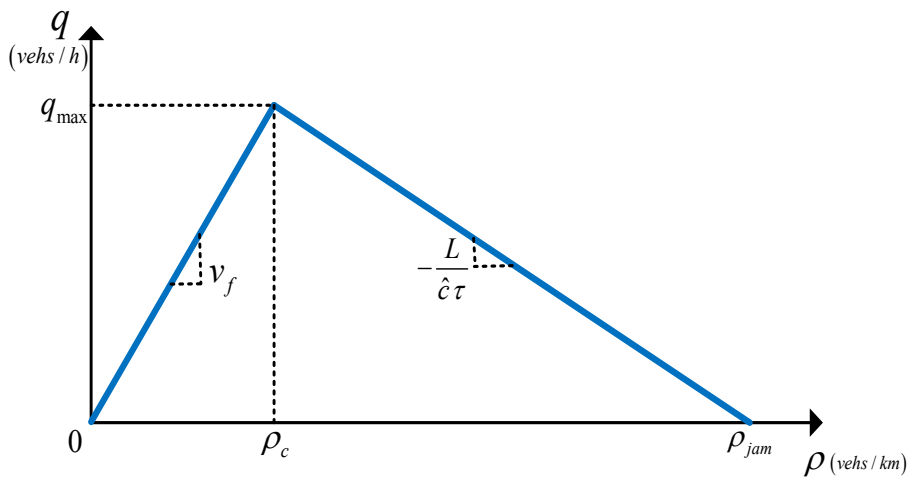

Figure 5.1: Time-gap-based traffic model.

key parameters: the maximum free-flow velocity defined in a free-flow region, an average safety length of vehicles, and a mean value of the time gap of traffic data defined during congested conditions.

Let q, ρ, and v denote traffic flow, density, and velocity per lane, respectively. Traffic flow means the number of vehicles passing over the unit time (in vehs/h) and traffic density is the number of vehicles traveling over the unit distance (in vehs/km). The unit of velocity is km/h. The flow-density fundamental diagram of the time-gap-based traffic model, which specifies a relation among traffic flow, density, and velocity, is given by

$$q = \min\left\{\rho\, v_f, \frac{1000 - \rho L}{\hat{c}\,\tau}\right\}, \tag{5.1}$$

where v_f is the maximum free-flow velocity (in km/h), L is an average safety length of vehicles (in m), τ is the mean value of the time gap defined in a congestion region (in s), and $\hat{c}$ is a constant of $1000/3600$. Here, the safety length of a vehicle is a summed value of its actual physical length and positive car spacing needed for safety when all vehicles stop completely, say 1 m.

As shown in Fig. 5.1, a vehicular traffic network attains the maximum capacity q_{max} at a value of the critical density ρ_c such that

$$\rho_c = \frac{1000}{\hat{c}\,\tau\, v_f + L}.$$

The corresponding maximal throughput is easily calculated from the relationship among traffic flow, density, and velocity, of $q = \rho v$. Also, we can define the jam density as $\rho_{jam} = 1000/L$.

The first argument of (5.1) is dominated in a free-flow traffic situation, while its second is attained in congested conditions. The traffic data measurement shows that the average and standard deviation of the time gap vary widely in a free-flow regime, whereas its average is nearly constant, and its standard deviation is small regardless of the value of traffic density, particularly when traffic density is larger than the critical density. A typical value of the time gap is a major parameter to describe traffic flow in a congestion region. Hence, this remarkable observation confirms that the time-gap-based traffic model is characterized as a well-defined macroscopic traffic flow model.

5.2.2 Target time-gap-based velocity update model

Contrary to a macroscopic fundamental diagram such as the time-gap-based traffic model, a microscopic traffic flow model specifies the interaction between consecutive vehicles traveling in the same lane by representing how a driver reacts to the changes in the relative velocity or position of the leading vehicle. A microscopic traffic flow model contains the flow dynamic properties such as the velocity and position of a single vehicle. The provision of a car-following model extended from the time-gap-based traffic model is meaningful owing to this fundamental diagram's merits.

Now, we provide a car-following model, called the target time-gap-based velocity update model, which reflects the time-gap-based traffic model well proposed by Cho *et al.* [37]. The target time-gap-based velocity update model considers a discrete-time and continuous-space vehicular traffic network.

Let $v_i\,(kT)$ denote the velocity of the ith vehicle at time kT for $i \in \mathbb{N}$ and for $k \in \{0 \cup \mathbb{N}\}$, where $\mathbb{N}$ is a set of natural numbers and T is the update time interval. That is, T is frequency of update in time to yield the new velocity and position of each vehicle. Also, the index of $(i-1)$ represents the lead of the ith vehicle. The new temporary velocity of the ith vehicle for next time step, which is determined from the

target time-gap-based velocity update model, is given by

$$\tilde{v}_i\left(\left(k+1\right)T\right) = \frac{s_i\left(kT\right)}{\hat{c}\,\tau_i\left(kT\right)}, \tag{5.2}$$

where $s_i\left(kT\right)$ is the car spacing between the ith vehicle and its leading $(i-1)$st vehicle, and $\tau_i\left(kT\right)$ denotes the time gap of the ith vehicle to the vehicle immediately ahead. This model shows that the newly calculated velocity of a vehicle is proportional to its forward car spacing, but is in inverse proportion to its time gap. Our proposed target time-gap-based velocity update model has the advantage that microscopic dynamic properties can be simply controlled by only two instantaneous variables of the car spacing and given target time gap. However, we need to take into account the limit of the new temporary velocity (5.2), since the acceleration and brake rates are practically bounded. Also, it is limited by both the zero velocity and the maximum free-flow velocity. Therefore, the new velocity of the ith vehicle at time $\left(\left(k+1\right)T\right)$ is given by

$$\begin{aligned} &v_i\left(\left(k+1\right)T\right) \\ &\quad = \max\left\{0, v_i\left(kT\right) + a_{max}^{-}\,T, \min\left\{v_f, v_i\left(kT\right) + a_{max}^{+}\,T, \tilde{v}_i\left(\left(k+1\right)T\right)\right\}\right\}, \end{aligned} \tag{5.3}$$

where a_{max}^{+} and a_{max}^{-} denote the maximum acceleration rate and maximum deceleration rate, respectively. These rates, $a_{max}^{+} > 0$ and $a_{max}^{-} < 0$, are finite bounded. This implies that $v_i\left(kT\right) + a_{max}^{+}\,T$ is the maximum realizable velocity and $v_i\left(kT\right) + a_{max}^{-}\,T$ is the minimum feasible velocity at next time step, when the current velocity is $v_i\left(kT\right)$. For simplicity of our analysis and simulation, we suppose that each vehicle has the same maximum acceleration rate and maximum deceleration rate. Hence, we can imagine that every vehicle has a discontinuous acceleration rate at every time step but continuous velocity with respect to time.

According to the target time-gap-based velocity update model (5.2), the only requisite information needed to determine the next velocity is the forward car spacing. The distance to the vehicle ahead can be reported by a measuring device such as radar or lidar, or be derived by the positions of the vehicle itself and its leading vehicle.

5.3 Vehicular Traffic Network

We need to investigate if our proposed model can perform the role of a car-following model and whether its various induced outcomes match the empirical traffic data. An investigation into the usability of the target time-gap-based velocity update model will determine its effectiveness as a car-following model. A consideration of its safety point of view is also needed; for example, what combinations of two key parameters, such as car spacing and target time gap, defined in our proposed model brings about incidents or guarantees collision-free movement. Furthermore, a comparison between the system capacity obtained from the empirical traffic data and the throughput of the vehicular traffic network where all vehicles apply our proposed car-following model is necessary. We will discuss the issues related to the usability, safety, and capacity analysis by microscopic traffic simulations using our proposed target time-gap-based velocity update model.

5.3.1 Description of the simulation environment

We assume that a platoon of vehicles is traveling on a long corridor of a 2 km looping road. In a looping road, the start and end points of the road are connected not physically but virtually. That is to say, as soon as a vehicle passes the end point of this roadway with some velocity, it appears at the start point at the same velocity. For instance, when we suppose that the number of vehicles moving on our considered roadway is $M \in \mathbb{N}$, the immediate lead of the 1st vehicle (i.e., the lead-most vehicle that is the closest vehicle to the end of a road) is the Mth vehicle (i.e., the last-most vehicle that is the closest vehicle to the start of a road) and the vehicle behind the Mth vehicle is the 1st vehicle. This implies that the velocity and position of the 1st vehicle are influenced by its virtual leading vehicle, M.

The main reason why we prefer a looping road rather than a straight road for computer simulation is because the given traffic density can be maintained constantly until simulation terminates as well as the fact that it is not necessary to include boundary conditions for the lead-most vehicle at every time step. In addition, Mason *et al.* [65] suggested that identical simulation results about system stability and the propagation of

disturbances can be observed irrespective of the type of road, when the simulation is executed on a long corridor. In practice, hence, many studies have considered a long corridor of a looping road for computer simulation.

We set the initial conditions for simulation that every vehicle starts to travel at zero velocity and at a random location on the roadway. We suppose that our considered vehicular traffic network is synchronous in time; that is, all vehicles on a given looping system use the target time-gap-based velocity update model to simultaneously refresh their dynamic properties, such as their velocity and position at every time step. We assume that the average safety length of vehicles is $L = 6.1$ m (i.e., 20 feet) and the maximum free-flow velocity is $v_f = 120.7$ km/h (i.e., 75 m/h) in (5.1).

5.4 Usability Analysis

In practice, loop detectors are normally used to measure and report local traffic data at their deployed spots every 30 s. The observed traffic data is converted to macroscopic traffic state representing the speed, flow, density, and so on, averaged over 30 s. Our simulation use an operation of a loop detector to obtain various results and thus collects the measurement data at the start point of a looping road every 30 s.

We set the update time interval T to 0.05 s. A small value of the update time interval implies a highly controlled vehicle enabling a high frequency communication or a cautious driver having his eyes on forward traffic conditions continuously without distraction. We assume that every vehicle uses a pre-defined same target time gap of $\check{\tau} = 1.8$ s, which is similar to the mean value of the time gap in a congestion region measured in San Diego, California, USA [37]. That is, $\tau_i\left(kT\right) = \check{\tau}$ for all $i \in \mathbb{N}$ and for all $k \in \{0 \cup \mathbb{N}\}$.

We change the values of traffic density for usability analysis simulation in which the range is from 1 to 100 vehs/km. The simulation for each density value is terminated once a vehicular traffic network reaches the steady-state in which all vehicles travel at the same velocity with respect to time without collisions. The simulation results per lane for all density values are combined together.

The relation between traffic density and average time gap is shown in Fig. 5.2.

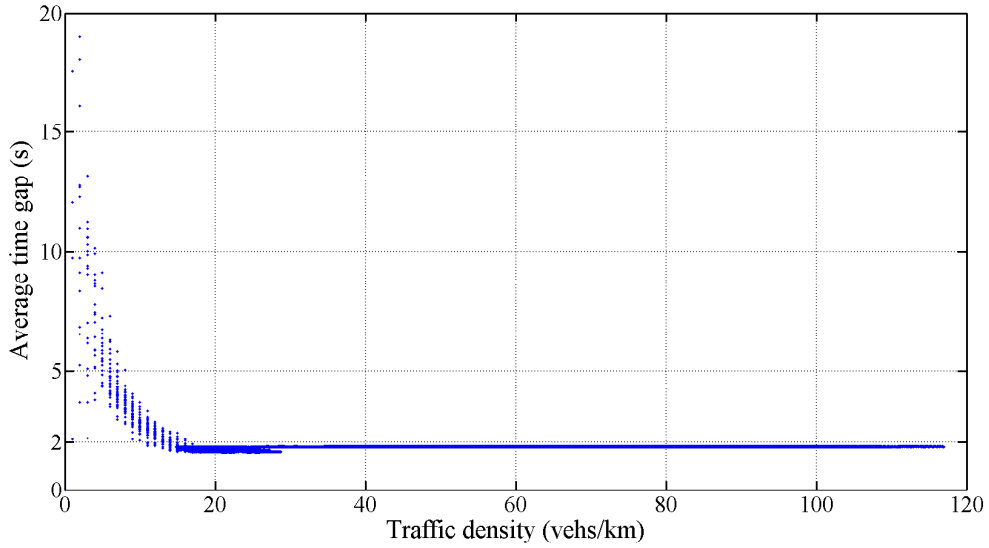

Figure 5.2: Average time gap with respect to traffic density under $T = 0.05$ s and $\tau_i\,(kT) = 1.8$ s for all i and for all k.

Each point in the scatter plot gives traffic density and average time gap, which are averaged over 30 s. The density scope obtained from the entire simulation is from 1 to around 118 vehs/km, which is different from the real density range we set. This gap exists because the density values calculated by the local observations at a loop detector is various in spite of a fixed given value of traffic density. It is observed that the time gap varies widely when traffic density is low. However, it converges to a pre-defined target time gap of $\check{\tau} = 1.8$ s in a congested area where traffic density is larger than the critical density of 17 vehs/km. This critical density value is similar to that measured in San Diego, California, USA [37]. The dispersion of the average time gap relies on the initial random position of vehicles in a free-flow regime, whereas a vehicular traffic network reaches an equilibrium state to where every vehicle has the constant time gap in a congested area. The pattern of this scatter plot is also similar to the empirical traffic data as presented in [37].

Fig. 5.3 shows the traffic flow and density pairs obtained from a microscopic traffic simulation and the time-gap-based traffic model drawn by (5.1). Each point in the scatter plot provides the traffic flow and density averaged over 30 s. Since the detectors deployed at the start point of our looping roadway count and report the number of vehicles passing on them during 30 s in integer units, the estimated traffic flow in vehs/h

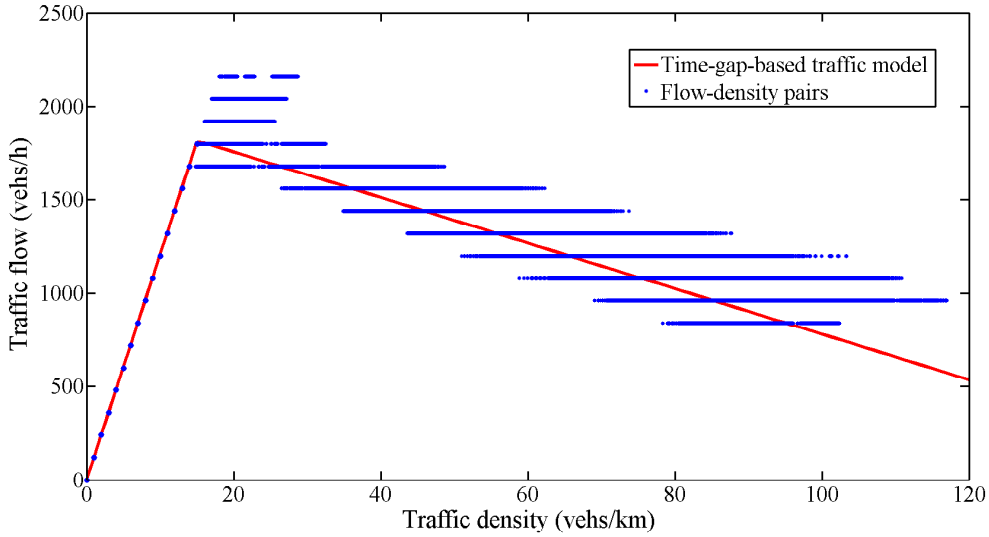

Figure 5.3: Traffic flow with respect to traffic density under $T = 0.05$ s and $\tau_i\,(kT) = 1.8$ s for all i and for all k.

is 120 times as large as the measured number of vehicles over 30 s. Thus, the traffic flow and density points in blue can be located only at the horizontal lines of 120 times of integers. Since every vehicle travels at the maximum free-flow velocity, v_f, when traffic density is low, the average speed of all vehicles in a vehicular traffic network is equal to v_f. In a congested area, on the contrary, the velocity of an individual vehicle is influenced by the forward traffic situation and traffic density, and it changes with time. Hence, the traffic flow-density pairs are scattered more widely near the congested branch. For reference, a red line in Fig. 5.3 represents the time-gap-based traffic model drawn with the given parameters: $v_f = 120.7$ km/h, $L = 6.1$ m, and $\tau = 1.8$ s in (5.1).

By comparing the blue flow-density pairs and the red line in Fig. 5.3, we can observe that the scatter points obtained from the simulation results of our proposed car-following model almost on average correspond to the time-gap-based traffic model, which is a good and simple fundamental diagram. In particular, the first argument of the time-gap-based traffic model, which is dominant in congestion conditions, is exactly identical to the simulation results. This implies that the target time-gap-based velocity update model mimics typical driving behavior accurately, and thus the vehicular traffic networks considering this model as an inter-vehicle velocity control produce the macroscopic results that tie in closely with the empirical traffic data.

Moreover, these traffic flow-density pairs support a prominent feature of vehicular traffic flow, which is the so-called capacity drop. The capacity drop is defined as a discharge flow drop after a localized disruption of traffic becomes active [74, 75, 76]. Particularly, Koshi *et al.* [74] claimed that the traffic flow-density relationship resembles a reversed λ shape and that the flow-density pairs disperse more widely near the right branch of the reversed λ symbol, which accords with the scattered blue points in Fig. 5.3. A reversed λ explains that the achievable maximum traffic flow in a free-flow regime is considerably larger than that in a congested region, and the phenomenon of this capacity drop happens by a difference of 1% to 18% [77, 78, 79, 80]. Fig. 5.3 also supports this numerical outcome, since the maximum capacity drop by a gap of around 17% can be observed at a traffic density of 28 vehs/km.

We have two additional simulation results under the same conditions except the values of the target time gap using $\check{\tau} = 1$ s and $\check{\tau} = 2.5$ s. The flow-density relationship, which aggregates the results obtained from the three different target time gap values, is shown in Fig. 5.4. No accident is observed during the execution of this simulation, since all drivers are so cautious that they can control the velocity frequently with the update time interval of 0.05 s to avoid collisions. The safety analysis to explain this phenomenon will be discussed in detail in the next Section. Each point in the scatter plot provides the traffic flow and density averaged over 30 s. The traffic flow-density pairs look like the empirical traffic data irrespective of the measurement location presented in a study by Cho *et al.* [37], and the shape of these fit, on average, the time-gap-based traffic model. The traffic flow-density pairs generated when the target time gap is 1 s locate above the scattered blue points presented in Fig. 5.3. In contrast, the flow-density relationship located below those blue points is obtained when the target time gap is 2.5 s. This observation is coherent to the slope variation of the second argument defined in the time-gap-based traffic model (5.1).

The microscopic simulation results, such as the time gap and traffic flow with respect to density, of vehicular traffic networks based on the target time-gap-based velocity update model accord closely with the empirical traffic measurements as well as support strongly the previous research outcomes about the capacity drop. Therefore, our proposed target time-gap-based velocity update model can be regarded as a car-following

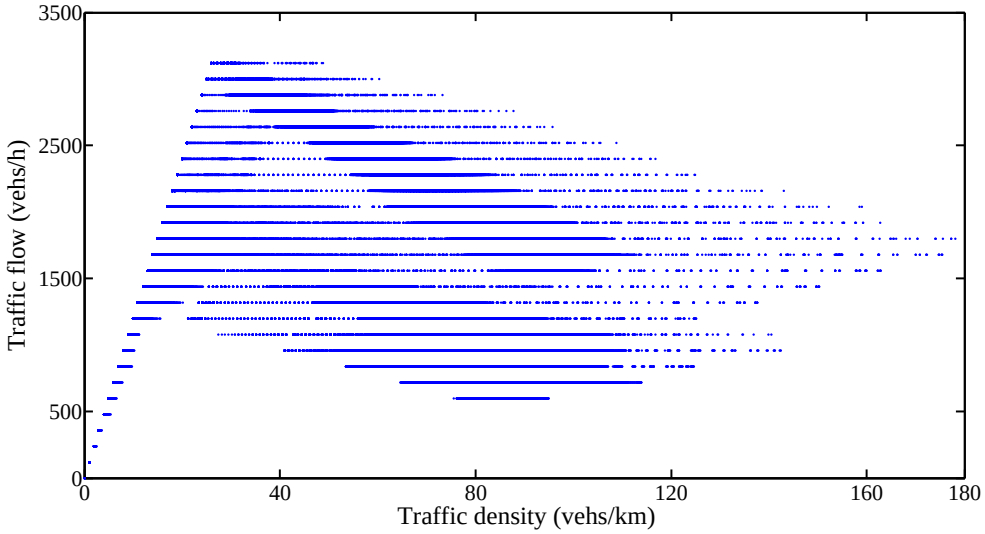

Figure 5.4: Traffic flow with respect to traffic density under $T = 0.05$ s and $\tau_i\,(kT) = 1$ s, $\tau_i\,(kT) = 1.8$ s, and $\tau_i\,(kT) = 2.5$ s for all i and for all k.

model for accurately mimicking the typical behavior of drivers.

5.5 Safety Analysis

In this Section, we adopt a traffic safety metric called an anterior safety marginal value (SMV) to analyze the safety of the target time-gap-based velocity update model. In a vehicular traffic network using our proposed car-following model, the selection of the target time gap and the update time interval with respect to traffic density value is critical in deciding collision-free movements of vehicles. Three different regions are introduced depending on the ratio of incident occurrence under various combinations of the following key parameters for the target time-gap-based velocity update model: the target time gap, the update time interval, and traffic density.

5.5.1 Traffic safety metric: Anterior safety marginal value

The anterior SMV initially introduced in Chapter 4 is a traffic safety metric to indicate the likelihood of a rear-end accident occurring. Unlike other studies about safety indicators, such as the time headway and the Time-to-Collision (TTC) [59, 63,

64], the anterior SMV provides a numerical value between 0 and 1, which indicates the safety level of rear-end collision risk as well as applies identically, irrespective of various traffic situations. In addition, it is verified as a strong and rigorous safety indicator, but it has a simple mathematical form. Thus, we use the anterior SMV to analyze the safety of the target time-gap-based velocity update model in our considered vehicular traffic network.

The anterior SMV is defined as the minimum value from a set of the continuous anterior collision avoidance likelihood function, representing the safety level of rear-end collision risk with leading vehicles, predicted by the collision avoidance (CA) margin time of a vehicle. The CA margin time is defined as the time required to stop completely with full application of the brakes. A set of vehicle states, including the position, velocity, and lane index, of all vehicles in a vehicular traffic network is used to determine the anterior SMV at every time step. A set of vehicle states at time kT for $k \in \{0 \cup \mathbb{N}\}$ is given by $\mathbf{C}\left(kT\right) = \{C_i\left(kT\right) \mid \text{for all } i \in \mathbb{N}\}$. Here, $C_i\left(kT\right)$ is the vehicle states of the ith vehicle at time kT given by $C_i\left(kT\right) = \{x_i\left(kT\right), v_i\left(kT\right), l_i\left(kT\right)\}$, where $x_i(kT)$, $v_i(kT)$, and $l_i(kT)$ denote the position, velocity, and lane index of the ith vehicle at time kT, respectively.

For the derivation of the anterior SMV, it is assumed that every vehicle has the same maximum acceleration rate a_{max}^{+} and deceleration rate a_{max}^{-}. It is also assumed that every vehicle knows the vehicle states of all other vehicles on a roadway at every discrete time step. Hence, each vehicle can accurately draw the maximum and minimum trajectories of other vehicles for some future time at every time step kT. The minimum trajectory is the trajectory of a traveling vehicle with the maximum brake rate a_{max}^{-}, whereas the maximum trajectory is that of a vehicle moving with the maximum acceleration rate a_{max}^{+}. Here, we note that when a vehicle travels with the maximum brake rate, once it stops completely, its minimum trajectory stays stationary. Let $d_{i,max}\left(kT + \Delta t\right)$ and $d_{i,min}\left(kT + \Delta t\right)$ denote the maximum and minimum trajectories of the ith vehicle at time $(kT + \Delta t)$ for all $\Delta t \geq 0$, which are calculated from the vehicle states $C_i\left(kT\right)$ of the ith vehicle at time kT, respectively. Let $h_i\left(kT\right)$ denote the CA margin time of the ith vehicle calculated at time kT. By the definition of the CA margin time, $h_i\left(kT\right) = -v_i\left(kT\right)/a_{max}^{-}$.

In particular, by the definition of the anterior SMV, the ith vehicle for $i \in \mathbb{N}$ needs a subset of vehicle states, $\{C_1(kT), C_2(kT), \ldots, C_i(kT)\}$, to determine its anterior SMV at time kT. Hence, the anterior SMV for the ith vehicle at time kT is

$$SMV_i^A(\{C_1(kT), C_2(kT), \ldots, C_i(kT)\}) \in [0,1]$$

for every $i \in \mathbb{N}$ and for every $k \in \{0 \cup \mathbb{N}\}$. $SMV_i^A(kT) = 1$ implies that the ith vehicle will not collide with vehicles ahead of it by its CA margin time $h_i(kT)$. That is, the ith vehicle is absolutely safe from collision risk by its CA margin time. On the contrary, $SMV_i^A(kT) = 0$ implies that the ith vehicle will absolutely crash into other leading vehicles before its CA margin time. $SMV_i^A(kT) \in (0,1)$ means that the ith vehicle is likely to crash into other leading vehicles by its CA margin time. The larger the anterior SMV, the safer the vehicle is; that is, the lower the likelihood of a crash.

The computational complexity in determining the anterior SMV described in Chapter 4 grows dramatically, particularly when the number of leading vehicles increases. Hence, they also introduced a finite anterior space horizon for the anterior SMV to substantially prune the computational complexity. The anterior space horizon is defined as the number of leading vehicles to affect non-unity anterior SMV. The statement that the ith vehicle has non-unity anterior SMV at time kT means $SMV_i^A(kT) \in [0,1)$. This implies that there exists a positive possibility of rear-end collision risk with the number of leading vehicles defined by the anterior space horizon.

The following Theorem 5.1 is the finite anterior space horizon and the corresponding anterior SMV presented in Chapter 4, which is used for analyzing the safety of our proposed target time-gap-based velocity update model.

Theorem 5.1. ***Finite anterior space horizon and anterior SMV***

Suppose that there exists $j_i = \max \mathcal{J}_i(kT)$ *for every* $i \geq 2$ *and for every* $k \in \{0 \cup \mathbb{N}\}$ *such that*

$$\mathcal{J}_i(kT) = \underset{l \in [1,i]}{\operatorname{argmin}} \{d_{l,max}(kT + h_i(kT))\}. \tag{5.4}$$

Then, the finite anterior space horizon of the i*th vehicle at time* kT *is given by*

$$SH_i^A(kT) = (i - j_i) \tag{5.5}$$

and its corresponding anterior SMV is

$$SMV_i^A(kT) = \min_{\Delta t \in (0, h_i(kT)]} \left\{ \left[\frac{\min\limits_{l \in [j_i,(i-1)]} \{d_{l,max}(kT+\Delta t)\} - d_{i,min}(kT+\Delta t)}{\min\limits_{l \in [j_i,(i-1)]} \{d_{l,max}(kT+\Delta t)\} - \min\limits_{l \in [j_i,(i-1)]} \{d_{l,min}(kT+\Delta t)\}} \right]_P \right\}. \tag{5.6}$$

5.5.2 Adoption of the anterior SMV for a target time-gap-based velocity update model

We showed that the target time-gap-based velocity update model can be used as a representative car-following model, since it mimics the typical behavior of drivers accurately. However, the safety assurance of our proposed car-following model does not follow its usability. Hence, we use the anterior SMV to investigate its safety in a vehicular traffic network.

We set traffic density, ρ, to around 93 vehs/km (i.e., 150 vehs/mile) for the considered vehicular traffic network. Fig. 5.5 represents the anterior SMV evolution in simulation time under the different target time gaps and update time intervals, when all vehicles use the target time-gap-based velocity update model to refresh their dynamic properties. The minimum anterior SMV of all vehicles at every time step is depicted with a red line. If this minimum anterior SMV evolution is equal to 1, then every vehicle in a vehicular traffic system has a safety indicator of 1 and thus ensures collision-free trajectory at that moment. Once a vehicular traffic network reaches the steady-state in which all vehicles move at the same velocity with respect to time without crashes and the minimum value of the anterior SMVs of all vehicles indicates perfect safety, this implies the guarantee of permanent collision-free movements. The simulation for each experiment is terminated when either everlasting collision-free movements of all vehicles are confident or rear-end incidents occur. A red line shown in Fig. 5.5 represents the minimum anterior SMV evolution for each experiment, and the blue circle refers to the time of collision occurrence.

We consider four scenarios: (1) the target time gap of 1.8 s, which is similar to the mean value of the time gap in a congestion regime measured in San Diego, Califor-

nia, USA [37], and the small value of the update time interval of 0.05 s, (2) the target time gap of 0.6 s, which is less than its empirical mean value in San Diego, USA, and the same update time interval as the first experiment, (3) the target time gap of 0.1 s, which is much less than its average value observed in San Diego, USA, and the same update time interval as the first experiment, and (4) the same target time gap as the first experiment, but with the update time interval of 1 s, which is much larger compared to the other three experiments. The results of these four experiments are shown in Figs. 5.5(a), 5.5(b), 5.5(c), and 5.5(d), respectively. As the target time gap gets smaller, drivers can be considered as tailgaters closely following frontward vehicles. In addition, a small value of the update time interval implies a highly controlled vehicle enabling a high frequency operation or a cautious driver having his eyes on forward traffic situations consistently without distraction.

The anterior SMV of every vehicle keeps being identical to 1 for the first experiment, since all vehicles travel with enough car spacing and steadily update their velocity in order to prevent incidents. This result helps explain why drivers unconsciously maintain a typical time gap of around 1.8 s for frontward safety, which is the essential point of the empirical traffic data about the time gap measured in San Diego, California, USA. Figs. 5.5(b) and 5.5(c) show decreases in the target time gap and the consequential variations in the minimum anterior SMV, but retaining the same update time interval. When the target time gap is 0.6 s, there exist vehicles with non-unity anterior SMV from around 3 s in simulation time. However, since this given target time gap does not induce the severe tailgating phenomenon, the vehicles with positive collision risk can escape gradually from a dangerous accident zone. Finally, it is observed that a vehicular traffic network can be assured of collision-free movements of all vehicles from about 6 s in simulation time. To top it off, when all vehicles in a vehicular traffic system use the given target time gap of 0.1 s, the vehicles appear with non-unity anterior SMV. Unlike the second experiment, the vehicles adhere to aggressive driving to leading vehicles and thus make collisions in simulation time of 11 s. Now, the minimum anterior SMV evolution, where only frequency of update for new velocity in time is larger compared to the first experiment, is shown in Fig. 5.5(d). Even though the vehicles in a vehicular traffic network try to move with enough distance to leading vehicles, since they update

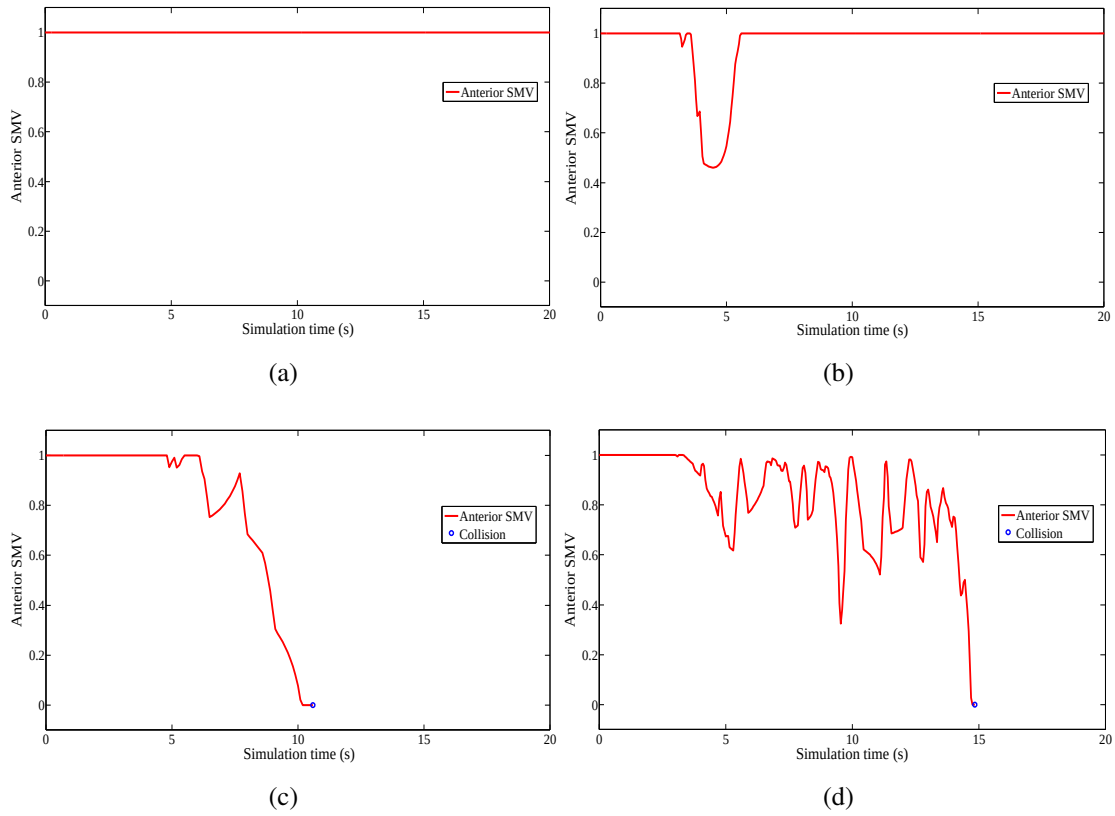

Figure 5.5: Minimum anterior SMV evolution according to the target time gap and the update time interval under 93 vehs/km (i.e., 150 vehs/mile). (a) $\check{\tau} = 1.8$ s and $T = 0.05$ s. (b) $\check{\tau} = 0.6$ s and $T = 0.05$ s. (c) $\check{\tau} = 0.1$ s and $T = 0.05$ s. (d) $\check{\tau} = 1.8$ s and $T = 1$ s.

their dynamic properties with one second old car spacing information, there exists the positive likelihood of a rear-end collision among vehicles. The abrupt fluctuation of the minimum anterior SMV eventually culminates with incidents in a time of 15 s.

An investigation of the target time-gap-based velocity update model with the help of the anterior SMV gives the conjecture that either a small value of the target time gap or a large value of the update time interval can cause a rear-end collision in a vehicular traffic network using our proposed car-following model. Therefore, the detailed safety analysis for the target time-gap-based velocity update model is necessary depending on its three key parameters: the target time gap, the update time interval, and traffic density.

5.5.3 Traffic safety relationship among three parameters

The target time gap, update time interval, and traffic density for our proposed car-following model are the primary parameters determining collision-free movements of vehicles in a vehicular traffic network. Hence, the collision ratio according to a combination of these primary variables needs to be examined. The collision ratio is defined as the ratio of the number of simulations that experience rear-end incidents over the total number of simulations to run. The total number of simulations is 200 times for each case. The simulation for each case is terminated when either permanent collision-free trajectories of all vehicles are confident or rear-end collisions occur as was done in earlier simulation for the usability analysis. The values of traffic density to be examined are around $\rho = 12$ vehs/km (i.e., 20 vehs/mile), $\rho = 31$ vehs/km (i.e., 50 vehs/mile), and $\rho = 93$ vehs/km (i.e., 150 vehs/mile). We note that these traffic densities are representative density values for describing a free-flow regime, a low-congestion regime, and a high-congestion regime, respectively. The range of the target time gap is from 0.1 to 3.0 s at an interval of 0.1 s. Also, the scope of the update time interval is from 0.05 to 4.0 s with 0.05-seconds intervals additionally including 0.01 s. Thus, the total number of simulation cases for each traffic density value is 2430.

We introduce three different regions depending on the frequency of collision occurrence with respect to the key parameters for the target time-gap-based velocity update model, which are a collision-free region, a transition region, and a catastrophe region. A collision-free region is defined as the sub domain of the target time gap and the update time interval under the given traffic density, which is always assured the collision-free movements of all traveling vehicles in a vehicular traffic network unless an abrupt perturbation exists. On the contrary, a catastrophe region is the sub domain that will result in rear-end accidents before a vehicular traffic system reaches a steady-state. A transition region is the area between a collision-free region and a catastrophe region with a positive ratio of collision occurrence. The entire domain constructed by the target time gap and the update time interval consists of these three non-overlapping regions: a collision-free region with collision ratio of 0, a catastrophe region with collision ratio of 1, and a transition region with the lower and upper open bounds of collision ratio range between 0 and 1.

Figs. 5.6(a), 5.6(b), and 5.6(c) depict the collision ratio according to a combination of the target time gap and the update time interval under the different traffic densities of 12, 31, and 93 vehs/km, respectively. The surface in red with the collision ratio of 1 describes a catastrophe region, whereas that in blue having the collision ratio of 0 is a collision-free region. Three different regions are obviously observed irrespective of traffic density. However, as traffic density increases, the catastrophe region gets wider, whereas both the collision-free region and the transition region become narrower. In addition, a transition region under high density has a steeper slope between catastrophe and collision-free regions compared to low density. This is because the small value of average car spacing of vehicles caused by high density augments rear-end collision risk. This reason also explains that a platoon of vehicles in high traffic density is more vulnerable to crashing into other vehicles compared to those in low density.

The large value of the update time interval implies that vehicles in our considered vehicular traffic network use old car spacing data to update their dynamic properties; that is, there is a long interval before they intermittently refresh their velocities and positions. In this case, the cause of a rear-end incident can be explained as follows: if the newly calculated velocity of a vehicle is much higher than that of its leading vehicle and a long time is needed to update the velocities of two consecutive vehicles owing to the large update time interval, a vehicle can collide into the vehicle in front of it. In general, hence, the collision ratio will grow irrespective of traffic density, as the update time interval increases.

Under the highest traffic density of around 93 vehs/km, the collision ratio is commonly inversely proportional to the target time gap. Unfortunately, a vehicular traffic system stays a catastrophe region when the target time gap is set to 0.2 s over the entire given range of the update time interval. We define the abysmal target time gap set as the values of the target time gap that have the longest range of the update time interval and result in a catastrophe region. The abysmal target time gap set exists for each traffic density. For instance, the abysmal target time gap set is 0.2 s in the highest traffic density. Unlike the general relationship between the target time gap and the collision ratio, as the former decreases, particularly where it is less than the abysmal target time gap set, the latter also drops off. The abysmal target time gap set contains the values of the target

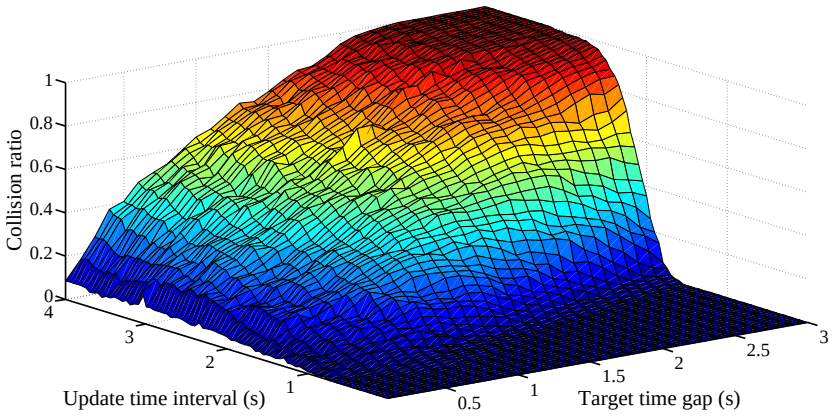

(a)

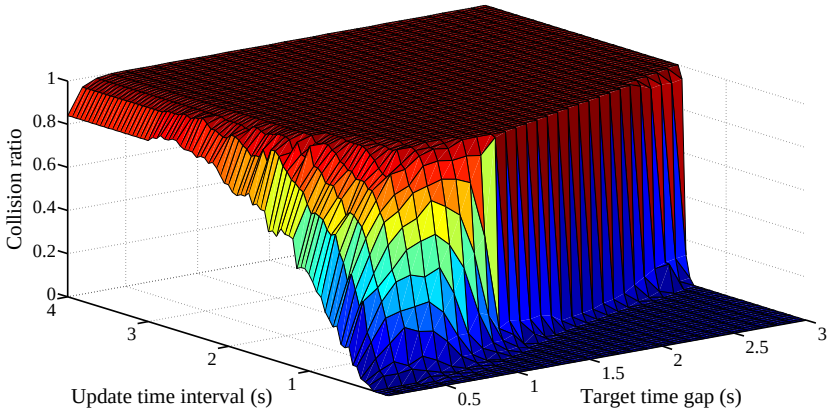

(b)

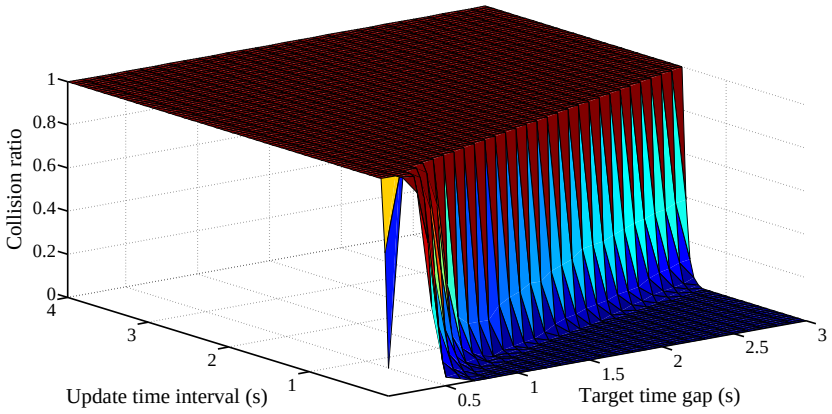

(c)

Figure 5.6: Collision ratio with respect to the target time gap and the update time interval for various traffic densities, ρ. (a) $\rho = 12$ vehs/km (i.e., 20 vehs/mile). (b)$\rho = 31$ vehs/km (i.e., 50 vehs/mile). (c) $\rho = 93$ vehs/km (i.e., 150 vehs/mile).

time gap from 1.0 s to 1.3 s, when traffic density is 31 vehs/km. Since our considered upper bound of the target time gap is 3.0 s, the corresponding exact abysmal target time gap set can not be examined for the density of 12 vehs/km. In this case, however, the abysmal target time gap set might be 3.0 s with the limited simulation results. Hence, it is observed that the abysmal target time gap set diminishes, whereas the relevant update time interval range belonging to a catastrophe region becomes wider as traffic density increases. This observation is consistent with a proportional connection between the size of a catastrophe region and traffic density in a vehicular traffic network. The reason why the collision ratio is a non-increasing curve at which the target time gap is less than the abysmal target time gap set under the fixed values of traffic density and update time interval can be explained as follows: even though the given target time gap value is small, if all vehicles on a roadway have enough car spacing, such as even car spacing, at the initial time step, then their practical time gaps are larger than the given target time gap, and thus they do not apply sudden full brakes. In this case, several strings of vehicles in which some vehicles travel close together in packs can be observed. This enables a vehicular traffic network to reach a steady-state without incidents.

In conclusion, the larger target time gap and the shorter update time interval are necessary to achieve collision-free movements in a vehicular traffic network using the target time-gap-based velocity update model. For safety, however, if vehicles are controlled with the shorter target time gap, they need to frequently measure their frontward car spacings and to update their dynamic properties. That is, the vehicles require high bandwidth operation. Although the vehicles travel in a collision-free region, even small adverse changes in either the target time gap or the update time interval can make a vehicular traffic system unexpectedly fall into a catastrophe region, in particular when traffic density is high.

Boundaries of collision-free regions and catastrophe regions for three different traffic densities are shown in Fig. 5.7. The dotted lines represent collision-free region boundaries for every traffic density, whereas the solid lines describe catastrophe region boundaries for each density value. The blue, red-circled, and green-squared lines refer to boundaries for traffic densities of 12, 31, and 93 vehs/km, respectively. As traffic density decreases, the area between a catastrophe region and a collision-free region, called a

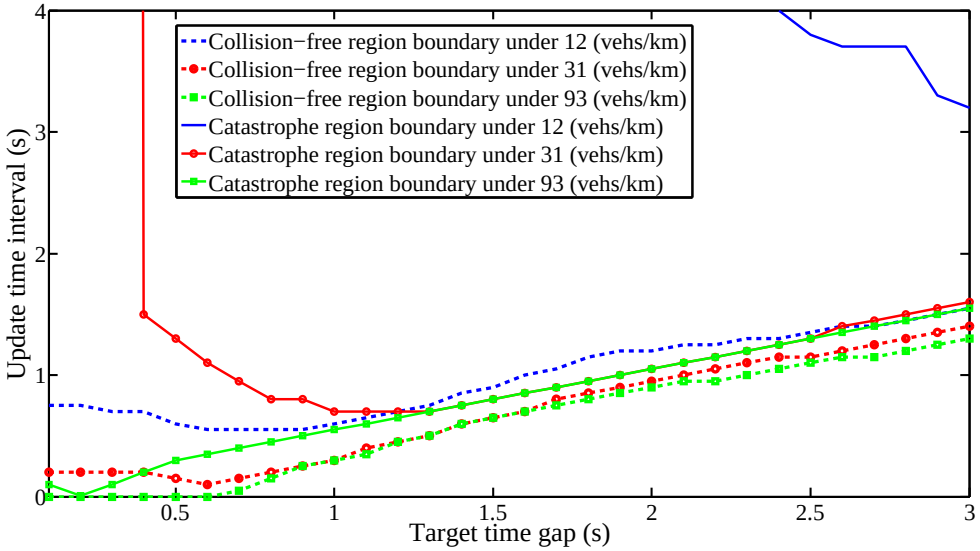

Figure 5.7: Boundaries of collision-free regions and catastrophe regions for various traffic densities, $\rho = 12$, $\rho = 31$, and $\rho = 93$ vehs/km.

transition region, becomes narrow as discussed in Fig. 5.6. The fact that more attention in collision-free driving is necessary in high density conditions is also easily supported by Fig. 5.7. A catastrophe region obtained when traffic density is high contains that in low density. On the contrary, a collision-free region under high traffic density is a subset of that when density is low. The abysmal target time gap set can be easily observed in Fig. 5.7 by finding the target time gap that has the longest range of the update time interval that results in a catastrophe region; the abysmal target time gap sets are 3.0 s, from 1.0 s to 1.3 s, and 0.2 s in an ascending order of traffic density.

An investigation of a collision-free region guaranteeing perfect traffic safety with respect to three key parameters, such as the target time gap, the update time interval, and traffic density, for the target time-gap-based velocity update model is a basic essential for analyzing the capacity of our proposed car-following model.

5.6 Capacity Analysis

In this Section, an analysis of average practical time gap and average system velocity under a steady-state for our considered vehicular traffic networks is performed.

We regard a steady-state as the state where all vehicles in a vehicular traffic network travel at the same time-invariant velocity without collisions. Also, a comparison between the empirical capacity obtained from traffic measurement data and the numerical capacity of a vehicular traffic network using the target time-gap-based velocity update model is drawn. The achievable system capacity ensuring safety and capacity enhancements is then provided.

5.6.1 Numerical analysis under a steady-state

We assume that our considered system reaches a steady-state. Then, $v_i\,(kT) = v^*$ for all $i \in \mathbb{N}$ and for all $k \geq K$ in a steady-state, where $K \in \{0 \cup \mathbb{N}\}$. Let $\bar{s}^*$ and $\bar{\tau}^*$ denote the average car spacing (in m) and the average practical time gap in a steady-state, respectively. Even though every vehicle refreshes its velocity with the given target time gap of $\check{\tau}$, the practical time gap averaged over all vehicles can be different from the target time gap according to traffic density and the upper bound of the velocity limited by the maximum free-flow velocity of v_f. The average car spacing in a steady-state is given by

$$\bar{s}^* = \frac{1000}{\rho} - L. \tag{5.7}$$

In addition, the average system velocity, $\bar{v}^*$, is equal to v^* in a steady-state. By substituting (5.7) into (5.1), the relationship between the average practical time gap and the average system velocity in a steady-state is given by

$$\bar{\tau}^* = \frac{\frac{1000}{\rho} - L}{\hat{c}\,\bar{v}^*}. \tag{5.8}$$

Fig. 5.8 shows the average practical time gap with respect to the given target time gap under various traffic densities. The red solid, green dotted, and blue dash-dotted lines represent the average practical time gap for various traffic densities, such as $\rho = 12$, $\rho = 31$, and $\rho = 93$ vehs/km, respectively. When steady-state traffic flow is in a free-flow regime, all vehicles travel at the same velocity of the maximum free-flow velocity, v_f. The corresponding average measured time gap is denoted by $\bar{\tau}_f^*$, which is easily calculated by substituting $\bar{v}^* = v_f$ into (5.8). That is, the average practical time gap keeps being identical to $\bar{\tau}_f^*$, which depends on traffic density, in a steady-state

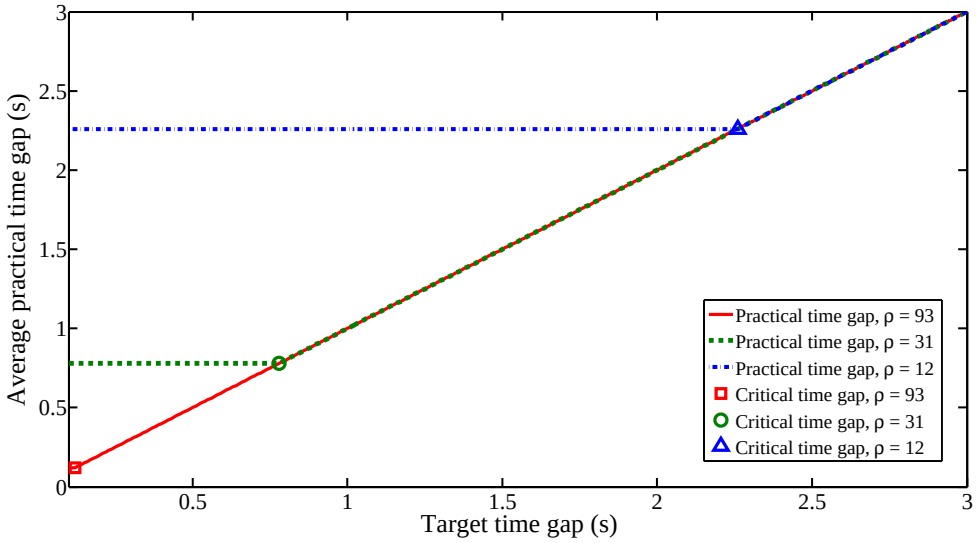

Figure 5.8: Average practical time gap with respect to the target time gap for traffic densities, such as $\rho = 12$, $\rho = 31$, and $\rho = 93$ vehs/km.

free-flow situation. However, if vehicles in a vehicular traffic network use the given target time gap of $\check{\tau}$ being larger than $\bar{\tau}_f^*$, then the given target time gap overrides as a mean value of the practical time gap. We define the critical target time gap as the largest value of the target time gaps to make the average system velocity attain the maximum free-flow velocity; that is, the critical target time gap is $\check{\tau} = \bar{\tau}_f^*$. The red square, green circle, and blue triangle depict the critical target time gap under traffic densities, $\rho = 12$, $\rho = 31$, and $\rho = 93$ vehs/km, respectively. These critical target time gaps are around 0.12, 0.78, and 2.26 s in a descending order of the considered traffic density. We observe that if the given target time gap is less than or equal to the critical target time gap in which a vehicular traffic network stays in a free-flow regime, the average measured time gap is equal to $\bar{\tau}_f^*$, but otherwise it is the same as the given target time gap. In other words, we have

$$\bar{\tau}^* = \max\{\check{\tau},\, \bar{\tau}_f^*\}. \tag{5.9}$$

The average system velocity according to the target time gap for each traffic density is shown in Fig. 5.9. All vehicles travel at the maximum free-flow velocity of around 117.5 km/h when the given target time gap is less than or equal to the critical time gap as explained in Fig. 5.8. On the contrary, the average system velocity in a congestion regime is directly obtained from (5.8). Hence, the average system velocity

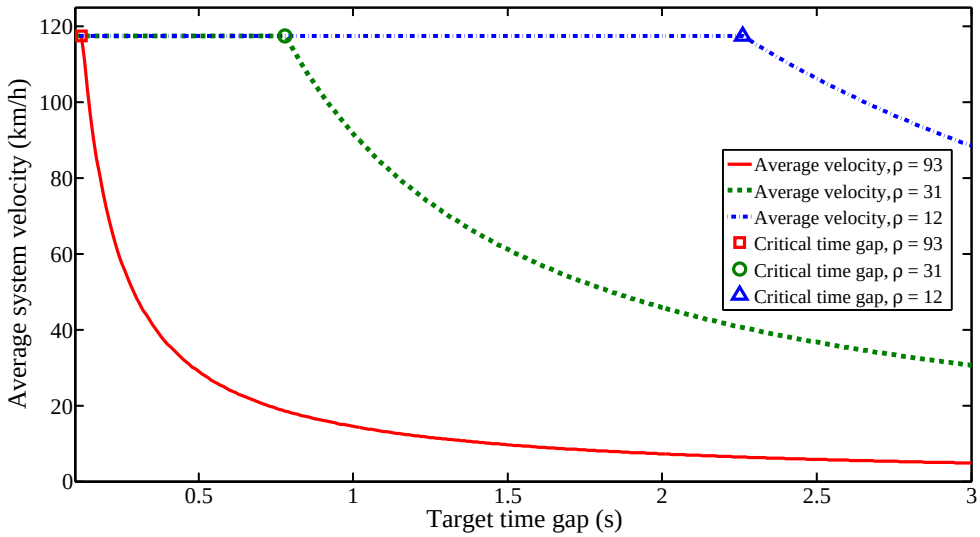

Figure 5.9: Average system velocity with respect to the given target time gap for various traffic densities, $\rho = 12$, $\rho = 31$, and $\rho = 93$ (vehs/km).

of all vehicles in a steady-state is

$$\bar{v}^* = \begin{cases} \bar{v}_f^* & \text{if } \check{\tau} \leq \bar{\tau}_f^*, \\ \frac{\frac{1000}{\rho} - L}{\hat{c}\,\bar{\tau}^*} & \text{if } \check{\tau} > \bar{\tau}_f^*. \end{cases} \tag{5.10}$$

In general, the average system velocity is a non-increasing curve with respect to traffic density under the same target time gap. A similar phenomenon also occurs in the increasing target time gap under the same traffic density.

We note that Figs. 5.8 and 5.9, represented by the numerical analysis of a steady-state for the target time-gap-based velocity update model, are exactly identical to the simulation results obtained when our considered vehicular traffic system reaches a steady-state without collisions.

Fig. 5.10 shows the average system velocity with respect to traffic density and the target time gap, which is a simulation result of our proposed car-following model only when no collision is observed. As we discussed in the previous Section on safety analysis, a small value of the update time interval, $T = 0.01$ s, is used to guarantee collision-free movements of all vehicles during simulation. As traffic density value or the target time gap increases, the average system velocity decreases in principle. A plain of the maximum free-flow velocity, which is the average system velocity in a free-flow

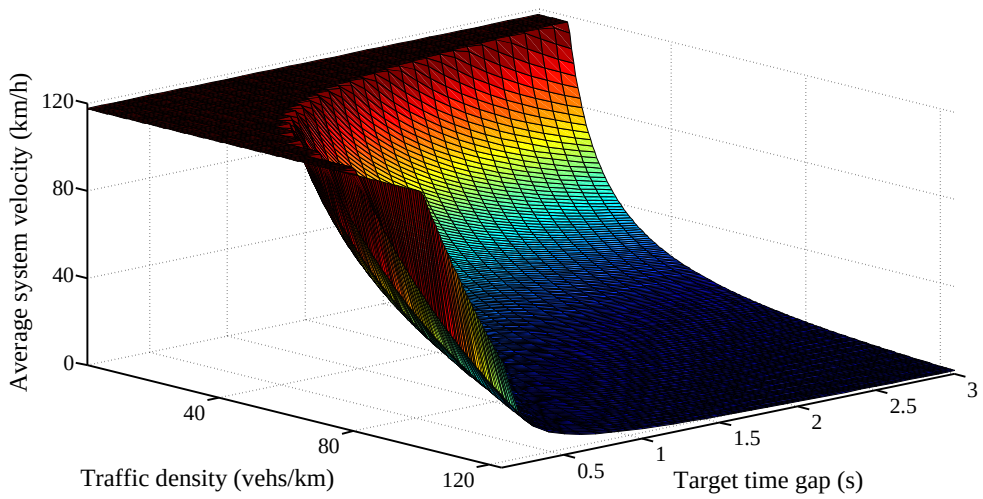

Figure 5.10: Average system velocity with respect to traffic density and the given target time gap.

regime, can be observed when either of them is small. However, once the target time gap increases beyond the critical target time gap for each traffic density, the average system velocity plummets like a waterfall.

5.6.2 Comparative results for capacity

Table 5.1 shows the empirical capacity per lane based on the measurement data in San Diego, California, USA, which was provided by Cho *et al.* [37]. When traffic is in a free-flow regime, such as a low density of 12 vehs/km, since vehicles in a vehicular traffic network travel at the maximum free-flow velocity, the corresponding empirical capacity is 1460 vehs/h. As traffic density increases to 31 vehs/km, slightly congested traffic can be observed and thus the empirical capacity of 2650 vehs/h is less than the maximal throughput achieved at the critical density. In situations where vehicles are in a high-congestion regime caused by a high density of 93 vehs/km, the empirical capacity dramatically decreases to 450 vehs/h.

A comparison between the numerical capacity and the empirical capacity is drawn in Fig. 5.11. The numerical capacity, which is the maximum achievable traffic flow per lane in a steady-state, is calculated by (5.10) and by the relation among traffic flow, density, and velocity satisfying with $q = \rho\, v$. The numerical capacity is also

Table 5.1: Empirical capacity based on the measurement data in San Diego, California, USA.

Traffic density (vehs/km)	Traffic condition	Empirical capacity (vehs/h)
12	A free-flow regime	1460
31	A low-congestion regime	2650
93	A high-congestion regime	450

identically supported by the simulation results. These numerical capacities for various traffic densities, such as $\rho = 93$, $\rho = 31$, and $\rho = 12$ vehs/km, are represented by the red solid, green dotted, and blue dash-dotted lines, respectively. The empirical capacity for each traffic density presented in Table 5.1 is depicted by a diamond in relevant color.

When traffic is in a seriously congested situation caused by a high density of 93 vehs/km, applying the target time-gap-based velocity update model to all vehicles improves the system throughput compared to the empirical capacity no matter what target time gap value is used. As traffic density decreases to 31 vehs/km, a lightly congested condition can be observed. In this situation, the use of a less than or equal to 1.0 s small target time gap value is recommended so as to enhance system throughput. However, in situations where vehicles are in a free-flow regime, such as a density of 12 vehs/km, letting drivers have power over the vehicles gives better performance than controlling vehicles with any value of the target time gap.

The achievable system capacity of a vehicular traffic network in which all vehicles use the target time-gap-based velocity update model needs to be considered. The achievable system capacity means the maximum traffic flow between the numerical capacity in using the target time-gap-based velocity update model and the empirical capacity, in particular while guaranteeing collision-free trajectories of all traveling vehicles. The range of the target time gap is from 0.1 to 3.0 s, and the scope of the update time interval is from 0.01 to 4.0 s, which we use, in order to examine the collision ratio as shown in Fig. 5.6. Even though the entire range of the target time gap for the high density of 93 vehs/km provides better performance in throughput, since its sub-range from 0.1 to 0.6 s makes vehicles reach a catastrophe region or a transition region, its sub-range is considered the domain that brings the zero capacity. When traffic density is 31 vehs/km, the small values of the target time gap, such as 0.1 to 1.0 s, induces the

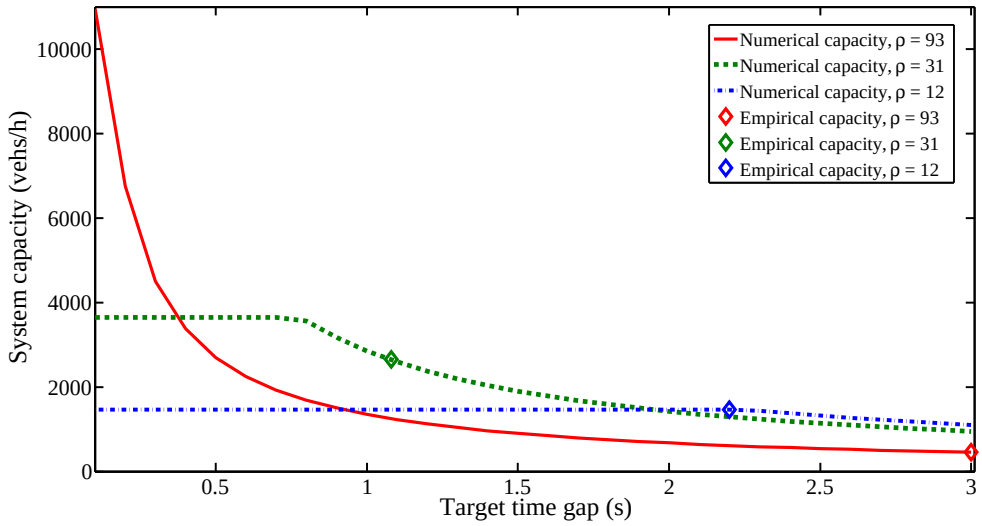

Figure 5.11: A comparison between the numerical capacity and the empirical capacity.

system throughput enhancement compared to the empirical traffic data. However, the achievable system capacity is dominated by the empirical capacity over the range of the target time gap from 1.1 to 3.0 s. This implies that only its sub-range from 0.1 to 1.0 s is preferred to use for system throughput improvement. The numerical capacity for a low traffic density of 12 vehs/km is more dominant than the empirical capacity over the target time gaps from 0.1 to 2.2 s, whereas the empirical capacity is the attainable system throughput over the rest of the target time gap range. Since the above provided sub-ranges, which are from 0.1 to 1.0 s for traffic density of 31 vehs/km and from 0.1 to 2.2 s for 12 vehs/km, have the corresponding update time interval values to have a vehicular traffic network stay in a collision-free region, the numerical capacity derived from these sub-ranges can be considered as the achievable system throughput.

As a result, we present the effective domain of the target time gap and the update time interval for each traffic density in Table 5.2. This effective domain guarantees both collision-free movements of all vehicles and system capacity improvement compared to the empirical capacity. When traffic density is 12 vehs/km, there exists the effective domain consisting of the target time gap of 0.1 to 2.2 s and the relevant update time interval of 0.01 to 0.55. The safety and system throughput enhancements for this effective domain are verified by Fig. 5.6(a). As traffic density increases, traffic becomes congested and the size of the effective domain gets narrower. The sub-range of the target time gap

Table 5.2: Effective domain of the target time gap and the update time interval for ensuring perfect safety and capacity enhancement.

Traffic density (vehs/km)	Target time gap (s)	Update time interval (s)
12	$0.1 \sim 2.2$	$0.01 \sim 0.55$
31	$0.1 \sim 1.0$	$0.01 \sim 0.10$
93	$0.7 \sim 3.0$	$0.01 \sim 0.05$

from 0.1 to 1.0 s shows an improvement in system capacity when traffic density is of 31 vehs/km. In addition, the update time interval should be from 0.01 to 0.10 s under its sub-range for collision-free movements in a vehicular traffic network as shown in Fig. 5.6(b). An increase in traffic density in a congestion regime widens the range of the target time gap, which induces system throughput enhancement; for instance, if traffic density increases to 93 vehs/km, the relevant range of the target time gap is from 0.1 to 3.0 s. However, since no value of the update time interval corresponding to the target time gap of 0.1 to 0.6 s makes a vehicular traffic system reach a collision-free region, the sub-range of the target time gap constituting the effective domain is from 0.7 to 3.0 s. Extremely small values of the update time interval, such as 0.01 to 0.05 s, are needed for perfect safety, particularly under the target time gap of 0.7 to 3.0 s.

5.7 Summary

We proposed the target time-gap-based velocity update model, which is an extension of the time-gap-based traffic model considered as a simple triangular fundamental diagram. Every vehicle in a vehicular traffic network updates its velocity and position for the next time step with the time-gap-based velocity update model. A simulation analysis for the proposed car-following model was conducted by a microscopic traffic simulator. In addition, the simulation results matched well with empirical traffic data. Hence, the target time-gap-based velocity update model is considered to be a representative car-following model that mimics the typical behavior of drivers. Since typical driving behavior is itself a creative and superior algorithm, the proposed car-following model describing it specifically and accurately deserves a similarly outstanding model. A safety analysis of the target time-gap-based velocity update model was conducted

through the anterior safety marginal value (SMV). Three different regions were introduced depending on the frequency of collision occurrence with respect to traffic density, the given constant target time gap applied for all vehicles in vehicular traffic networks, and the update time interval needed to refresh the velocity and position of vehicles. These regions include a collision-free region, a transition region, and a catastrophe region. A collision-free region is defined as the sub domain of the target time gap and the update time interval under the given traffic density, which is always assured the collision-free movement of vehicles, if there is no perturbation. In contrast, a catastrophe region is the sub domain that will result in incidents before reaching a steady-state. A transition region is the area between a collision-free region and a catastrophe region with a positive ratio of collision occurring. The average practical time gap and the average system velocity in a steady-state of the target time-gap-based velocity update model was analyzed mathematically and verified by the identicalness with the corresponding simulation results. Moreover, when the proposed car-following model is used as a basis for inter-vehicle control, the effective reachable domain of the target time gap and the update time interval was presented, which guarantees both collision-free movements and system capacity enhancement compared to the empirical traffic data.

Chapter Acknowledgments

Chapter 5, in full, is a reorganized version of the following manuscript. Seokheon Cho and Ramesh R. Rao. “Usability, Safety, and Capacity Analysis for a Target Time-gap-based Velocity Update Model,” *in preparation*.

Chapter 6

Conclusions and Future Works

6.1 Conclusions

The presented research works provided various approaches described in Chapter 1 to enhance traffic safety and improve system capacity for vehicular traffic networks. In order to build a solid foundation for this interdisciplinary work, first the understanding phase of vehicular traffic flow was fulfilled by analyzing the empirical traffic data. As a result, a time-gap-based traffic model that is a triangular fundamental diagram was proposed in Chapter 2. Three different strategies were provided to reach the traffic safety and capacity enhancement goals of this dissertation. Two coordinated ramp-metering optimization problems were suggested with the objective function that attains the maximum average system throughput in Chapter 3. The comparative results showing better performance of these optimization problems were conducted by a macroscopic traffic simulator based on the proposed time-gap-based traffic model. In particular, the time-variant ramp-metering algorithm that also supports on-ramp queue control showed increases in the system-level capacity and prevention of on-ramp queue spillover onto neighboring arterial streets. A new and rigorous traffic safety metric called the anterior safety marginal value (SMV), which indicates the safety level of collision risk with other leading vehicles, was derived in Chapter 4. The anterior SMV has the strength of providing a numerical value between 0 and 1, which shows the likelihood of accident occurrence and applies identically for various traffic conditions, whereas it does not include the practical weakness of the existing safety indicators, which have recommended

safety limits that are not only various for different traffic situations, but also ambiguous for presenting the safety level of collision risk. The anterior SMV was qualified as a remarkable safety indicator to predict and prevent a rear-end collision through a safety analysis of the Gipps car-following model. In Chapter 5, the time-gap-based velocity update model that is a car-following model was provided. The proposed car-following model is an extended version of a microscopic traffic flow model from the time-gap-based traffic model. Its verification was carried out by a microscopic traffic simulator based on the time-gap-based velocity update model. A comparison between its simulation results and the empirical traffic data showed that it is a representative car-following model that can mimic typical driving behavior accurately. Moreover, the reachable domains of the time gap and the update time interval in vehicular traffic networks using the time-gap-based velocity update model were provided, which effect the simultaneous improvement of traffic safety and capacity. Therefore, a combination of the various compoundable strategies suggested in this dissertation creates a synergistic effect to improve safety and throughput for vehicular traffic networks.

When traveling, a driver generally maintains a positive safe distance between his vehicle and the vehicle immediately in front of it in order to prevent collisions. Because of this safe distance, there exists a time gap that is defined as the time required to travel the distance between the front end of a vehicle to the back end of its leading vehicle. In Chapter 2, we provided the time-gap-based traffic model for describing vehicular traffic flow. The proposed model explains the widely known triangular flow-density fundamental diagram introduced by Newell, in particular by using three primary parameters: the maximum free-flow velocity, a typical safety length of vehicles, and a mean value of the time gap calculated from the traffic data in congested conditions. In addition, we suggested two different analysis methods to estimate the time gap from empirical traffic data measured by single-loop and double-loop detector systems. It was observed that the average and standard deviation of the time gap vary widely when traffic density is low, whereas its average keeps nearly constant and its standard deviation is small in a congestion regime. The proposed time-gap-based traffic model was well validated by traffic measurement data using least squares matching and by previous research outcomes about driver reaction times as well as propagation velocity. This emphatically

declares that a mean value of the time gap is a critical factor to characterize vehicular traffic flow, particularly where the traffic is congested. Therefore, the proposed time-gap-based traffic model is a good and simple representative fundamental diagram for mimicking driving pattern and describing vehicular traffic flow specifically. Moreover, the time-gap-based traffic model can be used as a macroscopic traffic flow model in implementing optimal ramp-metering control or a macroscopic traffic simulator as exploited in this dissertation.

Numerous ramp-metering algorithms have been examined to relieve highway congestion. Unlike previous research, in Chapter 3, we provided two optimal coordinated ramp-metering controls for achieving the maximum average system throughput of vehicular traffic networks. The proposed ramp-metering strategies, the steady-state optimization problem and the time-variant optimization problem, use real-time measurement data along a system-wide highway corridor to regulate the metered rates at all entrance ramps. Also, both strategies are realistically implementable and reasonable algorithms, since they exploit only the limited traffic measurements collectable from existing field facilities and the time-gap-based traffic model introduced in Chapter 2. The steady-state ramp-metering programming problem regulates on-ramp flows so as to keep traffic densities of all homogeneous sections along a system-wide highway corridor below their critical densities. However, this strategy has the side effect of increased traffic jams from the highway mainline to its adjacent streets. Hence, the time-variant linear programming problem was provided with consideration of on-ramp queue control to prevent on-ramp queue spillover that is an adverse effect of most ramp-metering algorithms like the steady-state ramp-metering control. The time-gap-based fundamental diagram was used to demonstrate the constraints of the two proposed optimization problems as well as to estimate traffic flow. As a result of the comparative analysis through a macroscopic traffic simulation based on the time-gap-based traffic model, the time-variant optimization problem for maximizing the average system throughput was proven as an effective coordinated ramp-metering algorithm to provide higher system capacity, to increase the average system speed, particularly in congested traffic, and to mitigate on-ramp queue spillover onto neighboring arterial streets.

Current car-following models for collision avoidance describe the interactive

characteristics of vehicles such as velocity, acceleration rate, and time headway. However, they have the weak point that they cannot predict unexpected and risky driver behavior, as they were developed under unrealistic assumptions about driver behavior. In Chapter 4, therefore, we formulated the anterior SMV to be utilized as a safety indicator to prevent even unexpected vehicle-to-vehicle collisions on roadways. The anterior SMV is defined as the minimum value from a set of the continuous safety level of collision risk with other leading vehicles predicted by the collision avoidance (CA) margin time of each vehicle. Every vehicle in a vehicular traffic network uses a set of vehicle states, including the position, velocity, and lane index of all traveling vehicles, to determine the anterior SMV. The general, simple form of the anterior SMV needs dramatically growing computational complexity, particularly when the number of leading vehicles increases. Hence, the finite space horizon for the anterior SMV was defined in order to substantially reduce computational complexity. The space horizon for the anterior SMV is defined as the finite number of leading vehicles to be considered in determining non-unity anterior SMV. The usability for the anterior SMV was validated through a safety analysis of the Gipps car-following model, which is one of the best-known models. Three states were introduced according to the different variables defined in the Gipps car-following model: a global steady-state that guarantees collision-free movements of all vehicles with the same time-invariant velocity and car spacing along the entire traffic system, a local steady-state in which every vehicle travels on a collision-free trajectory with the same time-invariant velocity but with different constant car spacing, and a catastrophe state that results in collisions. The anterior SMV enables a vehicular traffic system to stay in either a global steady-state or a local steady-state by warning of relevant vehicles of non-unity anterior SMV and helping them by the collision avoidance to escape gradually from a dangerous accident zone. Hence, the anterior SMV can be used as a safety criterion to indicate the level of safety for a car-following model or as a main parameter of an objective function to maximize safety or minimize traffic congestion for vehicular traffic networks.

Existing car-following models specify the movement of vehicles traveling on a highway corridor, particularly by presenting the driver's response to the behavior of the vehicle in front. Unlike existing car-following models, in Chapter 5, we proposed

the target time-gap-based velocity update model, which is an extension of the time-gap-based traffic model considered as a simple triangular fundamental diagram, as described in Chapter 2. Every vehicle in vehicular traffic networks updates its velocity and position for the next time step with the time-gap-based velocity update model. A simulation analysis for the proposed car-following model was conducted by a microscopic traffic simulator. In addition, the simulation results matched well with empirical traffic data. Hence, the target time-gap-based velocity update model is considered to be a representative car-following model that mimics the typical behavior of drivers. Since typical driving behavior is itself a creative and superior algorithm, the proposed car-following model describing it specifically and accurately deserves an outstanding algorithm. A safety analysis of the target time-gap-based velocity update model was conducted through the anterior SMV proposed in Chapter 4. Three different regions were introduced depending on the frequency of collision occurrence with respect to the traffic density, the given constant target time gap applied for all vehicles in vehicular traffic networks, and the update time interval needed to refresh the velocity and position of vehicles. These regions include a collision-free region, a transition region, and a catastrophe region. A collision-free region is defined as the sub domain of the target time gap and the update time interval under the given traffic density, which always assures the collision-free movement of vehicles unless an abrupt perturbation exists. In contrast, a catastrophe region is the sub domain that will result in incidents before reaching a steady-state. A transition region is the area between a collision-free region and a catastrophe region with a positive ratio of collision occurring. A global steady-state of the target time-gap-based velocity update model was analyzed mathematically. Moreover, when the proposed car-following model is used as a basis for inter-vehicle control, the effective reachable domain of the target time gap and the update time interval was presented, which guarantee both collision-free movements and system capacity enhancement compared to the empirical traffic data.

In conclusion, this dissertation offered the following multilevel solutions to improve traffic safety and enhance the capacity of vehicular traffic networks: (1) a time-gap-based traffic model as a foundation for a simple representative macroscopic traffic flow model inferred from an understanding of traffic flow. (2) an optimal coordinated

ramp-metering control to achieve the maximum average system capacity. (3) an anterior SMV to indicate the safety level of rear-end collision risk with leading vehicles. (4) a target time-gap-based velocity update model as a representative car-following model that mimics typical driving behavior for the traffic safety and throughput enhancements.

6.2 Future Works

Diverse control strategies presented in this dissertation can be extended to the aspect of road safety for enabling perfect collision-free movement in vehicular traffic networks. To make this dissertation short, an optimal coordinated ramp-metering control was proposed in Chapter 3 in order to maximize the average system-level capacity and to prevent on-ramp queue spillover onto neighboring arterial streets. In Chapter 4, an effective and rigorous traffic safety metric called the anterior SMV was provided, which indicates the safety level of collision risk with other leading vehicles. Also, the target time-gap-based velocity update model proposed in Chapter 5 was verified as a representative car-following model to mimic typical driving behavior accurately.

As an extended research of Chapters 4 and 5, a hypothesis can be formulated that every vehicle using the target time-gap-based velocity update model always travels along a collision-free trajectory. To support this hypothesis, the derivation of the numerical bounds of the time gap and velocity for the next time step is meaningful, which guarantees collision-free movement. That is, its purpose is to control all traveling vehicles so as to maintain their calculated anterior SMV with a value of 1. Moreover, the system throughput can be presented when this perfect inter-vehicle safety control is applied to a vehicular traffic network, and it can be compared with the field capacity analyzed from the empirical traffic data.

The concept of the posterior SMV was introduced in Chapter 4 and is used as a collision indicator to show the likelihood of accident occurrence with following vehicles. By the characteristics of the posterior SMV, it is helpful to a vehicle in performing lane changing models. As a future work, however, the mathematical derivation of the posterior SMV will be necessary. In addition, the simultaneous application of the anterior SMV and posterior SMV potentializes autonomous driving without accidents.

In conclusion, conducting research about how to constitute a combination of the diverse control strategies presented in this dissertation to attain the high utilization of vehicular traffic networks and guarantee collision-free movement is a significant and remarkable work.

Bibliography

[1] P. Hu, "Data requirements in transportation reauthorization legislation: Operations and security," Tech. Rep. 3, Oak Ridge National Laboratory, Dec. 2005.

[2] J. Kwon, M. Mauch, and P. Varaiya, "Components of congestion: Delay from incidents, special events, lane closures, weather, potential ramp metering gain, and excess demand," in *Proceedings of the 85th Annual Meeting of the Transporation Research*, pp. 84–91, 2006.

[3] J. Kwon and P. Varaiya, "The congestion pie: Delay from collisions, potential ramp metering gain, and excess demand," in *Proceedings of the 84th Transportation Research Board Annual Meeting*, pp. 9–13, 2005.

[4] M. DoT, "2009 Missouri state highway system: Traffic crash statistics," *Missouri Department of Transportation*, pp. 1–74, Aug. 2010.

[5] M. Papageorgiou and A. Kotsialos, "Freeway ramp metering: An overview," *IEEE Transactions on Intelligent Transportation Systems*, vol. 3, pp. 271–281, Dec. 2002.

[6] M. Papageorgiou, H. Hadj-Salem, and J. M. Blosseville, "ALINEA: A local feedback control law for on-ramp metering," *Transportation Research Record*, vol. 1320, pp. 58–64, 1991.

[7] M. Papageorgiou, H. Hadj-Salem, and F. Middelham, "ALINEA local ramp metering: Summary of field results," *Transportation Research Record*, vol. 1603, pp. 90–98, 1997.

[8] H. Jadj-Salem, J. M. Blosseville, and M. Papageorgiou, "ALINEA: A local feedback control law for on-ramp metering; A real-life study," in *Proceedings of the Third International Conference on Road Traffic Control*, pp. 194–198, May 1990.

[9] E. Smaragdis and M. Papageorgiou, "A series of new local ramp metering strategies," in *Proceedings of the 82nd Transportation Research Board Annual Meeting*, pp. 74–86, 2003.

[10] L. Jacobsen, K. Henry, and O. Mahyar, "Real-time metering algorithm for centralized control," *Transportation Research Record*, vol. 1232, pp. 17–26, 1989.

[11] R. Lau, "Ramp metering by zone - The Minnesota algorithm," Tech. Rep. 1, Minnesota Department of Transportation, Jun. 1997.

[12] G. Paesani, J. Kerr, P. Perovich, and E. Khosravi, "System wide adaptive ramp metering (SWARM) in southern California," in *Proceedings of the 7th Annual Meeting, ITS America*, Jun. 1997.

[13] M. Papageorgiou, J. Blosseville, and H. Haj-Salem, "Macroscopic modelling of traffic flow on the Boulevard Périphérique in Paris," *Transportation Research Part B*, vol. 23, no. 1, pp. 29–47, 1989.

[14] M. Papageorgiou, J. Blosseville, and H. Haj-Salem, "Modelling and real-time control of traffic flow on the southern part of Boulevard Périphérique in Paris - Part I: Modelling," *Transportation Research Part A*, vol. 24, no. 5, pp. 345–359, 1990.

[15] M. Papageorgiou, J. Blosseville, and H. Haj-Salem, "Modelling and real-time control of traffic flow on the southern part of Boulevard Périphérique in Paris - Part II: Coordinated on-ramp metering," *Transportation Research Part A*, vol. 24, no. 5, pp. 361–370, 1990.

[16] A. Kotsialos, M. Papageorgiou, C. Diakaki, Y. Pavlis, and F. Middelham, "Traffic flow modelling of large-scale motorway networks using the macroscopic modelling tool METANET," in *Proceedings of TRAIL Expert Seminar on Recent Advances in Traffic Flow Modelling and Control*, no. Chapter 6, Sep. 1999.

[17] A. Kotsialos, M. Papageorgiou, C. Diakaki, Y. Pavlis, and F. Middelham, "Traffic flow modelling of large-scale motorway networks using the macroscopic modelling tool METANET," *IEEE Transactions on Intelligent Transportation Systems*, vol. 3, no. 4, pp. 282–292, 2002.

[18] B. Greenshields, "A study of highway capacity," in *Proceedings of the 14th Annual Meeting of the Highway Research Board*, vol. 14, pp. 448–477, 1934.

[19] M. J. Lighthill and G. B. Whitham, "On kinematic waves. II. A theory of traffic flow on long crowded roads," in *Proceedings of the Royal Society of London. Series A, Mathematical and Physical Sciences*, vol. 229, pp. 317–345, 1955.

[20] P. I. Richards, "Shock waves on the highway," *Operations Research*, vol. 4, no. 1, pp. 42–51, 1956.

[21] G. F. Newell, "A simplified theory of kinematic waves in highway traffic, Part I: General theory," *Transportation Research Part B*, vol. 27, no. 4, pp. 281–287, 1993.

[22] J. H. Banks, "Average time gaps in congested freeway flow," *Transportation Research Part A*, vol. 37, no. 6, pp. 539–554, 2003.

[23] M. Green, "'How long does it take to stop?' Methodological analysis of driver perception-brake times," *Transportation Human Factors*, vol. 2, no. 3, pp. 195–216, 2000.

[24] A. Mehmood and S. M. Easa, "Modeling reaction time in car-following behaviour based on human factors," *International Journal of Engineering and Applied Sciences*, vol. 5, no. 2, pp. 93–101, 2009.

[25] G. T. Taoka, "Brake reaction times of unalerted drivers," *ITE Journal*, vol. 59, no. 3, pp. 19–21, 1989.

[26] R. H. Wortman and J. S. Matthias, "Evaluation of driver behavior at signalized intersections," *Transportation Research Record*, no. 904, pp. 10–20, 1983.

[27] M. S. Chang, C. J. Messer, and A. J. Santiago, "Timing traffic signal change intervals based on driver behavior," *Transportation Research Record*, no. 1027, pp. 20–30, 1985.

[28] M. Sivak, P. L. Olson, and K. M. Farmer, "Radar measured reaction times of unalerted drivers to brake signals," *Perceptual and Motor Skills*, vol. 55, p. 594, 1982.

[29] H. S. Mika, J. B. Kreer, and L. S. Yuan, "Dual mode behavior of freeway traffic," *Highway Research Record*, no. 279, pp. 1–12, 1969.

[30] J. R. Windover and M. J. Cassidy, "Some observed details of freeway traffic evolution," *Transportation Research Part A*, vol. 35, no. 10, pp. 881–894, 2001.

[31] J. C. Muñoz and C. F. Daganzo, "The bottleneck mechanism of a freeway diverge," *Transportation Research Part A*, vol. 36, no. 6, pp. 483–505, 2002.

[32] B. A. Zielke, R. L. Bertini, and M. Treiber, "Empirical measurement of freeway oscillation characteristics," *Transportation Research Record*, vol. 2088, no. 1, pp. 57–67, 2008.

[33] K. R. Smilowitz and C. F. Daganzo, "Reproducible features of congested highway traffic," *Mathematical and Computer Modelling*, vol. 35, no. 5, pp. 509–515, 2002.

[34] M. Schönhof and D. Helbing, "Empirical features of congested traffic states and their implications for traffic modeling," *Transportation Science*, vol. 41, no. 2, pp. 135–166, 2007.

[35] C. I. Chen, J. B. Cruz, and J. G. Paquet, "Entrance ramp control for travel-rate maximization in expressways," *Transportation Research Part C*, vol. 8, no. 6, pp. 503–508, 1974.

[36] M. Papageorgiou, E. Kosmatopoulos, L. Papamichail, and Y. Wang, "Alinea maximises motorway throughput - An answer to flawed criticism," *Traffic Engineering and Control*, vol. 48, no. 6, pp. 271–276, 2007.

[37] S. Cho, A. Badii, R. L. Cruz, and R. R. Rao, "Time-gap based traffic model for vehicular traffic flow," in *Proceedings of IEEE Vehicular Technology Conference, VTC 2014 Spring*, pp. 1–5, May 2014.

[38] R. L. Gordon, "Algorithm for controlling spillback from ramp meters," *Transportation Research Record*, no. 1554, pp. 162–171, 1996.

[39] A. D. Spiliopoulou, D. Manolis, I. Papamichail, and M. Papageorgiou, "Queue management techniques for metered freeway on-ramps," *Transportation Research Record*, no. 2178, pp. 40–48, 2010.

[40] C. F. Daganzo, "Urban gridlock: Macroscopic modeling and mitigation approaches," *Transportation Research Part B*, vol. 41, pp. 49–62, 2007.

[41] N. Geroliminis and J. Sun, "Hysteresis phenomena of a macroscopic fundamental diagram in freeway networks," *Transportation Research Part A*, vol. 45, pp. 966–979, 2011.

[42] D. C. Gazis, R. Herman, and R. B. Potts, "Nonlinear follow the leader models of traffic flow," *Operations Research*, vol. 9, no. 4, pp. 545–567, 1961.

[43] P. G. Gipps, "A behavioural car following model for computer simulation," *Transportation Research Part B*, vol. 15, pp. 105–111, 1981.

[44] R. E. Wilson, "An analysis of Gipps's car-following model of highway traffic," *IMA Journal of Applied Mathematics*, vol. 66, no. 5, pp. 509–537, 2001.

[45] M. Brackstone and M. McDonald, "Car-following: A historical review," *Transportation Research Part F*, vol. 2, no. 4, pp. 181–196, 1999.

[46] K. Chang and K. Chon, "A car-following model applied reaction times distribution and perceptual threshold," *Journal of the Eastern Asia Society for Transportation Studies*, vol. 6, pp. 1888–1903, 2005.

[47] A. Tordeux, S. Lassarre, and M. Roussignol, "An adaptive time gap car-following model," *Transportation Research Part B*, vol. 44, no. 8-9, pp. 1115–1131, 2010.

[48] D. Anup, B. T. Morris, and M. M. Trivedi, "On-road prediction of driver's intent with multimodal sensory cues," *IEEE Pervasive Computing*, vol. 10, pp. 22–34, Jul. 2011.

[49] J. C. McCall, D. Wipf, M. M. Trivedi, and B. D. Rao, "Lane change intent analysis using robust operators and sparse bayesian learning," *IEEE Transactions on Intelligent Transportation Systems*, vol. 8, pp. 431–440, Sep. 2007.

[50] A. Vahidi and A. Eskandarian, "Research advances in intelligent collision avoidance and adaptive cruise control," *IEEE Transactions on Intelligent Transportation Systems*, vol. 4, pp. 143–153, Sep. 2003.

[51] W. Prestl, T. Sauer, J. Steinle, and O. Tschernoster, "The BMW active cruise control ACC," *SAE Transactions*, pp. 1–8, 2000.

[52] P. Venhovens, K. Naab, and B. Adiprastito, "Stop and go cruise control," *International Journal of Automotive Technologies*, vol. 1, pp. 61–69, Dec. 2000.

[53] N. Oliver and A. P. Pentland, "Driver behavior recognition and prediction in a smartcar," in *Proceedings of SPIE 4023, Enhanced and Synthetic Vision*, pp. 280–290, May 2000.

[54] N. Kuge, T. Yamamura, O. Shimoyama, and A. Liu, "A driver behavior recognition method based on a driver model framework," *SAE Transactions*, vol. 109, no. 6, pp. 469–476, 2000.

[55] J. C. Hayward, "Near-miss determination through use of a scale of danger," in *Proceedings of the 51st Annual Meeting of the Highway Research Board*, vol. 384, pp. 22–34, Aug. 1972.

[56] H. Chin and S. Quek, "Measurement of traffic conflicts," *Safety Science*, vol. 26, pp. 169–185, Aug. 1997.

[57] C. Oh and T. Kim, "Estimation of rear-end crash potential using vehicle trajectory data," *Accident Analysis and Prevention*, vol. 42, pp. 1888–1893, Nov. 2010.

[58] L. Evans and P. Wasielewski, "Do accident-involved drivers exhibit riskier everyday driving behavior?," *Accident Analysis and Prevention*, vol. 14, pp. 57–64, Feb. 1982.

[59] P. G. Michael, F. C. Leeming, and W. O. Dwyer, "Headway on urban streets: Observational data and an intervention to decrease tailgating," *Transportation Research Part F*, vol. 3, pp. 55–64, Jun. 2000.

[60] K. Vogel, "A comparison of headway and time to collision as safety indicators," *Accident Analysis and Prevention*, vol. 35, pp. 427–433, May 2003.

[61] K. Bevrani and E. Chung, "Car following model improvement for traffic safety metrics reproduction," in *Proceedings of the Australasian Transport Research Forum*, pp. 1–14, 2011.

[62] Å. Svensson, *A method for analysing the traffic process in a safety perspective*. PhD thesis, Department of Traffic Engineering, Lund University, Sweden, Mar. 1998.

[63] Å. Svensson and C. Hydén, "Estimating the severity of safety related behavior," *Accident Analysis and Prevention*, vol. 38, pp. 379–385, Mar. 2006.

[64] J. Maretzke and U. Jacob, "Distance warning and control as a means of increasing road safety and ease of operation," in *Proceedings of the XXIV FISITA*, pp. 105–114, 1992.

[65] A. D. Mason and A. W. Woods, "Car-following model of multispecies systems of road traffic," *Physical Review E*, vol. 55, pp. 2203–2214, Mar. 1997.

[66] H. J. Payne, "Models of freeway traffic and control," in *Simulation Council Proceedings*, vol. 1, pp. 51–61, 1971.

[67] G. B. Whitham, *Linear and nonlinear waves*. John Wiley and Sons Inc., 1974.

[68] A. Aw and M. Rascle, "Resurrection of "second order" models of traffic flow," *SIAM Journal on Applied Mathematics*, vol. 60, no. 3, pp. 916–938, 2000.

[69] H. M. Zhang, "A non-equilibrium traffic model devoid of gas-like behavior," *Transportation Research Part B*, vol. 36, no. 3, pp. 275–290, 2002.

[70] D. Helbing, "Improved fluid dynamic model for vehicular traffic," *Physical Review E*, vol. 51, pp. 3164–3169, Apr. 1995.

[71] R. M. Michaels, "Perceptual factors in car following," in *Proceedings of the 2nd International Symposium on the Theory of Road Traffic Flow*, pp. 44–59, Apr. 1963.

[72] R. Wiedemann and U. Reiter, "Microscopic traffic simulation: The simulation system MISSION, backgroud and actual state," tech. rep., CEC Project ICARUS (V1052) Final Report, 1992.

[73] H. T. Fritzsche, "A model for traffic simulation," *Traffic Engineering and Control*, vol. 35, pp. 317–321, May. 1994.

[74] M. Koshi, M. Iwasaki, and I. Ohkura, "Some findings and an overview on vehicular flow characteristics," in *Proceedings of the 8th International Symposium on Transportation and Traffic Theory*, pp. 403–426, 1981.

[75] J. H. Banks, "Flow processes at a freeway bottleneck," *Transportation Research Record*, no. 1278, pp. 20–28, 1990.

[76] B. S. Kerner, "Experimental features of self-organization in traffic flow," *Physical Review Letters*, vol. 81, no. 17, pp. 3797–3800, 1998.

[77] J. H. Banks, "Two capacity phenomenon at freeway bottlenecks: A basis for ramp metering?," *Transportation Research Record*, no. 1320, pp. 83–90, 1991.

[78] M. J. Cassidy and R. L. Bertini, "Some traffic features at freeway bottlenecks," *Transportation Research Part B*, vol. 33, pp. 25–42, Feb. 1999.

[79] L. Zhang and D. Levinson, "Some properties of flows at freeway bottlenecks," in *Proceedings of the 83rd Transportation Research Board Annual Meeting*, no. 1883, pp. 122–131, 2004.

[80] K. Chung, J. Rudjanakanoknad, and M. J. Cassidy, "Relation between traffic density and capacity drop at three freeway bottlenecks," *Transportation Research Part B*, vol. 41, pp. 82–95, Jan. 2007.

[81] H. M. Zhang, "A mathematical theory of traffic hysteresis," *Transportation Research Part B*, vol. 33, pp. 1–23, Feb. 1997.

[82] D. Chen, J. A. Laval, S. Ahn, and Z. Zheng, "Microscopic traffic hysteresis in traffic oscillations: A behavioral perspective," *Transportation Research Part B*, vol. 46, pp. 1440–1453, Dec. 2012.

[83] W. S. Levine and M. Athans, "On the optimal error regulation of a string of moving vehicles," *IEEE Transactions on Automatic Control*, vol. AC-11, pp. 355–361, Jul. 1966.

[84] J. G. Bender and R. E. Fenton, "A study of automatic car following," *IEEE Transactions on Vehicular Technology*, vol. 18, pp. 134–140, Nov. 1969.

[85] S. Sheikholeslam and C. A. Desoer, "Longitudinal control of a platoon of vehicles," in *Proceedings of IEEE American Control Conference*, pp. 291–296, May 1990.

[86] K. C. Chu, "Optimal decentralized regulation for a string of coupled systems," *IEEE Transactions on Automatic Control*, vol. 19, pp. 243–246, Jun. 1974.